Stellar activity in high-precision photometric and spectroscopic transit observations
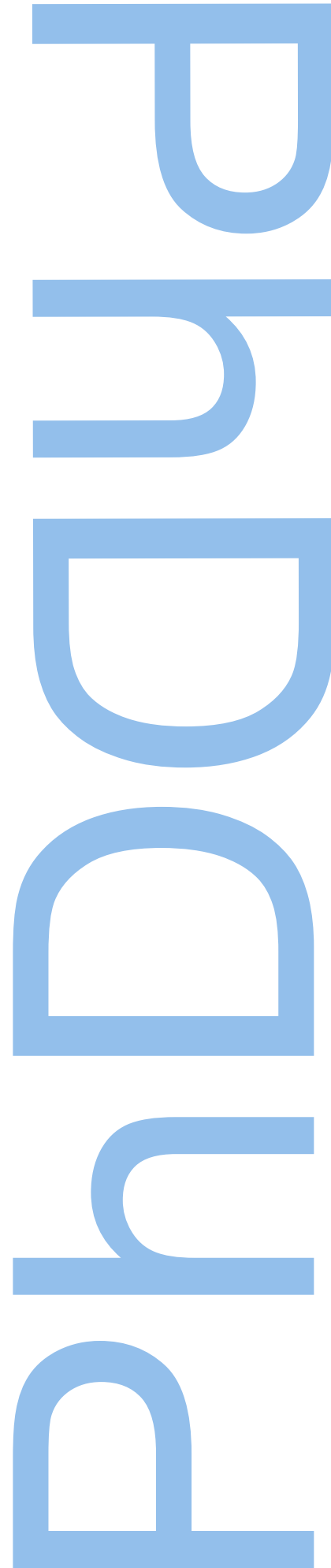
Mahmoudreza Oshagh

Tese de Doutoramento apresentada à

Faculdade de Ciências da Universidade do Porto

Departamento de Física e Astronomia

2014

PhD

Stellar activity in high-precision photometric and spectroscopic transit observations
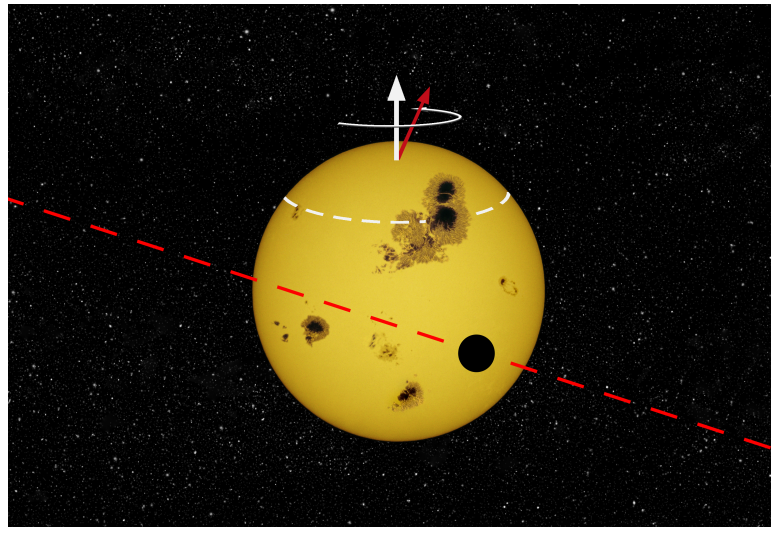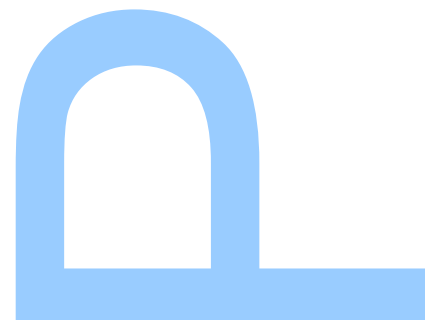
Mahmoudreza Oshagh

Doutoramento em Astronomia
Departamento de Física e Astronomia

Orientador
Nader Haghighipour, Professor of Astronomy, University of Hawaii

Coorientador
Nuno Miguel Cardoso Santos, Researcher in Center for Astrophysics of University of Porto
Faculdade de Ciências da Universidade do Porto
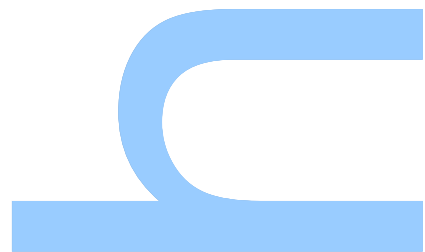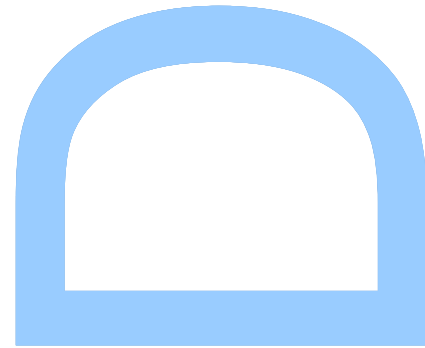
To my loving parents, Shirin and Mohammad, as a small token of my gratitude to their unconditional love and support throughout my life.

اجرام که ساکنان این ایوانند			اسباب تردد خردمندانند

هان تا سر رشتهٔ خرد گم نکنی			کانان که مدبرند سرگردانند

خیام

Acknowledgements

First of all, I would like to express my sincere gratitude to my PhD supervisors Prof. Nuno Santos and Prof. Nader Haghighipour, for supporting me during these past four years. Nuno not only was my supervisor, he was also a very close friend. His patience, motivation, enthusiasm, and trust in me enabled me to be an independent researcher and moreover enjoy my life while earning my PhD. Nader, despite the long distance supervising, has given me numerous crucial advice during my PhD research which helped me to stay on the right track of science.

I would also like to give special thanks to Gwenael. Gwenael and I have worked closely on most of my research project even when he was not at CAUP any more. I very much appreciate his enthusiasm and caring. I would also like to thank Isabelle for her kind help during developing the SOAP-T code, which I could not have done without.

I would like to express my special thanks to my friend and my colleague Pedro for his understanding, encouragement, and personal attention which helped me to get through challenging times during my PhD, and dealing with issues related to living in a foreign country. I thank my lovely friend and colleague Vardan for all friendly conversations which helped me to learn a lot from him about Galaxy astrophysics and in general about science.

I wish to thanks all the EXO-Earth team members in the CAUP for their contribution to my PhD research. I would like to thank especially my office mates, Maria, Annelies, and Diana for the warm and friendly environment which gave me the positive energy that I needed to work harder on my PhD project.

I would like to thank my lovely parents, Shirin and Mohammad, for their unconditional love and encouraging me to be independent, and have confidence in my abilities to go after new things in my life. I would also like to thank my lovely brothers, Morteza and Reza, for their support throughout my life and I especially appreciate them for taking care of my parents during my absence for my PhD.

Finally, a heartfelt thanks goes out to my beloved girlfriend Banafsheh for all her love, support , understanding, and patience during my PhD study.

Abstract

The quest for Earth-like extra-solar planets, especially those located inside the habitable zone of their host stars, requires detection techniques sensitive enough to detect the faint signals produced by those planets. The Radial Velocity (RV), transit, and transit timing variation methods are the most used and also the most efficient methods for detecting and characterizing exoplanets. Surveys of the currently known exoplanets indicate that many of these planets orbit stars with high levels of activity. Stellar-activity features such as spots can complicate the detection and characterization of exoplanetary systems through all these methods. In this thesis, I concentrate on the problem of stellar activity for planet detection and characterization using the above mentioned methods.

The transit timing variation method is based on measuring transit timing deviations from constant period and interpreting this deviations to be due to the gravitational interaction of a perturber. Most of the methodologies which have been used to measure the transit times are model-dependent and are vulnerable to systematic errors. To overcome this problem, we proposed a model-independent method to determine the transit times through calculating the barycenter of the transit light curve.

However, the results of all the methodologies including our proposed method would be offseted in the case that the transit light curve symmetry is broken, for instance due to the overlap of the transiting planet and the stellar activity features on the stellar surface. To tackle this issue we developed a software "SOAP-T" which can simulate systems consisting of a rotating star with active zones and a transiting

planet. Because this tool generates the light curves with anomalies inside, we can use these synthesis light curves to remove the anomalies in the observed transit light curves, and reproduce realistic symmetric light curves. However, in most studies which have been done on the TTV method, the impact of the stellar activity features in the transit light curve and derived transit timing estimations have not been taken into account. We performed a quantitative study on the impact of stellar spot on the planetary parameters estimations, especially the transit timing. The results of our study show that spot anomalies might lead to a maximum underestimation of a planet radius by about 4%. The effects on the transit duration can also reach to the order of 4%, longer or shorter. Depending on the size and distribution of spots, anomalies can also produce transit timing variations with significant amplitudes (200 seconds). For instance, TTVs with signal amplitudes of 200 seconds can be produced by an Earth-mass planet in a mean-motion resonance with a Jovian type body transiting a solar-mass star in a three-day orbit , or by an Earth-mass exomoon on a Neptune mass transiting planet.

Transmission spectroscopy (multiband photometry) is the most powerful technique to explore exoplanetary atmospheres. Since the transmission spectroscopy is basically based on the high-precision transit observations at different wavelengths, one of its main limitations could be the stellar activity, which is usually taken into account only by assessing the effect of non-occulted stellar spots. We found that the anomalies inside the transit light curve at different wavelengths due to occultation of stellar spot/plage by the transiting planet can lead to a significant underestimation or overestimation of the planet-to-star radius ratio as a function of wavelength. Especially at short wavelengths, the effect can reach up to a maximum difference of 10% in the planet-to-star radius ratio, mimicking the signature of light scattering in the planetary atmosphere. Furthermore, we demonstrated that the transmission spectroscopy measurements of the active stars HD 189733b and GJ 3470b, and especially their excess of the planet

radius in the bluer part of the spectra, can almost exactly be reproduced by assuming the occultation of the HD 189733b and GJ 3470b with the active region (plage) of their host star.

Resumo

A busca de planetas extra-solares semelhantes à Terra, especialmente aqueles localizados na zona de habitabilidade da sua estrela, requer técnicas de detecção suficientemente sensíveis para detectar os diminuto sinais por eles produzidos. Os métodos da velocidade radial (VR), dos trânsitos e da variação do tempo de trânsito são os mais utilizados e os mais eficientes na detecção e caracterização de exoplanetas. Uma pesquisa aos exoplanetas actualmente conhecidos indica que muitos destes orbitam estrelas com altos níveis de atividade . Os indicadores de actividade estelar, como manchas podem complicar a detecção e caracterização de sistemas extrasolares através dos métodos da VR, dos trânsito e da variação do tempo de trânsito.

O método da variação do tempo de trânsito é baseado na medição do desvio do tempo de trânsito de um período constante e na intrepretação destes desvios como fruto da interacção gravitacional de um corpo perturbador.

A maioria das metodologias utilizadas para medir os tempos de trânsito são são dependentes do modelo e são vulneráveis a erros sistemáticos . Para superar este problema propusemos um método independente do modelo para determinar o tempo de trânsito através de cálculo do baricentro da curva de luz do trânsito .

Contudo , os resultados de todas as metodologias , incluindo o método do baricentro apresentam um desvio no caso em que a simetria da curva de luz do trânsito é quebrada, por exemplo, devido à sobreposição do planeta em trânsito com as características da atividade estelar na superfície estelar. Para resolver esta questão causada por anomalias

na curva de luz, desenvolvemos um programa de computador " SOAP-T ", que simula sistemas constituídos por uma estrela em rotação com zonas activas e um planeta em trânsito . Como o pragrama gera as curvas de luz com anomalias no interior , podemos assim usar a curva de luz sintética para remover as anomalias presentes nas curvas de luz de trânsito observadas e reproduzir uma curva de luz realista e simétrica. No entanto , na maioria dos estudos feitos sobre o método variação do tempo do trânsito, o impacto das característica de atividade estelar na curva de luz do trânsito e consequentes estimativas para os tempos de trânsito não foram levados em consideração. Portanto, realizamos um estudo quantitativo sobre o impacto das manchas estelares nas estimativas dos parâmetros planetários, especialmente no tempo de trânsito . Os resultados do nosso estudo mostram que as anomalias provocadas pelas manchas podem levar a subestimas o raio de um planeta em 4% interio ao seu valor real. Os efeitos sobre a duração do trânsito podem também ser da ordem de 4 % , a mais ou a menos longo. Dependendo do tamanho e distribuição das manchas , as anomalias podem também produzir variaçõesno tempo de trânsito com amplitude significativas. . Por exemplo , uma variação no tempo do trânsito com uma amplitude de sinal de 200 segundos pode ser induzida por um planeta com a massa da Terra com um movimento médio em ressonância com um corpo tipo joviano a transitar uma estrela com massa solar, numa órbita com um período de três dias, ou por uma exolua com a massa da Terra à volta de um planeta com a massa de Neptuno em trânsito.

A espectroscopia de transmissão (fotometria em multibanda) é a técnica mais poderosa para explorar atmosferas exoplanetárias. Uma vez que a espectroscopia de transmissão é basicamente baseada nas observações de alta precisão de trânsitos em diferentes comprimentos de onda, uma das principais limitações desta técnica é a atividade estelar, que normalmente é levada em conta apenas avaliando o efeito das manchas estelares não-ocultadas. Constatamos que as anomalias no interior da curva de luz de trânsito em diferentes comprimentos

de onda, devidas à ocultação estelar de manchas / plage pelo planeta em trânsito, pode levar a uma subestimação ou sobrestimação significativa da razão entre o raio do planeta e o raio estelar em função do comprimento de onda. Especialmente em comprimentos de onda curtos, o efeito pode atingir até uma diferença máxima de 10 % na razão entre o raio do planeta o raio da estrela, imitando a assinatura de dispersão de luz na atmosfera planetária. Para além disso, foi demonstrado que as medidas de espectroscopia de transmissão das estrelas activas HD 189733b e GJ 3470b, e especialmente o excesso no raio do planeta na banda mais azul do espectro, pode ser quase exactamente reproduzido assumindo a ocultação de HD 189733b e GJ 3470b uma a região activa (plage) da sua estrela.

Contents

List of Figures

Chapter 1

Introduction

Attempting to answer a historical question "are we alone in the universe?" is the main objective of searching for the extra-solar planets (hereafter exoplanets). Since the first discovery of an exoplanet (51 Peg b) around a Sun-like star, by Mayor & Queloz (1995), this new field in Astrophysics has been growing up quickly. Nowadays, around one thousand seven hundred exoplanets in around thousand hundred planetary systems have been discovered through different detection techniques. The large majority of them have been detected through the spectroscopic Doppler shift of the spectral lines technique which is known as the Radial Velocity method (hereafter RV), and also through the transit method. Some of planets are found that have mass or radius close to that of the Earth, such as Alpha Centauri Bb with the mass close to Earth mass (Dumusque et al., 2012) and the Kepler-186f with a radius similar to Earth's which is located in the habitable zone of its host star (Quintana et al., 2014).

By continuously increasing the number of known exoplanets and also precisely characterizing them, we are able to put strong constraints on the planet formation scenarios (Alibert et al., 2005; Boss, 1998; Lin et al., 1996; Mordasini et al., 2009; Pollack et al., 1996). Furthermore, this allows us to have a more precise idea about the frequency of planets in the Galaxy, including potentially habitable worlds. Determining the frequency of planets in the Galaxy will allow to define the role of environment on the planet formation and evolution. For instance, it will reveal that how likely the metallicity and the mass of star can be a main factor

in formation of planet around the star (e.g., Alibert et al., 2011; Mordasini et al., 2012; Udry & Santos, 2007; Valenti & Fischer, 2008). Because of these reasons the planet searches and characterizations are now in the main focus of several space and ground based project (namely TESS, PLATO, CHEOPS, NGTS, HARPS-N, ESPRESSO).

In section 1.1, we briefly introduce the exoplanet detection and characterization methods. We describe with more details the most used ones in detecting and characterizing exoplanets, which are also the more relevant to this PhD thesis. In section 1.2 we provide some useful information about the *Kepler* space telescope and also about using the *Kepler* data. Chapter 2 is dedicated to the study of stellar activity, mostly the stellar spots. We describe the methods which are suitable to study the stellar spots and furthermore we present the main properties of stellar spots. In chapter 3, we explain the *Barycenter* method which is a model independent method to measure the transit time accurately. In chapter 4, we discus the issues arising due to the stellar activities when dealing with high-precision transit light-curve, such as wrong estimations on the transit times, planet radius, etc. We also introduce the SOAP-T tool. SOAP-T generates the RV signal and light curve of that system. Especially, the SOAP-T is capable of reproducing the same features as obtained from observations for the outside of transits modulation, as well as the anomalies inside the transits. In chapter 5, we describe the quantitative study on the impact of stellar spots on the planetary parameters estimations. In chapter 6, we present the result of our study on the impact of the occultation of stellar active regions, such as stellar spots or plages, on transmission spectroscopy measurements. Finally, in chapter 7 we conclude the overall conclusions of my PhD project, and we discuss shortly about future prospects.

1.1 Detection and characterization methods

Several techniques have been used to detect and characterize exoplanets, namely, radial velocity, transit, transit timing variations, astrometry, direct imaging, gravitational microlensing, and pulsar timing. In this section, we briefly introduce
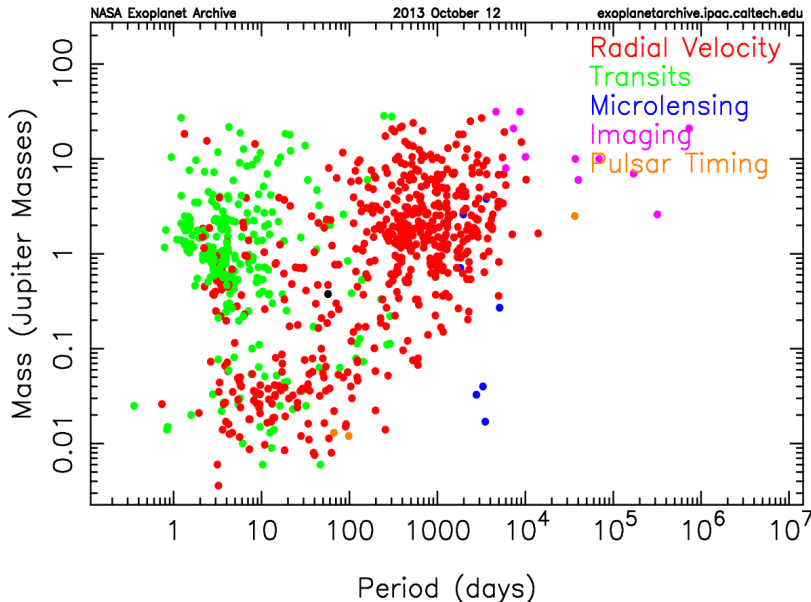
Figure 1.1: Diagram of the confirmed exoplanets masses verse their orbital period (Plot is taken from http://exoplanetarchive.ipac.caltech.edu/).

them. We describe with higher level of detail the ones more relevant to this thesis, the radial velocity, the transit, and the transit timing variations methods.

1.1.1 Radial Velocity technique

While a planet orbits its host star, it induces a reflex on motion on the star. The star orbits around the center-of-mass of the star-planet system. Despite the fact that the orbital radius of this motion is much smaller than that of the motion of planet around the center-of-mass, the planet has a millionth of their parent star's brightness. Therefore, measuring accurately the shifts of the spectral lines in the stellar spectrum due to the movement of the star (which is known as the Doppler effect), enables us to estimate the radial velocity of the star (the velocity of star along the line-of-sight of observer) by using the Doppler's equation

$$\frac{\Delta\lambda}{\lambda} = \frac{v}{c} \tag{1.1}$$

3
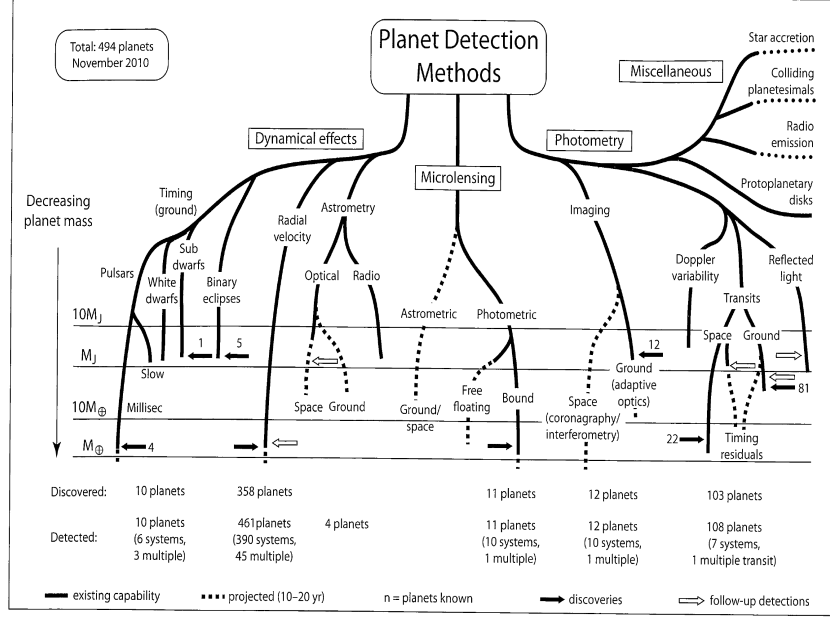
Figure 1.2: Diagram of exoplanet detection techniques, taken from Perryman (2011).

where c is the speed of light, v is the radial velocity of the star, and $\delta\lambda$ denotes the shift in the specific spectral line with respective wavelength of λ.

Therefore, by monitoring the variations of the RV measurements of the star, the detection of the planetary system around the star can be possible. Furthermore, by using Kepler's law of motion important information about the planetary system's configuration can be extracted from the RV signal. For instance, the planet orbital period (P), argument of periastron of planet (ω_p), periastron passage time (T_0), the orbital eccentricity (e), and the average radial velocity of the system (γ) can be estimated by fitting the functional form of radial velocity variations (equation 1.2) to the observed radial velocity measurements.

$$V(t) = K[\cos(\nu + \omega_p - \pi) + e\cos\omega_p - \pi] + \gamma \tag{1.2}$$

where ν, the true anomaly, is related to e and eccentric anomaly (E) as

$$\tan\frac{\nu}{2} = \sqrt{\frac{1+e}{1-e}}\tan\frac{E}{2}, \tag{1.3}$$

where E is also related to T_0 and P through the mean anomaly (M) as

$$E - e \sin E = \frac{2\pi(t - T_0)}{P} = M. \tag{1.4}$$

Moreover, the amplitude of RV's variation signal (K) can be described in the terms of the stellar mass (M_*), and the minimum planet mass $(M_p \sin i)$ as

$$K = \left(\frac{2\pi G}{P}\right)^{1/3} \frac{M_p \sin i}{(M_p + M_*)^{2/3}} \frac{1}{\sqrt{1 - e^2}}, \tag{1.5}$$

where G is the gravitational constant (these equations are taken from the Celestial Mechanics of J. B. Tatum [1]). As an example, the amplitude of RVs signal on the Sun due to Earth is around 8 cms^{-1}. It is clear from the equation 1.5 that the amplitude of RV signal strongly depends on the mass of planet and depends inversely on the orbital period. Thus, the massive planets which are orbiting on the short period orbits induce higher amplitude signals and are thus easier to be detected. This introduced a bias in the RV surveys which lead to the discoveries of comparatively large number of "Hot Jupiters" (Hot Jupiters are the Jupiter mass planet on the short period orbit, hence they have high surface temperatures).

Because the RVs measurements of the stars are obtained in the direction of the observer, the estimation on the planet mass is only a minimum mass $(M_p \sin i)$, and not the actual mass. This is one of the strongest limitations of the RV method (Santos, 2008), even if it has been shown that statistically is not an crucial issue (Lovis & Fischer, 2011). Considering that the inclination angle of the planet orbital plane is randomly (isotropically) distributed in space, the probability that the value of $\sin i$ is larger than 0.5 is around 87%, which means that the edge-on systems are more frequent. The only way to determine the actual planet mass is by measuring the orbital inclination through the transit method.

The first exoplanet orbiting Sun-like star (51 Pegasi b) was discovered in 1995 by using ELODIE spectrograph, a echelle type spectrograph, at 1.93 cm telescope in Observatoire de Haute-Provence (OHP). Later, in 2006, the spectrograph on 1.93 cm telescope was replaced with the SOPHIE spectrograph, which could reach to 3-4 ms^{-1} precision in the RV measurement. The CORALIE spectrograph, which is also a echelle type spectrograph, was installed on the Swiss 1.2 meter

---

[1]http://astrowww.phys.uvic.ca/ tatum/celmechs.html
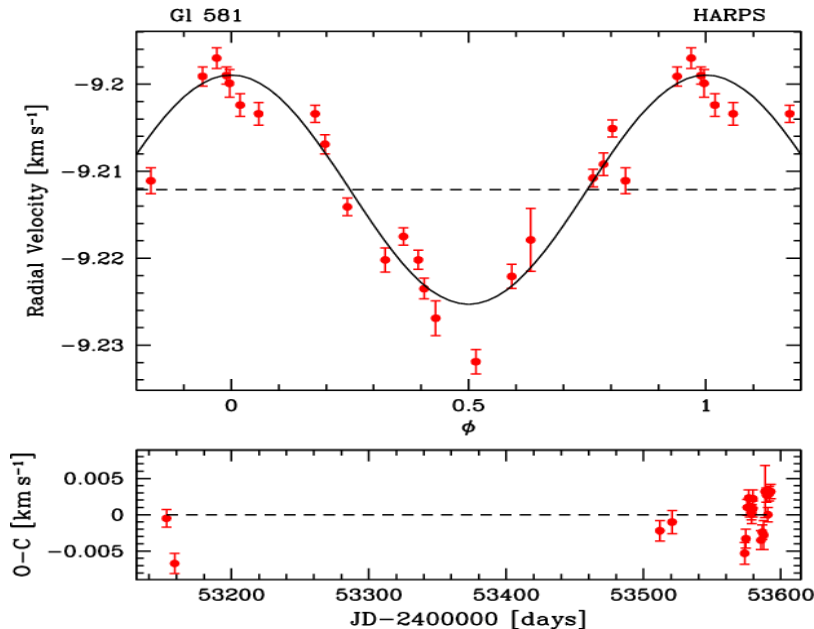
Figure 1.3: Upper panel: phased radial velocities for Gl 581 which indicates presence of a planet around that star. The lower panel shows the residuals between observation and the fitted solution (Bonfils et al., 2005).

telescope at La Silla ESO in 1998. CORALIE spectrograph could reach to 2-7 ms^{-1} precision in the RV measurement for long-term observations. The FIES spectrograph a high-resolution Fiber-fed Echelle Spectrograph was installed on 2.56 m the Nordic Optical Telescope in 2006. FIES could reach to the 2-8 ms^{-1} precision in the RV measurement for long-term observations (Telting et al., 2014). HIRES spectrograph (High Resolution Echelle Spectrometer) which is operating on the Keck Telescope is also able to push down the precision of RV measurements to ms^{-1} (Vogt et al., 1994).

Need for reaching to 1 ms^{-1} precision in the RV measurement, for the slow-rotating stars to be able to detect Earth like mass planets signal around those stars, led to the design of HARPS (High Accuracy Radio Velocity Planetary Searcher). HARPS is a high-precision and high resolution spectrograph which was installed on the 3.6m ESO telescope, at La Silla in Chile. It was designed to reach to $1ms^{-1}$ precision in the RV measurement for the slow-rotating star, in order to be able to detect Super-Earth like mass planets signal around them. By

implementing optimized observational strategy and modeling and removing the activity-induced noises, Dumusque et al. (2012) could reach an on-sky precision of around $0.51 ms^{-1}$ with HARPS.

ESPRESSO (Echelle SPectrograph for Rocky ECoplanets and Stable Spectroscopic Observations) is the near future high spectrograph which will be installed on the VLT telescope of ESO at Paranal observatory, Chile. ESPRESSO will be able to combine the light of four large Unit Telescopes (UT) of VLT and its principle objective is to achieve $10 cms^{-1}$ precision on RV measurements, which is crucial to detect the Earth-like planet in habitable zone of solar like star (Pepe et al., 2010).

1.1.2 Transit Photometry technique

Assuming that a planet orbiting around its host star passes in front of the stellar disk as seen from the observer, it will cause a reduction in the total flux of the star as measured by a photometric observation. This phenomena generates the well-known transit light-curve feature (see Figure 1.4). The schematic illustration of the transit is shown in Figure 1.5. The transit events are low-chance events to occur, since the passage of the planet in the same line-of-sight as the star as seen by observer is a geometrically and temporally low probability event.

The angle of the shadow's cone produced by the transiting planet (as shown in Figure 1.6) can be written as

$$\sin \Theta = (R_* + R_p)/a \tag{1.6}$$

where a is the semimajor axis of the planet orbit, R_p is planet radius and R_* stellar radius. The edge-on probability of the orbiting planet to transit also can be obtained from the requirement of $|b| < 1 + \frac{R_p}{R_*}$, which means for the transit to occur we need the projected distance between the planet position and the center of the star to be smaller than the stellar radius. In this equation b is the impact parameter

$$b = \frac{a \cos i}{R_*} \left(\frac{1 - e^2}{1 + e \sin \omega} \right), \tag{1.7}$$
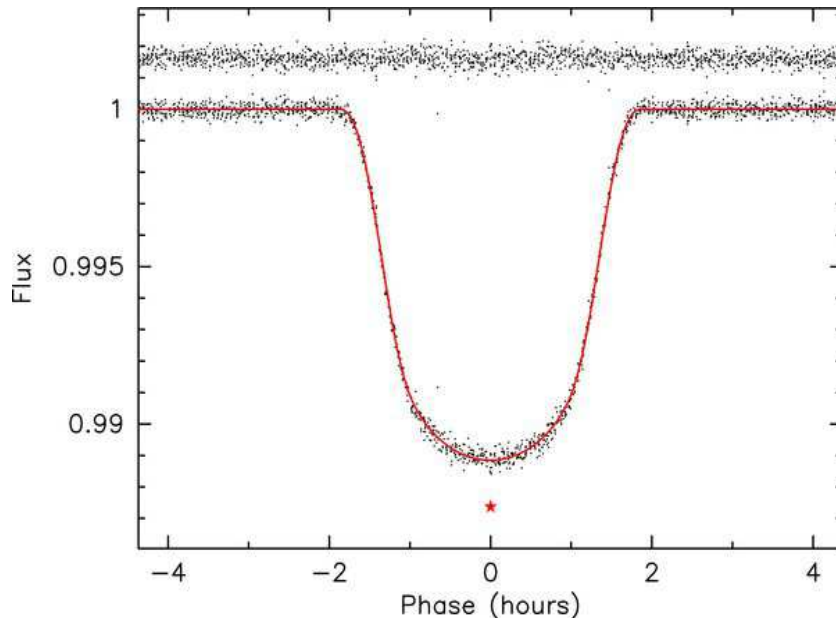
Figure 1.4: The phased transit light curve of Kepler-15. The dots denotes the observation while the red line shows the best-fit transit model. The residuals between them showed offset above the light curve. The star shows the mid transit time (Endl et al., 2011).

in which i is the inclination of orbital plane with respect to the line of sight of observer (Winn, 2010).

By multiplying the angle of the shadow's cone by the edge-on probability, and taking into account the uniform distribution of $\cos i$ while averaging over ω, we are able to derive the geometric probability of a transit event as

$$Prob_{tran} = \frac{R_* + R_p}{a} \left(\frac{1}{1 - e^2} \right),$$

(1.8)

The temporal probability is proportional to the inverse of planet orbital period. The best strategy to overcome the low probability issue is by running the long-term photometric observation of large number of stars, and then try to detect the periodic transit signal in the light curves.

Since the planet radius is in comparison much smaller than its host star, the depth of the transit light-curve is a tiny signal, and as consequence detecting
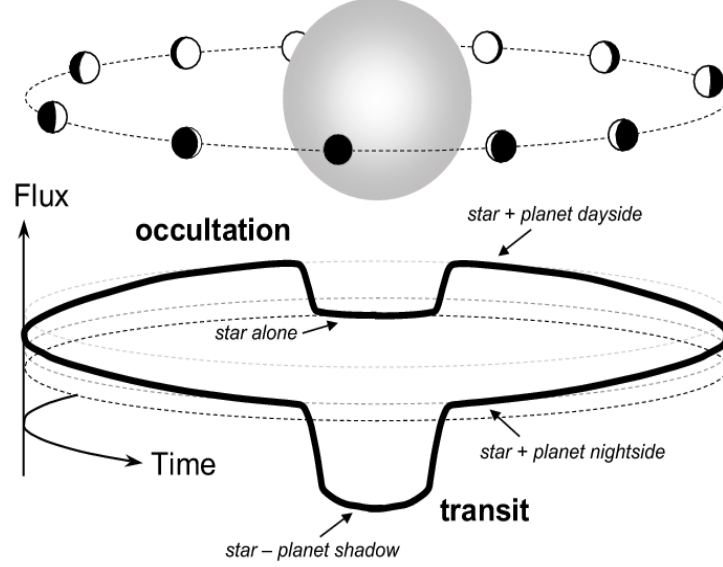
Figure 1.5: Illustration of transits and occultations, which is taken from Seager (2011).

the transit signal requires high precision photometric observation. For instance, an Earth-size planet with radius of 0.01 of the star will cause a 0.01% reduction in the flux. Nowadays, this precision is accessible on the space-based telescopes thanks to the CCDs technology. Considering the fact that the transit depth is related to the lose of flux during the transit and thus it can be written as

$$\frac{\Delta f}{f} = \frac{L_* - L_{*,planet}}{L_*}, \tag{1.9}$$

where $L_* = 2\pi R_*^2 F_*$ is the stellar luminosity and $L_{*,planet} = L_* - (2\pi R_p^2 F_*)$ is the luminosity of star while the planet blocks part of it. F_* is the stellar flux. By doing simple algebra manipulation the transit depth can be converted in terms of the planet and star radius as

$$\frac{\Delta f}{f} = \left(\frac{R_p}{R_*}\right)^2. \tag{1.10}$$

This equation indicates that by accurately determining the transit depth, the value of the planet radius (in units of stellar radius) can be estimated.
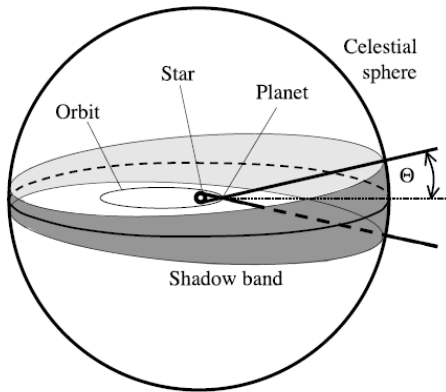
Figure 1.6: Schematic configuration of the transiting planet system. As a planet transit its host star, it generates a shadow cone with the angle of the cone Θ (Seager, 2011).

More parameters of the exoplanetary system can be estimated through the transit light-curve study, such as the inclination of the orbital plane of the planet with respect to the observer, the semimajor axis of planet orbit, and the coefficients of stellar limb darkening. For instance, for the common situation in which e, ω, and the orbital period (P) are know from RV measurements, the transit duration allows us to determine the inclination of the planet orbit. The transit duration can be formulated as

$$T_D = \frac{PR_*}{\pi a}\sqrt{1 - b^2}. \tag{1.11}$$

Stellar limb darkening phenomena causes the transit light curve to become rounded off at the bottom and also curved in the egress and ingress. Considering the optical depth, the light that we receive from the center of the stellar disk were generated on the deeper surface of photosphere compare to those from the limb of the stellar disk (see Figure 1.7). Thus, by looking at the limb of star, systematically we obverse higher layer in the photosphere which are cooler and

so less bright. This phenomena causes the limb of star become darker when compared to the center and is known as the stellar limb darkening effect. The general theoretical nonlinear form of limb-darkening law which reproduces the observed limb-darkening was proposed by Claret (2000) and is defined as
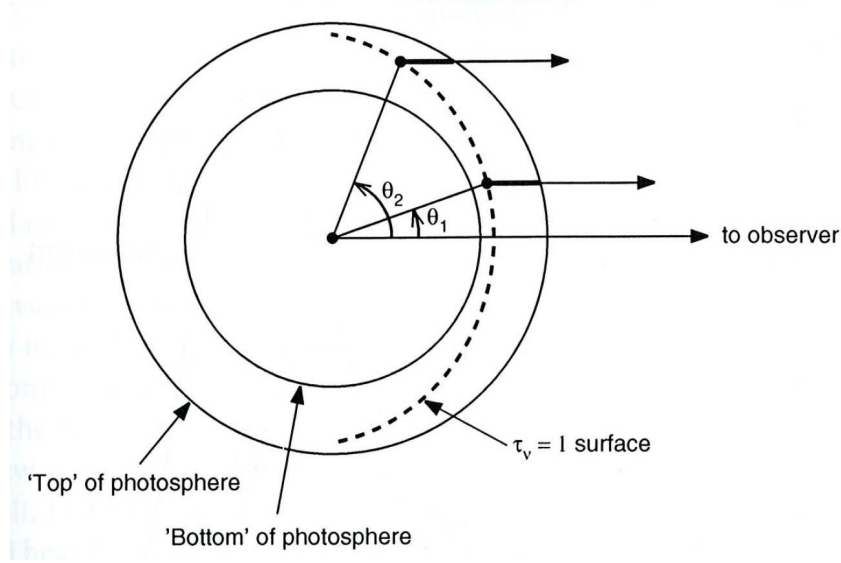
Figure 1.7: Schematic illustration of stellar limb darkening taken from (Gray, 2005). The dashed line shows the surface of unit optical depth from the top of photosphere.

$$I(x, y) = 1 - \sum_{n=1}^{4} c_n (1 - \mu^{n/2}), \tag{1.12}$$

which gives the stellar intensity at the given point of $I(x, y)$ on the stellar disk plane. In this equation μ is defined as $\mu = \cos \theta = \sqrt{1 - x^2 - y^2}$. Generally in the exoplanet field the quadratic limb darkening law for the stellar intensity is considered, which can be written as

$$I(x, y) = 1 - u_1 (1 - \mu) - u_2 (1 - \mu)^2, \tag{1.13}$$

where u_1 and u_2 are the quadratic limb darkening coefficients. The quadratic limb

darkening coefficients of the star can be estimated through studying the shape of transit light curve (Mandel & Agol, 2002).

Despite the fact that the transit method is capable to determine most of the planetary system parameters it has its main limitation which is the weakness in the estimation of the planet mass. Furthermore, the transit method is not a an error-free technique for discovering planets, since there are several physical phenomena (such as the eclipsing binary stars) which can mimic same signal as the transit light-curve (the false positive). Subsequently, all the transiting planet candidates have to be confirmed by one of the other detection methods, most commonly the RVs technique. Moreover, the combination of the transit and the RV observations allow us to fully characterize the planetary system. For example, the density of the planet can be determined precisely by combining these two method results, which provides valuable clues to the planet formation scenario.

The first planet which was detected through the transit method was HD 209458b (Charbonneau et al., 2000; Henry et al., 2000). Since then, several ground-based surveys have been started looking for the transiting planet sings in the long-term photometric observations of stars, such as the OGLE survey (Udalski et al., 1992), TrES (Alonso et al., 2004), HATNet (Bakos et al., 2004), MEarth (Charbonneau et al., 2008), and WASP (Pollacco et al., 2006). The transit surveys, like the RV surveys, favor large planets on the short period orbits, "Hot Jupiters", since they have a higher transit probability and are also easier to be detected. This introduces a bias on transit surveys. In order to tackle this issue, space telescopes such as *MOST* (Walker et al., 2003), *CoRoT* (Baglin et al., 2006) and *Kepler* (Borucki et al., 2010), came to push forward the detection limits in the transit surveys to the Earth-like planets on long period orbits. In this thesis we mostly work with *Kepler* public data. For this reason in the section 1.2 we describe in detail the *Kepler* space telescope.

In transit observations the stellar activity features such as spots which are not occulted by a transiting planet can produce out of transit light-curve variations that can lead to a wrong estimation of planet parameters such as its radius (e.g., Pont et al., 2008). The overlap of a transiting planet and stellar spots can produce anomalies in the transit light-curve that may also lead to an incorrect

determination of planetary parameters, such as the planet radius and the limb-darkening coefficients of the host star (Ballerini et al., 2012; Berta et al., 2011; Csizmadia et al., 2013; Czesla et al., 2009; Désert et al., 2011; Pont et al., 2007) . In chapter 2, we will discuss with more detail the issues caused by stellar activity in high precision photometry and how to settle down these issues.

1.1.2.1 Rossiter-McLaughlin effect

As a star revolves around its rotational axis, a given point on its surface will be blue-shifted when the star rotates toward the observer, and red-shifted when it rotates away. During the transit of an exoplanet in front of the host stellar disk, the corresponding rotational velocity of the portion of the stellar disk that is blocked by the planet disk is removed from the integrated stellar velocity over the entire star creating an anomaly in the RV measurement of the star known as Rossiter-McLaughlin effect (McLaughlin, 1924; Rossiter, 1924). Figure 1.8 illustrates schematically the RM effect. There have been several analytical studies which attempt to model the observations of RM effect (e.g., Boué et al., 2013; Hirano et al., 2011; Ohta et al., 2005). In general to calculate the RV anomaly due to the RM effect the profile of the spectral lines (or of the Cross-Correlation function[1]) has to be defined, which can be written as

$$F(v) = \frac{\iint I(x,y)M(x,y,v)\,dx\,dy}{\iint I(x,y)\,dx\,dy},$$ (1.14)

where $I(x,y)$ is the stellar surface intensity at (x,y) which was defined in the equation (1.13), and $M(x,y,v)$ is the velocity profile associated with each point (x,y) due to both the stellar rotation and macro-turbulence (Gray, 2005) which can be written as

$$M(x,y,v) = \left\{ \frac{1}{2\sqrt{\pi}\sigma_\parallel} \text{Exp}\left[-\left(\frac{v - v(x,y)}{\sigma_\parallel} \right)^2 \right] + \frac{1}{2\sqrt{\pi}\sigma_\perp} \text{Exp}\left[-\left(\frac{v - v(x,y)}{\sigma_\perp} \right)^2 \right] \right\}$$ (1.15)

---

[1]Cross-Correlation function(CCF) can be defined as an average of several spectral line in velocity space (more details can be found in Baranne et al. (1996)

the quantities $\sigma_\parallel$ and $\sigma_\perp$ are given by

$$\sigma_\parallel^2 = \sigma_0^2 + \zeta^2 \cos\theta^2 \quad , \quad \sigma_\perp^2 = \sigma_0^2 + \zeta^2 \sin\theta^2 \,, \tag{1.16}$$

where $\cos\theta = \sqrt{1 - x^2 - y^2}$, and ζ is the macro-turbulence velocity [1] and can be considered to have a value of ζ=3.98 km s^{-1} for the solar-type stars, which is equal to that of the Sun (Hirano et al., 2011; Valenti & Fischer, 2005). The quantity σ_0 is the instrumental broadening which is set to approximately 2.2 km s^{-1}. This is equivalent to the broadening of a typical spectrograph with a high-resolution of $R \sim 110000$, similar to that of HARPS. The velocity $v(x, y)$ in equation 1.15 is defined as

$$v(x, y) = (v \sin i)\frac{x}{r_*} + (v_{\text{CB}})\mu \,, \tag{1.17}$$

where v_{CB} is the convective blue-shift and is set to -300 m s^{-1}, similar to its value for the Sun (Shporer & Brown, 2011).

There are at least two different ways to estimate the RVs during transit due to the RM effect. One relies on the iodine cell technique which consists in fitting $F(v)$ with a stellar CCF (Butler et al., 1996), and the other is based on a Gaussian fit to $F(v)$ (Baranne et al., 1996; Pepe et al., 2002).

In the first order approximation the apparent RM effect signal can be expressed as (Ohta et al., 2005)

$$\Delta RV = v \sin i \frac{\iint I(x, y)x \, dx \, dy}{\iint I(x, y) \, dx \, dy}. \tag{1.18}$$

In the case of an edge-on transiting planet with zero misalignment between its orbital plane and stellar spin axis, the amplitude of RM effect signal can be approximated by

$$K_{RM} \simeq \left(\frac{R_p}{R_*}\right)^2 (v \sin i), \tag{1.19}$$

where R_p is planet radius and R_* stellar radius (Winn et al., 2008).

---

[1]macro-turbulence velocity is large-scale motions in the stellar atmosphere which can affect the spectral line width.
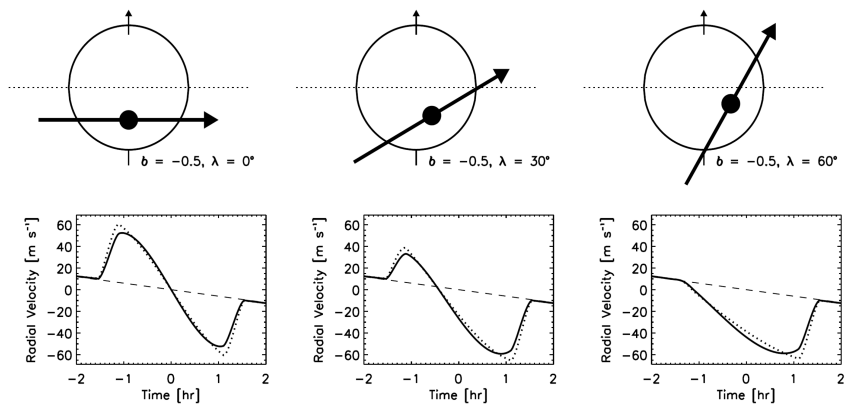
Figure 1.8: Schematic illustration of RM effect (Gaudi & Winn, 2007). The shape of the RM signal can be used to estimate the projected angle between the stellar spin axis and planetary orbital axis.

This effect has been used to constrain the projected rotational velocity of a star ($v \sin i$), and the angle between the sky-projections of the stellar spin axis and the planetary orbital plane (λ), known as misalignment angle (e.g., Albrecht et al., 2012; Hébrard et al., 2008; Hirano et al., 2011; Simpson et al., 2010; Triaud et al., 2010, 2009; Winn et al., 2009, 2010). Measuring the misalignment angle can allow us to better constrain models of planet formation, and evolution. It is important to note that the determination of $v \sin i$ and λ can be influenced by second order effects such as differential stellar rotation (Albrecht et al., 2012).

1.1.3   Astrometry
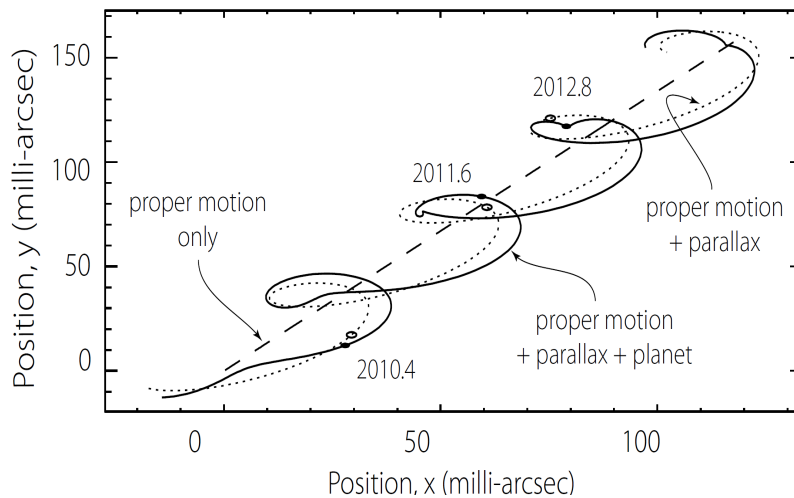
Figure 1.9:   Illustration of the stellar oscillation on the sky plane as result of an orbiting planet (Perryman, 2013).

Astrometry is a similar method to the RVs method, except that in the astromerty the quantity which has to be measured is the sky-projected displacement of star due to its orbit around the center-of-mass of the star-planet system. The amplitude of displacement of a sky-projected position of a star can be expressed by

$$\alpha \simeq \frac{a}{d} \left(\frac{M_p}{M_p + M_*} \right), \qquad (1.20)$$

where M_p is the planet mass and M_* is the mass of the star, a denotes the semimajor axis of planet orbit, and d is the distance between the star and the Earth (Hilditch, 2001). As an example a Jupiter-mass planet causes a solar-type star to move by 1 mas(milliarcsecond) over 12 yrs when viewed from a distance of 10 pc.

This equation shows that the largest displacement of the star occurs when a close-by star harbors a massive planet on a long period orbit. As a result, the astrometry technique tends to be more sensitive to the detection of massive planets located on long period orbits.

GAIA (Global Astrometric Interferometer for Astrophysics) is an ESA(European Space Agency) space telescope which was launched in December 2013. The main objective of GAIA is to determine precisely the positions of a very large sample of stars in our Galaxy, which can be used to discover hundreds of thousands of new objects orbiting those stars, such as exoplanets, brown dwarfs (Casertano et al., 2008; Sozzetti, 2011).

1.1.4 Gravitational Microlensing

One of the most interesting predictions of General relativity theory was that a massive body can bend the path of light, and in some sense, it can work as a lens, focusing the light behind it (Einstein, 1936). Assuming a foreground star passes in front of a far background source of light (star, galaxy, etc), it would cause a temporary amplification in the total flux of the background source. In the case of a star which hosts a planet, this amplification will take place twice (once due to the mass of star, once due to the planet mass) with a short time delay. However, the amplification due to the planet mass has a much smaller amplitude and also shorter duration.

It can be shown that this technique favors massive planets at large separation from its host star. One of the biggest disadvantages to using this technique is that, the event of microlensing occurs just once and there is no chance of follow-up of the target, in order to confirm the nature of the exoplanet. It should be noted
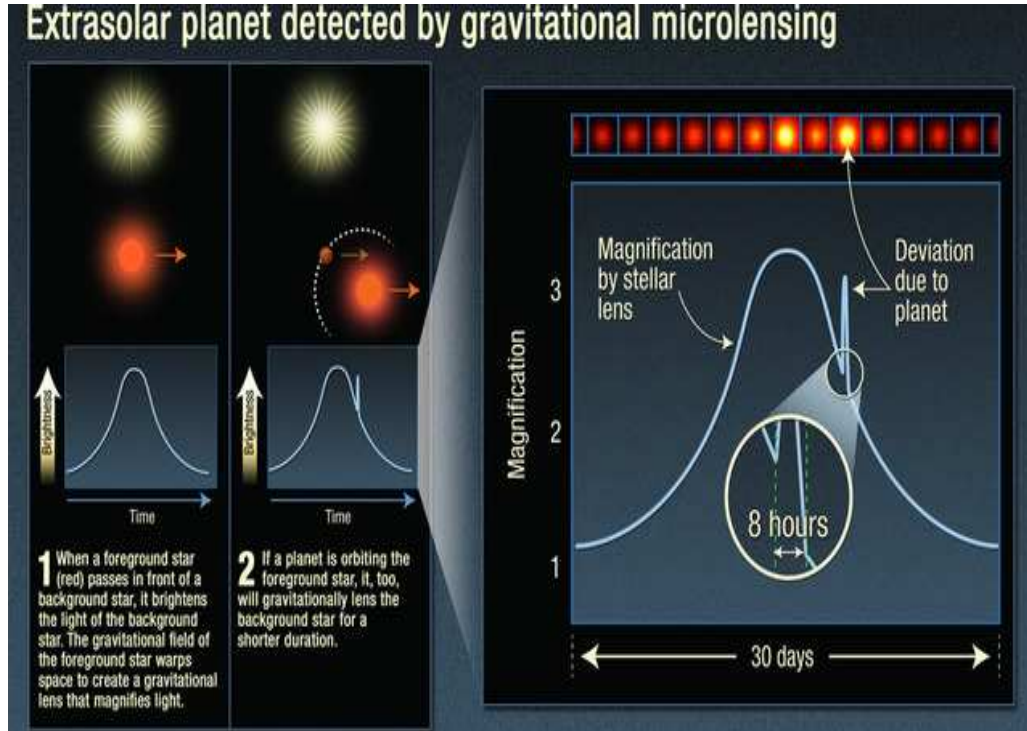
Figure 1.10: Sketch of one case of gravitational microlensing involving a planet in the lens system http://blogs.scientificamerican.com/life-unbounded/2012/03/07/gravitational-mesolensing-and-the-hunt-for-exoplanet/.

that the microlensing technique results allow us to do statistics of long period planets, and as well it allowed to detect free-floating planets [1] (Sumi et al., 2011).

Several ground-base surveys exist, such as OGLE survey (Udalski et al., 1992) and MOA survey (Bond et al., 2002), which have been monitoring large areas of the sky to detect microlensing events.

EUCLID, is an ESA space telescope, to be launched in 2020. As one of the by-products of EUCLID is to overcome the detection bias of microlensing technique, and detect Earth-mass planets on short period orbits, which maybe located in the habitable-zone of their host star (Laureijs et al., 2010).

---

[1]Free-floating planets, also known as rogue planets, are planetary-mass objects that are not orbiting a star but instead orbit the galaxy directly. They have either been ejected from the planetary system in which they were formed or never been gravitationally bound to any star.

1.1.5 Pulsar timing

Pulsars are fast rotating neutron stars. Since they are highly magnetized and rotating rapidly, they emit intense beam of radio emission along its magnetic axis, which does not necessarily lined up with the stellar rotation axis. When the direction of those radiations is pointing toward the Earth, we would be able to receive regular and precisely spanned time pulses.
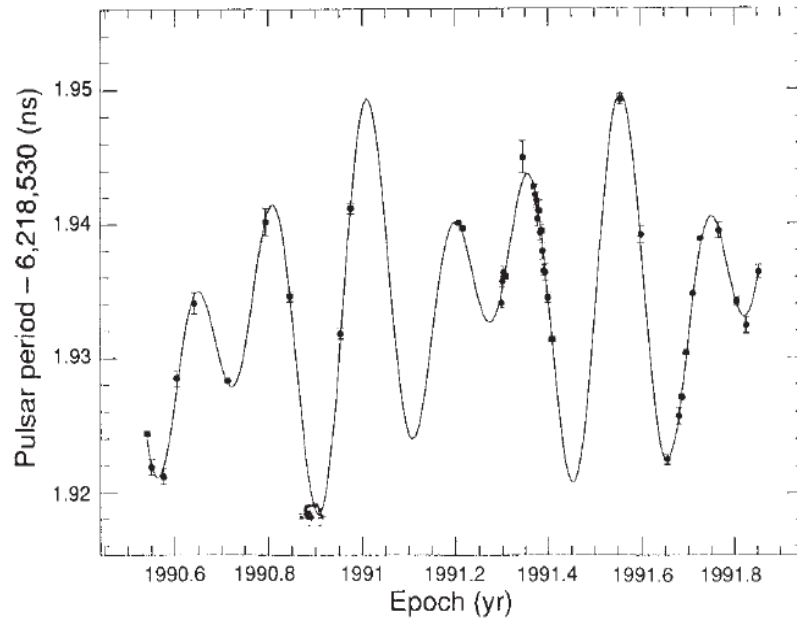
Figure 1.11: The first Pulsar timing variation signal observed for pulsar PSR1257 + 12 by Wolszczan & Frail (1992).

Like in the RV method, the motion of the star around the center-of-mass of the star and its planet, induces a variation in the timing between the pulses (see figure 1.11, the first observed pulsar timing variations signal (Wolszczan & Frail, 1992)). By determining the variations in the timing of a pulsar's pulses, it is possible to estimate the planetary parameters, such as the orbital period, semi major axis, and the minimum planet mass.

1.1.6 Direct imaging

Probably one of the theoretically most straightforward method for detecting exoplanet is direct imaging. In this technique the image of the exoplanet has to be spatially resolved form its host star. The diffraction limited spatial resolution which can be resolved by a telescope with the diameter of D is defined as
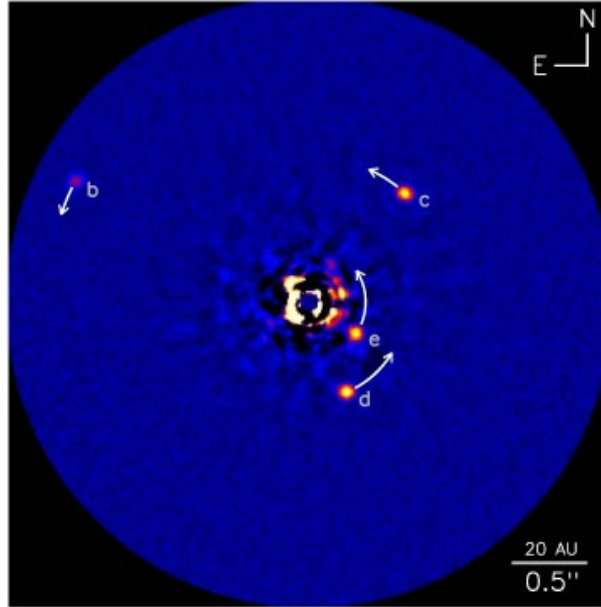
Figure 1.12: Image of a direct imaging of a multiplanets system around HR 8799 (Marois et al., 2010).

$$\alpha = \frac{1.22\lambda d}{D}, \tag{1.21}$$

where d is the distance of the star to the observer, and λ is the wavelength which is used in the observation (Oswalt, 2003). From this equation, it can be seen that detecting a planet on long period orbit around a nearby star with a large

telescope at a short wavelength is favored. However it should be noted that the Adaptive Optic[1] (AO) is needed to improve the image quality to reach to the diffraction limit of the telescope and since the AO technique is only available in the Infrared (IR) most of the exoplants detected through the direct imaging were observed in the IR (Kalas et al., 2005; Marois et al., 2008).

Despite the fact that this method cannot provide information about the planet mass, long-term direct imaging observations resolve the orbit of the exoplanet, which can yield an accurate estimation on the planet orbital parameters. However, it should be noted that for a long period orbit planet the observation should be done for a long time.

There will be several projects, in near future, which will be dedicated to perform high resolution direct imaging of exoplanets, such as the Large Binocular Telescope Interferometer (LBTI) (Hinz et al., 2008), the Gemini Planet Imager (GPI)at Gemini South Telescope in Chile (Macintosh et al., 2008), and the Spectro-Polarimetric High-Contrast Exoplanet Research (SPHERE) project at the VLT (Beuzit et al., 2008). The main goal of these projects is to be able to detect small-size planets, most likely young ones because they are hotter, on relatively short orbit around nearby stars.

1.1.7   Transit Timing Variation

One of the most recent method for detecting, characterizing, and confirming exoplanets, is that of transit timing variations method (hereafter TTV). By measuring the mid-transit times of several transit light-curves (time of the minimum of each transit light curve) of a transiting planet, the orbital period of transiting planet can be estimated accurately. Assuming that the transiting planet is orbiting unaccompanied around the star, its period has to be constant, thus the mid-transit times should occur in a strictly periodic fashion. In the case that mid-transit times show deviations form a constant period, these variations can

---

[1]Adaptive Optic is a new technology which is used to correct the wave-front distortions due to atmospheric distortion to improve the performance of optical systems. AO is based on measuring the distortions in a wave-front and compensating them in real-time with a device such as a deformable mirror.

be interpreted as a hint for the presence of another body in the system, such as a secondary planet, a large moon or even a stellar companion.
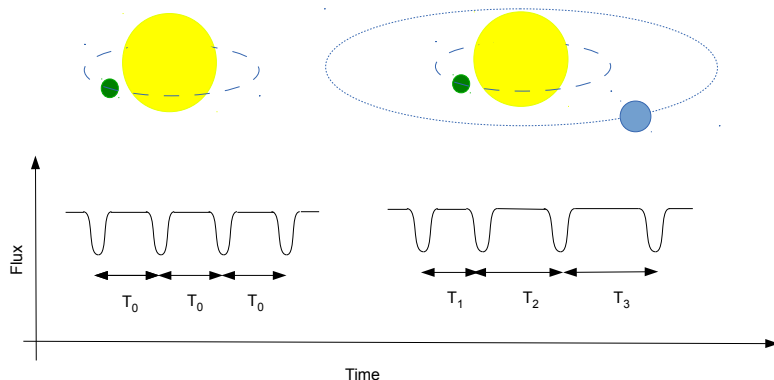
Figure 1.13: Illustrating the transit timing variation method due to gravitational perturbation on non-transiting planet. Left: A single planet transits its host star on a fix period. Right: A planet transiting time varies due to the gravitational perturbation of the non-transiting planet.

Regarding that the TTVs signal is generated by the gravitational perturbation of a hypothetical secondary object in the system, the amplitude of TTVs signal strongly depends on the mass and orbital architecture of the transiting planet and the perturber. Moreover, as shown by Holman & Murray (2005) and Agol et al. (2005) the TTV amplitude can be strongly amplified when the transiting planet and the pertuber are close to a mean-motion resonance. This amplitude, for a planet with period P and a perturbing planet on j:j+1 mean motion resonance with the transiting planet, can be written as

$$\delta t_{max} \sim \frac{P}{4.5j} \frac{m_{pert}}{m_{pert} + m_{tran}},$$ (1.22)

where m_{pert} is the mass of the perturber and m_{tran} is the mass of transiting planet

(Agol et al., 2005). In such a case, even a low-mass planets like Earth can induce large TTV signals on the transiting planet which can be easily detectable. As a result, the TTV method is suitable method for searching for small mass planets.

Recently the TTV method has been used for detection of non-transiting planets in the confirmed planetary systems of *Kepler* which showed strong TTV signals (strong TTV signal means periodic signal with a large amplitude). For instance, in the Kepler-19 system the Kepler-19b transiting planets showed strong TTV signals which is shown in the Figure 1.14 (Ballard et al., 2011). This TTV signal led to detection and characterization of Kepler-19c.

However, on the other hand the TTV signal depends on several parameters of the transiting planet and also the pertuber, and thus several configurations can produce the same TTV signal which means that the TTV signals are strongly degenerate (Boué et al., 2012). For instance, as shown by Boué et al. (2012), an Earth-mass planet is able to produce TTV signal comparable to that produced by a Saturn-mass planet. As a result, the TTV method often requires follow up RV observations in order to break the degeneracy and confirm and characterize non-transiting planets.

Despite the fact that in some cases we cannot conclude on the existence of a non-transiting planet in the system with the TTV technique, we can still make use of TTV signal to estimate and put upper limits on the parameters of an hypothetical non-transiting planet. For instance, there have been several systems on which weak TTV signal are present, and were used to set upper limits on the mass and period of non transiting planet, such as WASP-3b (Maciejewski et al., 2010), WASP-10b (Maciejewski et al., 2011a), WASP-12b (Maciejewski et al., 2011b), and LHS-6343c (Oshagh et al., 2012).

In addition, the TTV method has been used also in some cases to confirm the existence of multiplanets in the multiple transiting planets system, by determining anti-correlation between the TTVs of different planets in the same system, such as all the planets in the Kepler-9 system (Holman et al., 2010) and Kepler-11 (Lissauer et al., 2011) (see Figure 1.14).

Note that stellar activity features such as stellar spots can complicate the transit timing measurements. The overlap of the transiting planet and stellar spot can cause anomalies inside the transit light-curve, which can make an offset to the
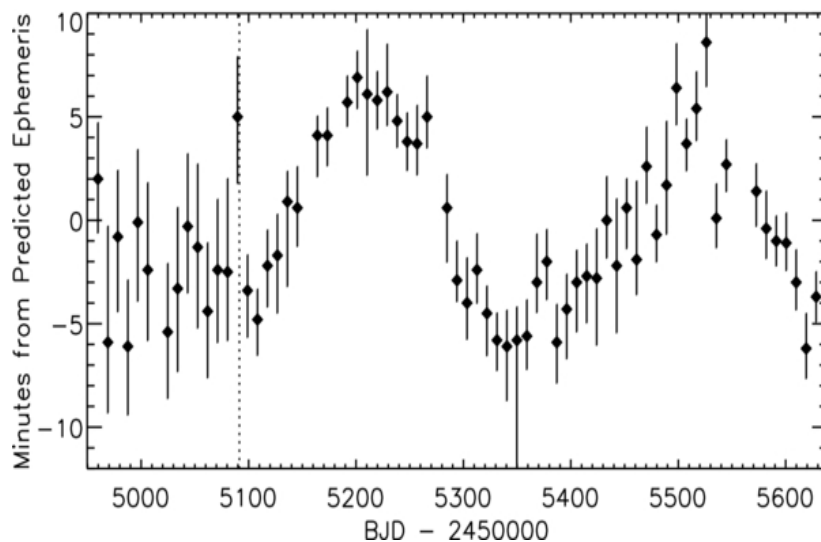
Figure 1.14: The TTV signal of Kepler-19b which was used to detect and characterize the non-transiting planet Kepler-19c (Ballard et al., 2011).

actual transit time values. These anomalies can produce TTV with significant amplitude(Oshagh et al., 2013b). In chapter 4 and 5, we will discuss the stellar activity issue in more detail and will propose a solution to settle down this issue.

1.2 Kepler Space Telescope

Kepler Space Telescope is a NASA telescope which was launched in March 2009. The principal aim of *Kepler* is to continuously monitor the brightness of over 150000 stars in a specific large region of our Galaxy (115 square degrees) in order to discover signs of Earth-size planets through the transit method (Borucki et al., 2010). Since its launch, more than 966 planets have been discovered and confirmed [1], and more than 3800 planet candidates have been detected (Batalha et al., 2013). The *Kepler* planet candidates are named *Kepler* Object of Interest (KOI) (Batalha et al., 2013). *Kepler* high precision photometric observation allow

---

[1]$http://www.nasa.gov/mission_pages/kepler/main/index.html.UmMoIvnWRao$
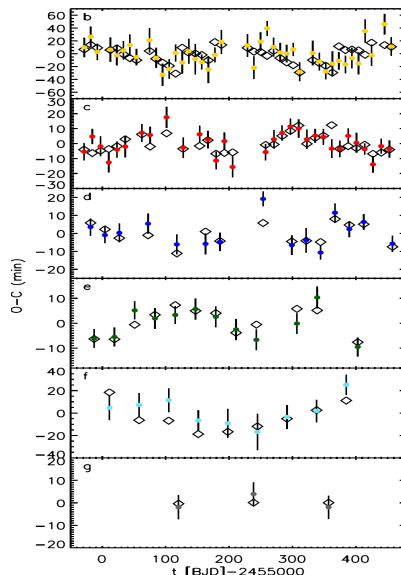
Figure 1.15: Observed transit times of planetary transits of Kepler-11 system minus a calculated linear ephemeris, plotted as dots with error bars. colors correspond to different planets in the Kepler-11 system. Dynamical models are shown by the open diamonds (Lissauer et al., 2011).

us to reach to the level of accuracy to detect small planets, such as two Earth-size planet in habitable zone of Kepler-62 (Borucki et al., 2013), and also moon-size planet Kepler-37b (Barclay et al., 2013).

Kepler camera exposure time is 6.02 seconds with the associated readout time of 0.52 seconds. *Kepler* offers two different options for the integration time. The Long Cadence (LC) which integrates over 270 exposures and provides one point each 29.4 min observations. The Short Cadence (SC) which integrates over 9 exposures and returns one data point each 58.9 seconds (Gilliland et al., 2010). All 150000 stars in the *Kepler* field of view have been observed in the LC. Only targets which are in the KOI or in the targets list of *Kepler* Asteroseismic Consortium (KASC) have been observed in the SC.

For each target in the filed of view of *Kepler* the flux is accessible in two different forms, the Simple Aperture Photometry (SAP) and the Pre-search Data Conditioning Simple Aperture Photometry (PDC-SAP). SAPs contain all the

instrumental effects such as data breaks, flux jumps, and drifts (García et al., 2011). The instrumental effects are partly corrected and detrended in the PDC-SAP. However, it has been shown that those correction affect the astrophysical signals which exist in the light curve, such as the stellar activity features and Asteroseismic signals (Murphy, 2012). The time for each time-series of fluxes is available also in two formats[1]. TIME which is the time of center of each cadence (presented in the Julian Day unit). The other format of time is the TIMECORR which is the barycenter corrected TIME .

Kepler data have been released in the form of package of quarters "Q". The LCs are in the format of Q_n and for the SCs each quarter is divided into three parts, $Q_{n,m}$ which $m = 1, 2, 3$. These data can be downloaded from the MAST (Mikulski Archive for Space Telescopes) webpage [2].

---

[1]$http://archive.stsci.edu/kepler/manuals/archive_manual_jul2011.pdf$
[2]http://archive.stsci.edu/kepler/publiclightcurves.html

Chapter 2

Stellar Activity

Stellar activity features similar to those on the Sun have been observed on the surface of most cool stars, through various observation techniques, such as periodic variation in brightness and Doppler imaging. Moreover, recent studies have demonstrated that most stars have a higher activity level than that of the Sun. For instance, in the *Kepler* field of view 25- 33% of the 150000 main sequence stars show an higher level of activity than the Sun (Basri et al., 2013) (see Figure 2.1).

Skumanich (1972) was the first to suggest that stellar activity might be related with stellar rotation. This idea was confirmed by the observation of strong correlations between the stellar rotational period and stellar magnetic field indicators, which led to the formulation of the "Dynamo theory" (Fekel et al., 1987; Mekkaden, 1985; Pallavicini et al., 1981; Walter & Bowyer, 1981). Dynamo theory is a description of a mechanism that explains how stellar rotation, coupled with a convective and electrically conducting fluid, can generate and maintain a magnetic field in a star. The stellar magnetic field generates turbulence in the convection zone of the star which leads to formation of intense localized magnetized area on the stellar surface. The strong magnetic filed produces magnetic pressure which causes a decrement in the surface temperature of magnetized area compared to the rest of the stellar surface (Ossendrijver, 2003).

Our understanding of stellar activity has advanced during the last two decades thanks to the improvement in observational facilities and diagnostic observa-
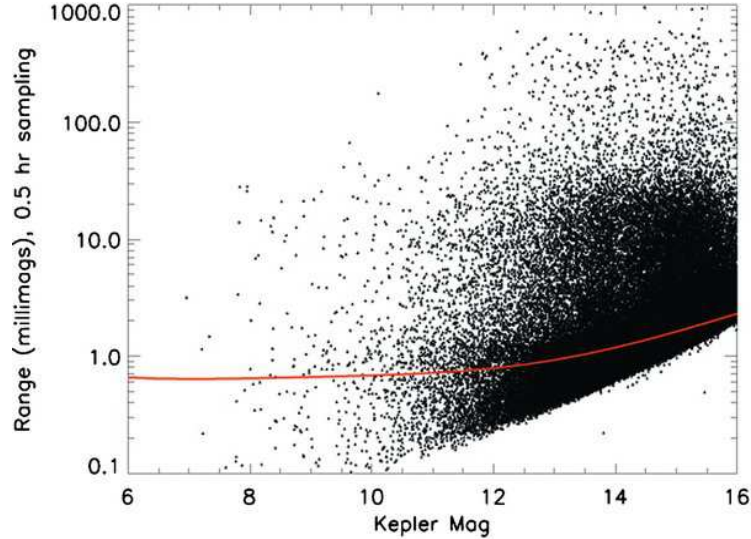
Figure 2.1: Comparison between the range of light curve modulation of Kepler targets and the Sun. The red line indicates the active Sun (Basri et al., 2010).

tional techniques, such as using long-term high-precision photometric observations (Borucki et al., 2010), high-resolution spectroscopy to perform Doppler imaging studies (Collier Cameron, 1992; Rice & Strassmeier, 2000; Vogt et al., 1987), observing molecular lines which provide crucial information on the spatially unresolved starspots (Berdyugina, 2002), performing spectropolarimetry to be able to achieve Zeeman-Doppler imaging that allows us to determine the distribution of magnetic field on the stellar surface(Donati et al., 1997).

2.1 Observational Tools for Studying Star spots

In this section, we briefly explain the observational tools which have been used to estimate the stellar spot's properties, crucial in our understanding about the nature of the stellar activity. We explain in more detail the most relevant observational tools (photometry and spectroscopy) to this thesis.
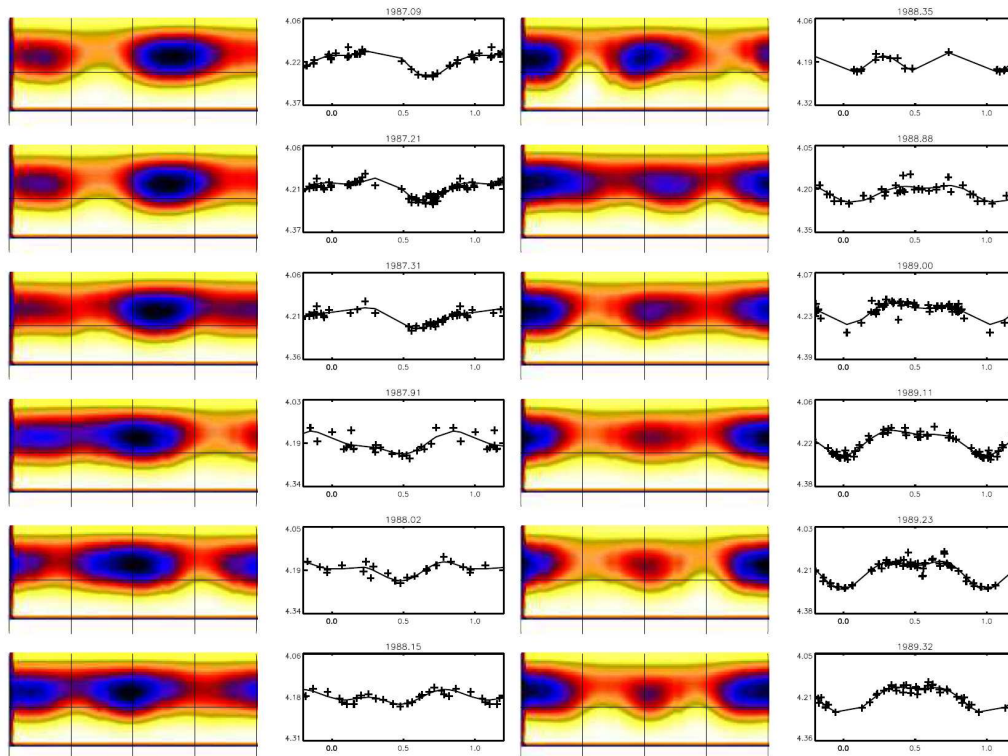
Figure 2.2: Long term photometric observation of RS CVn star σ Gem. The first and third column shows the spots positions and their filling factor by using inversion method on light curve (Berdyugina, 2005).

2.1.1 Long-term photometry

Following the discovery of variations in the brightness of star, which was interpreted as an indicator of the stellar activity (Kron, 1947), the long-term photometric observation has become the most common technique to monitor stellar activity. As an example, Figure 2.2 shows the long-term photometric observations on the σ Gem star, and the light-curve inversion technique used to determine the position and size of the stellar spots. Recently, exoplanet transit surveys also provided a large number of long-term photometric observations for the planet host star and also for the non-planet host stars. Space telescopes like *Kepler, CoRoT, MOST*, which are mostly dedicated to search for exoplanets, also provide long-term and more importantly, high-precision photometric observations which allow

us to put strong constraints on the stellar spot parameters.
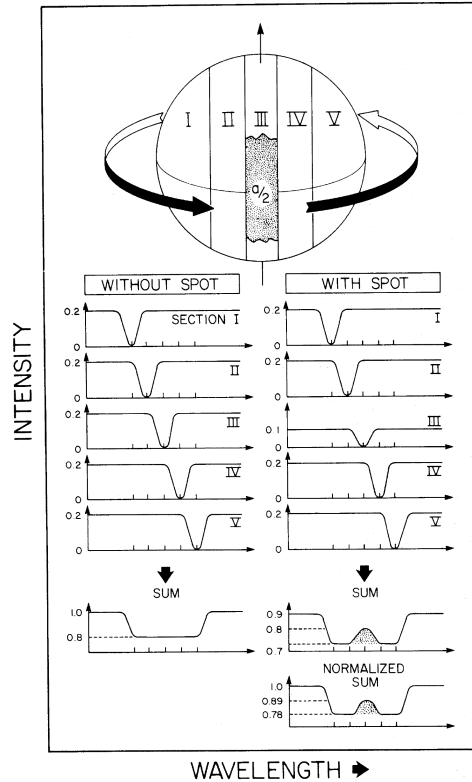
Figure 2.3: Schematic illustration of the effect of stellar spot on the CCF (Vogt & Penrod, 1983).

2.1.2   Spectroscopy

A stellar spot on a rotating star causes anomaly in the rotationally-broadened CCF (mean line of absorption line in spectra) of star. This anomaly in CCF appears at a velocity shift from line center corresponding to the spot projected distance from the stellar rotation axis (Collier Cameron, 1992) (see e.g Figure 2.3). The anomaly in the CCF induces variations of the measured RV of the star. Thus, high-precision RV measurements of a star could allow to estimate the position, size, and temperature contrast of stellar spots. We note here that determining the spot's temperature and its filling factor are strongly degenerate, and hence

any increment or decrement in the temperature contrast will be compensated by an increment or decrement of the spot's size.

Nowadays the high-resolution spectrographs with high-sensitivity detectors and stabilized, such as HARPS at ESO 3.6 telescope, UVES at VLT, and HIRES at Keck, allow us to reach to the level of precision which is needed to precisely estimate on the stellar spot characterization through the inverse problem solving. Furthermore, simultaneously spectroscopy and photometry observations allow to break the degeneracy between the stellar spots temperature contrast and its size, and precisely determine their values (Strassmeier, 2009).

2.1.3 Other techniques

2.1.3.1 Polarimetry

The nonzero polarization is a important indicator of breaking of the symmetry of the source. One of the most important astrophysical phenomena which breaks the spatial symmetry of a star is the magnetic field. The polarimetric technique is based on observing polarized light of stars and then using the Stokes vector to estimate the configuration of stellar magnetic field structure (Stenflo, 2013). The polarimetric technique is the most direct method for studying the stellar spot magnetic field. However, due to limited instrumental capabilities performing the polarimertic observation on the stars is a challenging task. Since the polarimetric signals from stellar spots has small amplitude, they require large telescopes to reach the required signal-to-noise. There is a small number of spectropolarimeters available which mostly are low resolution such as HARPS at ESO 3.6 telescope and FORS1 at Very Large Telescope (VLT) (Appenzeller et al., 1998). In near future PEPSI (Potsdam Echelle Polarimetric and Spectroscopic Instrument) at the double 8 meter Large Binocular Telescope (LBT) will provide high-resolution polarimetric observation on the stellar spots (Strassmeier et al., 2004).

2.1.3.2 Interferometry

By combing the beam of light from several separate telescopes, we are able to obtain higher angular resolution images when compared to single-telescope observed image. Thus, inhomogeneities on stellar surfaces such as stellar spots can

be identified using this method. The angular resolution of an interferometer can be defined as

$$R = \frac{\lambda}{B} \tag{2.1}$$

where B is the baseline distance, λ is the wavelength at which observation is performed, and R is angular resolution in radians. As a result, in order to reach a higher angular resolution, long baseline distance and shorter wavelengths are required. For an active star, interfrometric observations can provide critical information on the stellar spot size and also on the stellar rotation axis with respect to the observer (Rousselet-Perraut et al., 2004; Wittkowski et al., 2002), which can be combined with the information obtained from the spectroscopic and photometric observations of the same spotted stars.

2.1.3.3 Microlensing

While a massive body passes in front background source, due to the gravitational microlensing effect (Einstein, 1936), it will cause an amplification in the light of background source. This amplification of stellar brightness allows us to explore inhomogeneities on the stellar surface, thus we able to measure stellar spot size and their temperature (Fields et al., 2003; Udalski et al., 1995). Since this method does not depend on the stellar rotation velocity or on the stellar magnetic field, it provides an opportunity for studying the surface of slow rotating stars, which are mostly excluded from analysis by the other methods.

2.1.3.4 Asteroseismology

The internal stellar structure can be affected by the stellar magnetic field, thus the mode frequencies can be increased due to the magnetic activity. For instance, the 11-yr Sun activity cycle causes a shift in low degree mode frequencies of the order of 10^{-4} (Libbrecht & Woodard, 1990). Considering this fact, measuring the shifts in the frequencies of stars can be a powerful method to determine the stellar spot parameters, such as their magnetic field, latitude, and their size (Gizon,

2002; Lanza & Rodonò, 2002). Moreover, asteroseismology can provide important information on the stellar differential rotation for solar-type stars (Gizon & Solanki, 2004).

2.2 Star spot properties

In this Section, we briefly discuss the main properties of stellar spots, and also some stellar characteristics, such as the differential rotation, which were obtained through stellar spots studies.

2.2.1 Stellar spot's size

Estimating accurately the stellar spot's size is at the root of an active debate because it strongly depends on both the observational techniques and on the assumptions on the star. The best estimation on the stellar spot's size comes from the sunspot observations. Solar observations revealed that sunspot size varies over a large range. The largest sunspot which have been observed has filling factor of $f = 1\%$, which can be translated to diameters of 60000 km (Solanki, 2003). The filling factor is defined as

$$f = \frac{A_{spot}}{A_{1/2*}} = \left(\frac{R_{spot}}{R_*}\right)^2.$$
(2.2)

where A_{spot} is the area of the stellar spot, $A_{1/2*}$ is the area of the visible stellar disk, R_{spot} stellar spot radius, and R_* is the stellar radius.

The smallest sunspots have a size around 1500 km in diameter, which corresponds to filling factor of 0.001%(Bray & Loughhead, 1964; Meunier et al., 2010). Figure 2.4 shows the Sunspot size measurement during a solar cycle (since May 1996 to October 2007) by using SOHO observations (Meunier et al., 2010).

Bogdan et al. (1988), by performing extensive observations recorded at Mt Wilson between 1921 and 1982, concluded that the number of smaller sunspots are much higher that the large ones. They also found that the size distribution of sunspot can be well described by a log-normal function as
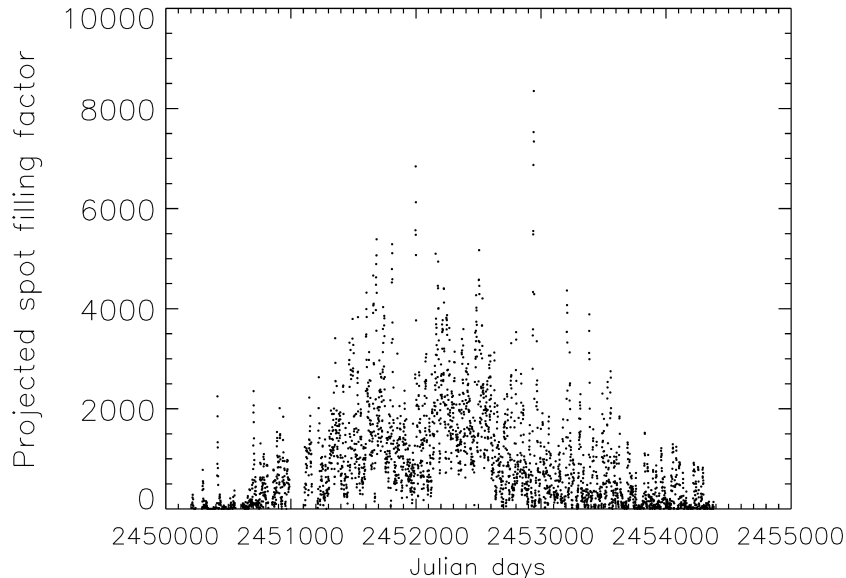
Figure 2.4: Sunspot filling factor in the unit of ppm of the solar disk area versus the time during one solar cycle (Meunier et al., 2010).

$$\frac{dN}{dA} = \left(\frac{dN}{dA}\right)_m \text{Exp}\left[-\frac{(lnA - ln\langle A\rangle)}{2ln\sigma_A}\right], \tag{2.3}$$

where $\left(\frac{dN}{dA}\right)_m = 9.4$ is the maximum that the distribution will reach, $\sigma_A = 4$ is the width of the log-normal distribution, and $\langle A\rangle = 0.55$ is the mean sunspot area (in units of $10^{-6}A_{\frac{1}{2}\odot}$) (Bogdan et al., 1988). The log-normal fit to the data is shown in Figure 2.5 (Solanki, 2003).

The largest photometric brightness variation ever observed, attributed to stellar spot, was obtained for two RS CVn-type stars HD12545 and II Peg (RS CVn stars are a class of close detached binaries where the primary is more massive being a G-K giant and the secondary is a G-M dwarf). The observed light-curve variation amplitude $\Delta V \simeq 0.63 mag$ on those two stars can be interpreted as the presence of the cool stellar spots which cover $\sim 40\%$ of the stellar disk as shown in Figure 2.6 (Strassmeier, 1999; Tas & Evren, 2000). The huge stellar spots with large filling factors on HD12545 and II Peg were also confirmed later by
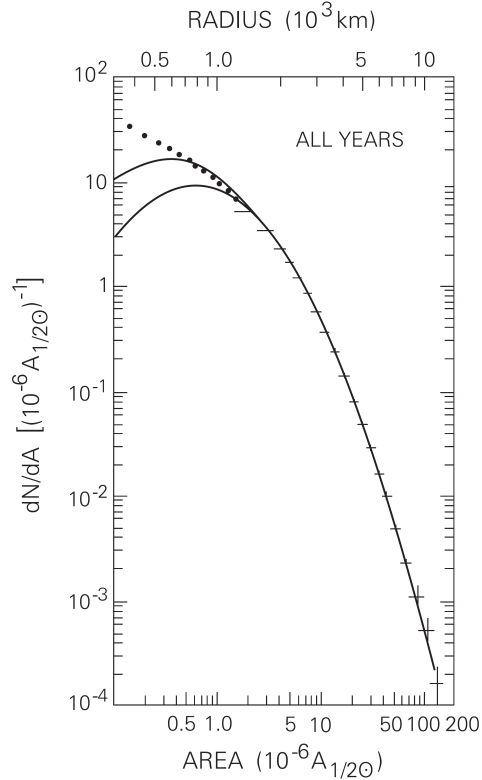
Figure 2.5: Sunspot's size distribution as function of sunspot filling factor (Solanki, 2003).

the Doppler imaging and modeling the observed molecular bands in the stellar spectra (O'Neal et al., 1996, 1998; Strassmeier, 1999).

We want to note here that the stellar spot size and its temperature are mathematically strongly correlated, thus measuring them is a degenerate problem (Poe & Eaton, 1985).

2.2.2 Stellar spot's temperature

Sunspots are composed of an inner region, called "umbra", much cooler and darker than outer region, called "penumbra". Solar observations showed that the sunspot umbra temperature is 1000- 1900 K cooler than the quiet Sun photosphere, and Sunspot penumbra is 250- 400 K cooler (Solanki, 2003).
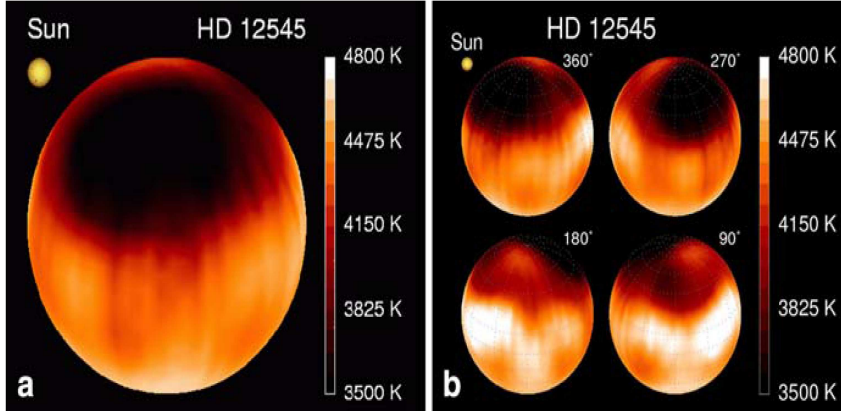
Figure 2.6: a: The huge stellar spot on the HD12545 obtained through the Doppler imaging technique. For comparison, the Sun surface temperature map while harbors the largest ever sunspot was plotted on the left side. b: The same as the left image but for different rotational phases (Strassmeier, 1999).

Several techniques have been used to measure the temperature of the stellar spots, namely, simultaneously modeling of brightness and color variations (Poe & Eaton, 1985), Doppler imaging (Collier Cameron, 1992), modeling of molecular bands (O'Neal et al., 2004), and line-depth ratios Gray & Johanson (1991).

The temperature measurements for other stars revealed that there is a strong correlation between stellar spot temperature and stellar photosphere temperature (Berdyugina, 2005), shown in the Figure 2.7. This result indicates that the temperature difference between the stellar spots and the stellar photosphere varies from 2000 K for the G-stars to 200 K for M-stars.

2.2.3 Stellar spot's magnetic field

Directly measuring the magnetic filed on the surface of star and also inside the stellar spot is a challenging task. The most common methods to measure the
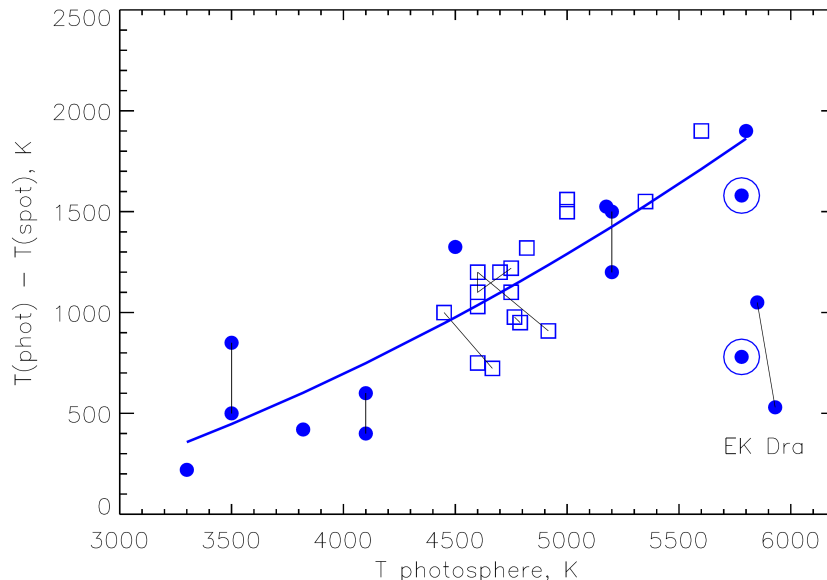
Figure 2.7: The difference between the temperature of stellar spot and stellar photosphere temperature as function of the stellar photosphere temperature for the sample of active stars. Dots in circles show sunspot umbra and penumbra (Berdyugina, 2005).

magnetic field on cool stars and their stellar spot is the Zeeman broadening technique (Robinson, 1980; Saar, 1988; Valenti & Johns-Krull, 2001). This technique is based on accurately measuring the Zeeman splitting on the stellar spectral lines due to the stellar magnetic field (detecting the Zeeman splitting, which is larger than the line width in the absence of the magnetic field). The Zeeman splitting can be written as

$$\Delta\lambda_{Zeeman} \propto \lambda^2 g_{eff} B. \tag{2.4}$$

where B is the magnetic field strength, λ is the wavelength, and g_{eff} is the Landé factor. In order to improve the efficiency of this method, the observations have to be done at long wavelengths, such as in the infrared(IR) or near-infrared(NIR), and line with large g_{eff} values, in order for the splitting to be detectable.

The sunspot's magnetic field measurements obtained a large range of values from 700- 1000 G in penumbra of sunspot to 1800- 3700 G inside the umbra of

sunspot (Livingston, 2002).

Stellar spot's magnetic field measurements indicated a trend for stellar spots magnetic filed both as a function of the stellar photosphere temperature and as a function of the stellar spot filling factor, shown in Figure 2.8 and 2.9, respectively. Figure 2.8 indicates that the cooler stars tend to have stronger magnetic field, and Figure 2.9 shows strong correlation between the stellar spot filling factor and the strength of the magnetic field (Berdyugina, 2005).
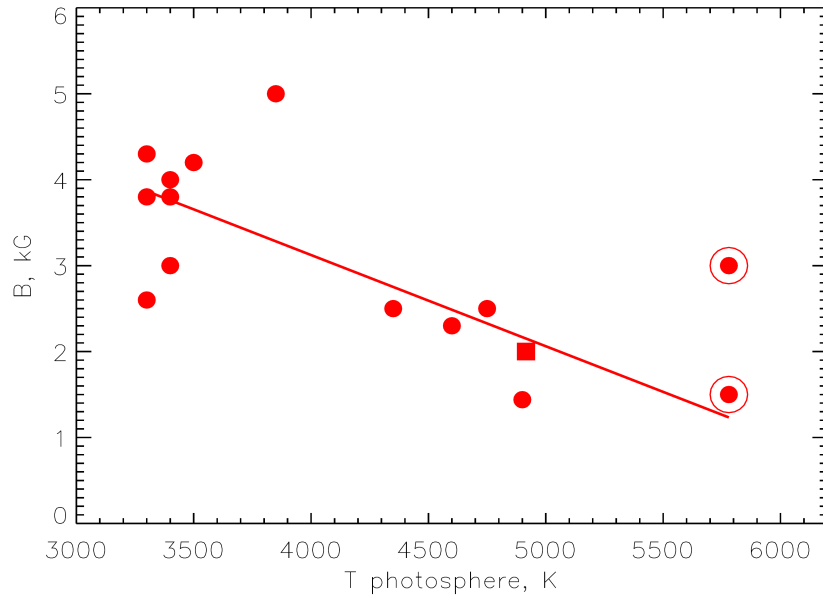
Figure 2.8: The behavior of the magnetic field for active stars as a function of the photosphere temperature. The red line indicates the linear fit to this behavior. Big circles show the sunspot umbra and penumbra (Berdyugina, 2005).

2.2.4 Stellar spot's life-time

Several studies showed that life-time of sunspots is strongly correlated to the size of the spot. The sunspot life-time can be formulated as

$$T_{life} = \frac{A}{W}, \tag{2.5}$$
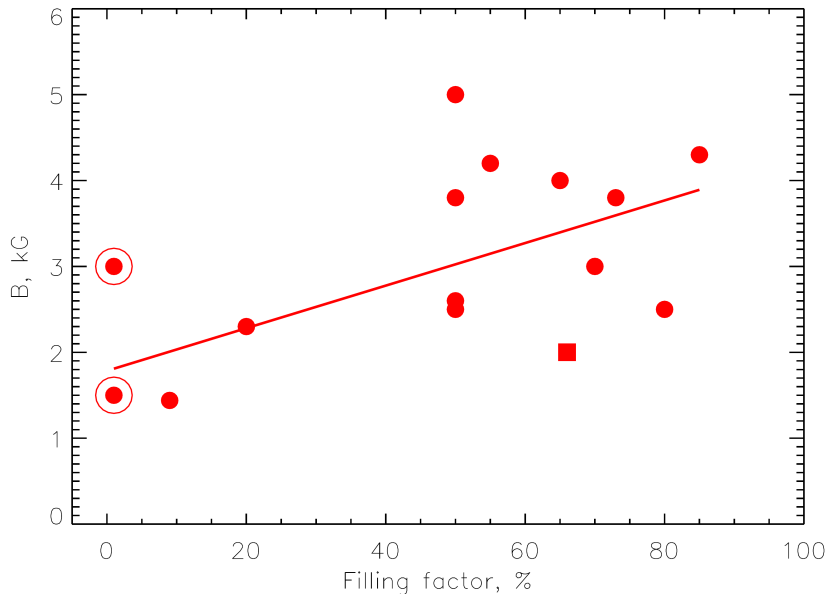
Figure 2.9: The behavior of the magnetic field for active stars as a function of the stellar spot filling factor. The red line indicates the linear fit to this behavior. Big circles show the sunspot umbra and penumbra (Berdyugina, 2005).

which is known as "Gnevyshev-Waldmeier rule", where A is the spot's area and $W = 10.89 \pm 0.18$ which is in units of $10^{-6} A_{\frac{1}{2}\odot} day^{-1}$ (Petrovay & van Driel-Gesztelyi, 1997; Waldmeier, 1955). Furthermore, recent long-term photometric observations have shown that the life time of stellar spots is proportional to their size (Hall & Henry, 1994), just like for the Sunspots.

2.2.5 Spot's latitude migration and the butterfly diagrams

Detailed and long-term observations of the position of sunspots indicates that these structures do not appear randomly on the surface of the Sun, but they are located on two different latitude bands around solar equator. At the beginning of each activity cycle of the Sun, the spots appears on two high latitude regions and then move toward the equator at the end of the 11 years cycle. This effect is known as the butterfly diagram, shown in Figure 2.10.

Measurements through the Doppler imaging and eclipse mapping of the eclips-
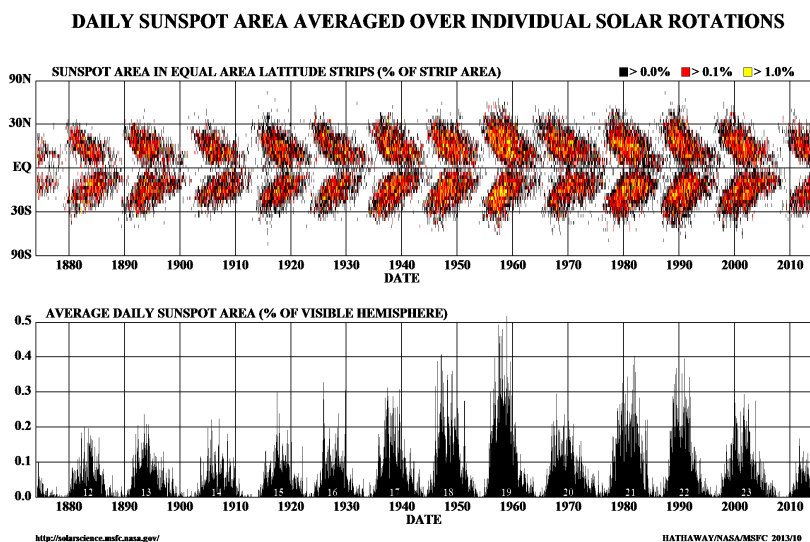
Figure 2.10: Top panel: The butterfly diagram which is the latitude of sunspots occurrence as a function of time. Bottom panel: Average sunspot area on the visible hemisphere of Sun as a function of time. Figure courtesy of D. Hathaway, http://science.nasa.gov/ssl/pad/solar/sunspots.htm.

ing binaries revealed that stellar spots are usually distributed over a wide range of latitudes, in clear opposition to what we see on the Sun (Berdyugina et al., 1999; Donati, 1999; Strassmeier, 1999). Since usually the time span for the Doppler imaging is short, it cannot be used either to detect the latitude variations of stellar spots or to recover the stellar spot butterfly diagram. However, long-term Doppler imaging on specific targets (such as HR1099) has been done, and the results showed that the stellar spots are located on the low latitude band and they change their latitude and migrate toward the pole on a scale of 16 years activity cycle (Berdyugina & Henry, 2007; Vogt et al., 1999), in contradiction to what is observed on the Sun. Further evidence for this pole-ward stellar spot migration was provided by Strassmeier & Bartus (2000) for the same star.

40

2.2.6 Stellar differential rotation

The Sun's differential rotation was discovered by Christoph Scheiner in 1630 by monitoring the relative motion of sunspots. Differential rotation is believed to be caused by the convection zone of the Sun, and can be described by

$$\Omega = \Omega_0 - \Delta\Omega \sin^2 \psi, \tag{2.6}$$

where ψ is the heliographic latitude, Ω_0 denotes the rotation velocity at the equator, and Ω is the difference between the rotation velocity at the pole and the equator (see Figure 2.11).
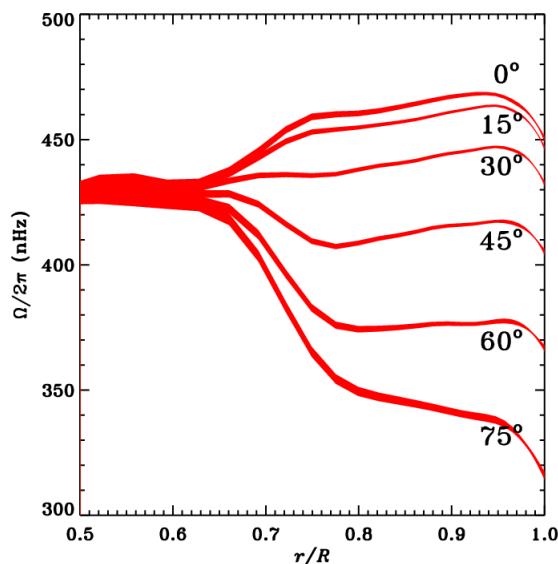
Figure 2.11: The rotational rates of the Sun as a function of radius for different latitudes. Image courtesy NSF's National Solar Observatory.

In order to explore the differential rotation behavior on other stars several techniques have been used, such as Fourier analysis of the long-term photometric observations (Hall, 1991b; Lanza et al., 1993), cross-correlation of the successive stellar Doppler images (Donati & Collier Cameron, 1997), direct star-spot tracking (Collier Cameron et al., 2002), Fourier transformed line profiles (Reiners & Schmitt, 2002), by using asteroseismology (Gizon & Solanki, 2004). For instance,

long-term photometric monitoring of stellar spots revealed the presence of differential rotation on the other stars (Hall, 1991a; Henry et al., 1995; Messina & Guinan, 2003).

In conclusion, recent surveys have suggested that most stars in our Galaxy may have higher activity level than that of the Sun. Accessing new observational facilities allows to probe in details the activity features on the stellar surface, and also be able to determine precisely the characteristics of them. Figuring out the behavior of stellar activity features on the stellar surface will play a key role in our understating about the Dynamo mechanism in other stars, and also will be crucial in distinguishing the signal of exoplanets orbiting those stars and the signal generated by the stellar activity feature. Stellar activity might also cause difficulties in accurately characterizing the detected exoplanets, so having insight about their properties will be significantly helpful.

Chapter 3

Barycenter method

Determining the variations in the transit timings requires precise measurements of the mid-transits time. To determine it, is necessary to develop a theoretical light-curve that reproduces in the best possible way the observational measurements of the flux of a star. When studying transiting planets, many authors use the analytical formulation developed by Mandel & Agol (2002) for this purpose. In this method, the synthetic light-curve of a star is produced using an analytical formula that contains several parameters, namely the coefficients of the star's limb darkening, the ratio of the radius of the planet to that of the star, the semimajor axis of the planet (or its orbital period), and the planet's orbital inclination. To measure the individual mid-transit time, it is customary to fix most parameters to their known value, except the mid-transit time, transit depth, and transit duration.

As a result, the measurement of the time of each mid-transit is particularly vulnerable to systematic errors. In other words, any wrong estimation of the value of any of the above-mentioned parameters (which may be obtained when observing the system for longer times) will change the model of the light-curve and result in different values of the times of mid-transits. Subsequently, the values of the TTVs obtained in these systems will also change.

Considering this issue, we proposed a model-independent methodology, which was first used by Szabó et al. (2006) in the field of the eclipsing binary star timing, to calculate the time of mid-transit of the exoplanet transits. We term

this technique the *barycenter* method because it calculates the mid-transit times by using the definition of barycenter of the transit light-curve. This method is based on a central assumption made also by Mandel & Agol (2002) namely symmetry of the transit light-curve.

In my first scientific paper during my PhD , which was entitled "Transit-timing measurements with the model-independent barycenter method: application to the LHS 6343 system", we presented the barycenter method and also its tests and comparison its results to that of other methods. Furthermore, we applied the barycenter method to one specific case "LHS 6343", which was observed by the *Kepler* Space Telescope, and we showed that the transiting brown dwarf around the LHS 6343A star shows a low-amplitude TTV signal. Furthermore we conclude that this TTV signal points to the possibility that a object with a mass larger than 1 M_{Jup} cannot exist around LHS 6343 A.

Astronomy & Astrophysics

Transit-timing measurements with the model-independent barycenter method: application to the LHS 6343 system[*]

M. Oshagh[1,2], G. Boué[1], N. Haghighipour[3], M. Montalto[1], P. Figueira[1], and N. C. Santos[1,2]

[1] Centro de Astrofísica, Universidade do Porto, Rua das Estrelas, 4150-762 Porto, Portugal
e-mail: moshagh@astro.up.pt
[2] Departamento de Física e Astronomia, Faculdade de Ciências, Universidade do Porto, Rua do Campo Alegre, 4169-007 Porto, Portugal
[3] Institute for Astronomy and NASA Astrobiology Institute, University of Hawaii-Manoa, 2680 Woodlawn Drive, Honolulu, HI 96822, USA

ABSTRACT

We present a model-independent technique for calculating the time of mid-transits. This technique, named "barycenter method", uses the light-curve's symmetry to determine the transit timing by calculating the transit light-curve barycenter. Unlike the other methods of calculating mid-transit timing, this technique does not depend on the parameters of the system and central star. We demonstrate the capabilities of the barycenter method by applying this technique to some known transiting systems including several *Kepler* confirmed planets. Results indicate that for complete and symmetric transit lightcurves, the barycenter method achieves the same precision as other techniques, but with fewer assumptions and much faster. Among the transiting systems studied with the barycenter method, we focus in particular on LHS 6343C, a brown dwarf that transits a member of an M+M binary system, LHS 6343AB. We present the results of our analysis, which can be used to set an upper limit on the period and mass of a possible second small perturber.

Key words. planetary systems – methods: data analysis

1. Introduction

The success of the transit-timing variation (TTV) method in characterizing planets around the stars Kepler 9 (Holman et al. 2010) and Kepler 11 (Lissauer et al. 2011) and in detecting a planet around star Kepler 19 (Ballard et al. 2011) strongly suggests that TTV method has come of age and is now among the main mechanisms for detecting extrasolar planets. This method, which is based on modeling the variations that appear in the times of the transits of a planet due to the perturbations of other objects, has been shown by many authors to be capable of detecting small Earth-sized planets, moons of giant planets, and stellar companions around variety of stars (Miralda-Escudé 2002; Holman & Murray 2005; Agol et al. 2005; Kipping 2009; Montalto 2010; Schwarz et al. 2011; Haghighipour & Kirste 2011).

Because the interaction between the transiting planet and the perturbing body(ies) is gravitational if there are no magnetic fields, the amplitude of the TTV strongly depends on the masses of these objects and their orbital architecture. As shown by Holman & Murray (2005), Agol et al. (2005), and Haghighipour & Kirste (2011), the amplitude of a TTV signal varies with the mass and distance of the perturbing body. The latter has been used in several null detections to place an upper limit on the mass and orbital parameters of a hypothetical perturber (Bean 2009; Csizmadia et al. 2010; Adams et al. 2010, 2011; Maciejewski et al. 2010, 2011a,b).

The TTV amplitude is strongly amplified when the transiting and perturbing planets are in a mean-motion resonance.

For instance, as shown by Agol et al. (2005); Steffen et al. (2007); Agol & Steffen (2007); Haghighipour et al. (2009); Haghighipour & Kirste (2011), a planet as small as Earth can produce large and detectable TTVs on a transiting Jupiter-like body in or near a resonance. This characteristic of resonant transiting systems makes the TTV method a powerful technique for detecting low-mass planets.

The fact that different orbital configurations of the transiting and perturbing bodies can produce similar TTVs has made the inference of the mass and orbital elements of the perturber from the measurements of the transiting planet's TTVs a very complicated task. Several attempts have been made to overcome these difficulties (Nesvorný & Morbidelli 2008; Nesvorný 2009; Nesvorný & Beaugé 2010; Meschiari & Laughlin 2010). However, the complications still exist, particularly when the system is in or near a resonance. As shown by García-Melendo & López-Morales (2011), continuous observations by *Kepler* and CoRoT are expected to resolve some of these difficulties.

Determining variations in transit timing requires precise measurements of the times of mid-transits. To compute a mid-transit time, it is necessary to develop a theoretical light-curve that best models the observational measurements of the intensity of the light of a star. When studying transiting planets, many authors use the analytical methodology developed by Mandel & Agol (2002) for this purpose. In this method, the light-curve of a star is calculated using an analytical formula that contains several parameters such as the coefficients of the star's limb darkening, the ratio of the radius of the planet to that of the star, the semimajor axis of the planet (or its orbital period), and the planet's orbital inclination. To measure the individual

---

[*] Table 1 is available in electronic form at http://www.aanda.org

mid-transit times, it is customary to hold all parameters (except mid-transit time) constant during the fitting procedure. As a result, the measurement of the time of each mid-transit will be vulnerable to systematic errors. In other words, any modification to the values of any of the above-mentioned parameters (which may be obtained when observing the system for longer times) will change the fitted light-curve and result in different values of the times of mid-transits. Subsequently, the values of the TTVs obtained in these systems will also change.

We used a model-independent methodology, first introduced by Szabó et al. (2006), to calculate the time of mid-transit. We call this technique the *barycenter method* because it calculates the mid-transit times by using the definition of the transit light-curve barycenter and its symmetry. We describe this methodology in Sect. 2 and present examples of its application to some of the already known transiting systems in Sect. 3. In Sect. 4, we apply this technique to the system of LHS 6343 and explain its implications for the transit timing of the system. We analyze the derived O–C diagram of LHS 6343 in Sect. 5, and in Sect. 6 we conclude this study by summarizing our analysis and reviewing the results.

2. Barycenter method

As mentioned earlier, to determine the variations in the transit timing of a planet, a precise calculation of the times of its mid-transits is required. The mid-transit times are determined by fitting an analytically obtained light-curve to the observational data, and calculating the time of the mid-point of each individual transit on the latter curve. When the transiting body is planetary, the synthetic light-curve is usually produced using the algorithm developed by Mandel & Agol (2002). In the majority of cases, the times of mid-transits are calculated by keeping all other parameters (e.g. stellar radius, planet radius, orbital period, and two limb darkening coefficients) constant during the fitting procedure. This is particularly important when the number of points inside a transit is small (e.g., 6–9 points). In such cases, fitting the observed data can lead to imprecise results.

Another technique for calculating times of mid-transits is the "trapezoid method" (Alonso et al. 2009). In this method, a trapezoid function is fitted to the observational data and the best light-curve is determined by varying the depth, duration, and shape of the trapezoid. The time of mid-transit is then calculated by identifying the mid-point of each transit on the best-fit trapezoidal curve.

In systems where the transiting/eclipsing body is a stellar companion, the time of each mid-transit/eclipse is calculated using the methodology developed by Kwee & van Woerden (1956). This method has been used by Deeg et al. (2000, 2008) to calculate eclipse timing variations of eclipsing binaries caused by a circumbinary planet, and is based on the assumption that in an unperturbed system, the light-curve of the transited/eclipsed star is symmetric. In this method, the mid-point of an eclipsing light-curve is determined by folding the light-curve around one point of the transit, and calculating the differences between the points on the two parts of the folded light-curve. The point where these differences become minimum corresponds to the point of mid-transit.

The method developed by Kwee & van Woerden (1956) has the advantage that unlike the method of Mandel & Agol (2002), it does not depend on the parameters of the central star. However, for the measurements of the mid-transit times to be accurate, this method requires very many points, which are obtained through the interpolation of points from the results of observation. As a
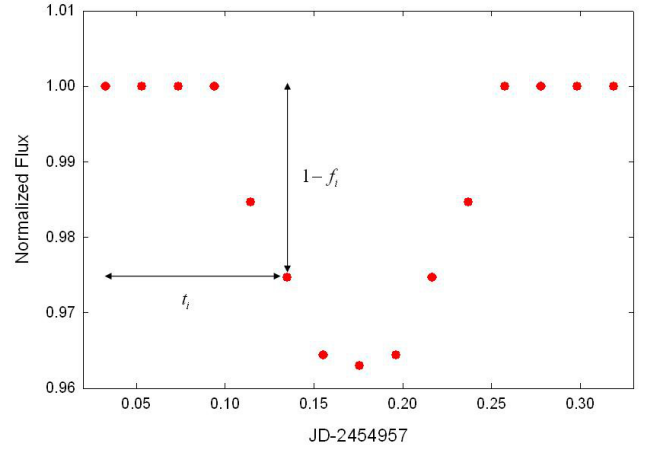
Fig. 1. Schematic view of the barycenter method.

result, in transiting systems with few data points (e.g., the transiting systems identified in the long cadence of Q0 to Q2 data sets from *Kepler*), using this method is not practical.

In this section, we explain a methodology that employs similar idea as the method by Kwee & van Woerden (1956) (i.e., using light-curve's symmetry) and as such is independent of the system's stellar parameters. This method was first presented by Szabó et al. (2006) and later used by Simon et al. (2007) and Kipping (2011) to study the possibility of the detection of exomoons. It calculates the exact moment of mid-transit using the definition of the transit light-curve barycenter. We call this methodology the "barycenter method". Unlike the method by Kwee & van Woerden (1956), the barycenter method can be applied to transit planetary systems with few data points.

To define the transit light-curve barycenter, we use a normalized graph of the flux of the central star. As shown in Fig. 1, the flux of the star outside the transit is detrended and normalized to 1. For a point i with a flux f_i inside the transit, the corresponding value of the light-loss of the system is equal to $1 - f_i$. Similar to the barycenter point of a number of massive objects, we now define a barycenter for the points on the graph of the normalized flux. In this definition, the time of mid-transit will then be given by

$$T = \frac{\sum\limits_{i=1}^{n} t_i(1 - f_i)}{\sum\limits_{i=1}^{n}(1 - f_i)}. \tag{1}$$

In Eq. (1), n represents the number (rank) of the data points in the observation, and t_i is Julian Day (JD) of the observation point i. To obtain more precise results, we only consider the points that are inside the transit light-curve. A point is inside the transit if its light-loss $(1 - f_i)$ is higher than the standard deviation of flux outside the transit.

3. Application of the barycenter method to known transiting systems

3.1. HAT-P-7b

To test the capability of the barycenter method and the validity of its results, we used this technique to calculate the times of mid-transits in several known transiting planetary systems. In addition to the timing, transits may also show variations in their

Fig. 2. Comparison between the results of mid-transit of HAT-P-7b first transit, obtained by the Mandel & Agol method (black circle), the trapezoid method (red square) and the barycenter method (blue triangle).

Fig. 3. Differences between the values of mid-transit timing obtained by the barycenter method and the Mandel & Agol method for Kepler-1b to Kepler-4b (Holman et al. 2010; Ford et al. 2011).

durations and depths. However, our focus is only on the variations in the times of mid-transits. Our first case was the transiting planet HAT-P-7b (Kepler-2b). HAT-P-7 was observed in short and long cadences as a calibration target for *Kepler*. In the short cadence mode, the light-curve of HAT-P-7 consisted of approximately 355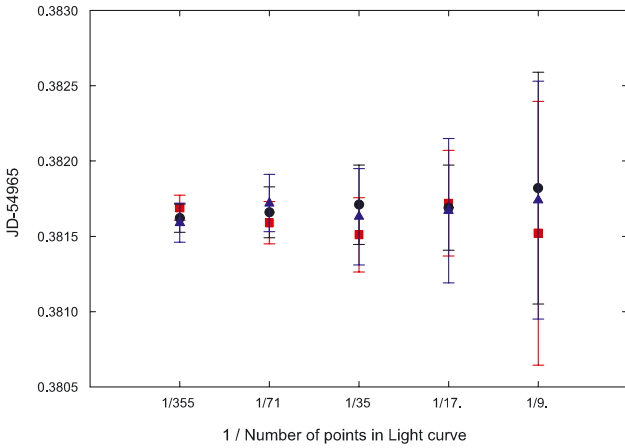 points in each transit. We used the results of the observations as reported in Q0 data set, and calculated the time of mid-transit for the first transit of this planet. Figure 2 shows the results (the first point from the left). The error bar on each point was determined using the bootstrap technique (Wall & Jenkins 2003). As shown here, the time of mid-transit obtained from the barycenter method is consistent with those obtained from the trapezoid method and the model by Mandel & Agol (2002).

To evaluate the sensitivity of each of these techniques to the number of points in a transit, we reduced the number of points in the light-curve by regular sampling, and calculated the time of mid-transit using all three methods. Results are shown in Fig. 2. As expected, the sizes of the error bars indicating the uncertainties at each point increase for fewer data points. However, as Fig. 2 shows, the times of mid-transits obtained by all three methods are close and agree with one another.

3.2. Kepler-1b to Kepler-9c

We also applied the barycenter method to the confirmed planets of the Kepler-1 to Kepler-9 systems. Table 1 shows the results and their corresponding uncertainties. The uncertainties were calculated using the equation

$$\sigma(T)^2 = \sum \left| \frac{\partial T}{\partial f_i} \right|^2 \sigma_i^2. \tag{2}$$

Table 1 also shows the values of the mid-transit times of these planets as reported by Holman et al. (2010) and Ford et al. (2011) using the model of Mandel & Agol (2002). As shown here, the results obtained from the barycenter method agree very well with the previously reported values.

Figures 3 and 4 show the differences between the values of mid-transit times obtained by the barycenter method and those reported by Holman et al. (2010) and Ford et al. (2011). The error bar at each point was calculated by taking the quadratic
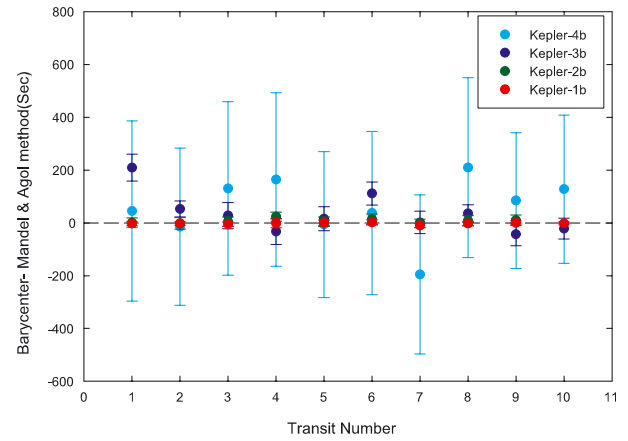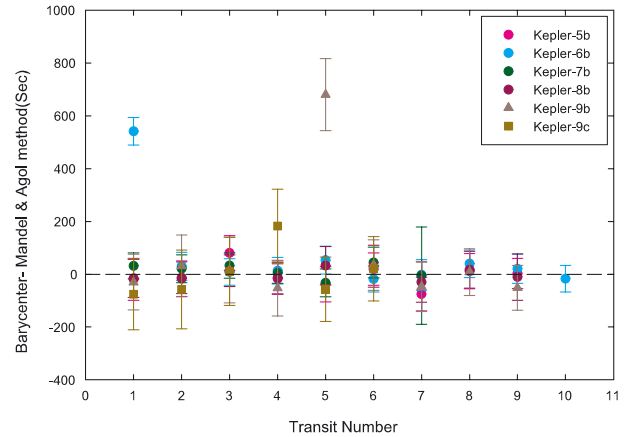
Fig. 4. Same as in Fig. 3 for Kepler-5b to Kepler-9c.

sum of the uncertainties shown in Table 1. Table 2 lists standard deviations of these differences and their average error bars. As can be seen from Fig. 3 and Table 2, Kepler-4b shows large error bars compared to those of other planets because of its shallow transits. This figure also shows that the standard deviation of Kepler-3b, as listed in Table 2, is larger than its average error, which can be attributed to the non-symmetric shapes of the first and sixth transits of this planet (see Fig. 5). These short-lived anomaly flux variations can be explained by different mechanisms such as the presence of active regions (dark spots) or a second transiting body (Rabus et al. 2009; Sanchis-Ojeda et al. 2011; Sanchis-Ojeda & Winn 2011; Silva-Valio 2008; Nutzman et al. 2011; Deming et al. 2011).

Since in both the barycenter method and the method of Mandel & Agol (2002) it is assumed that the light-curve is symmetric, these methods are sensitive to missing points in the observation of a transit. This can be seen from Table 2 for Kepler-6b and Kepler-9b. The standard deviations of these two planets are larger than their average errors, which could have been caused by a missing point in the observation of the first transit of Kepler-6b and fifth transit of Kepler-9b (Fig. 6). To illustrate this effect, we made an artificial light-curve for a transiting planet and calculated the time of its mid-transit using the

Table 2. Comparison of standard deviation of the difference between two methods and the average error bar obtained by quadratic sum.

Planet	Standard deviation (s)	Average error (s)
Kepler-1b	3.3	8.9
Kepler-2b	8.2	18.6
Kepler-3b	76.0	42.7
Kepler-4b	115.0	306.3
Kepler-5b	43.0	65.0
Kepler-6b	168.2	52.3
Kepler-7b	26.5	69.3
Kepler-8b	22.4	71.3
Kepler-9b	233.2	105.7
Kepler-9c	87.0	132.7
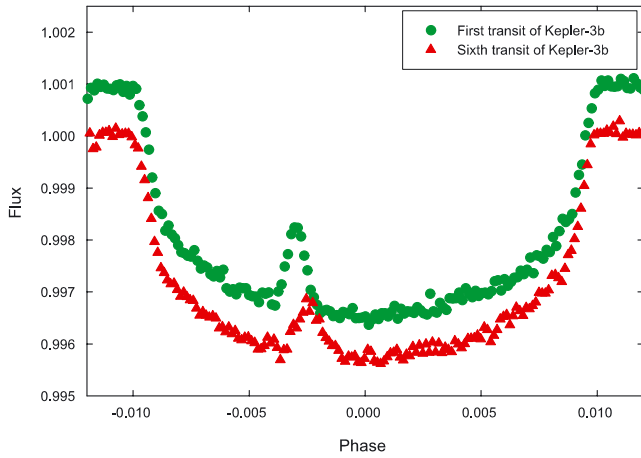
Fig. 5. Asymmetries in the first and sixth transits of Kepler-3b (maybe due to starspots).

Fig. 6. Asymmetries in the first transit of Kepler-6b and fifth transit of Kepler-9b, caused by missing point of observation.

Fig. 7. Deviations of mid-transit timing from the known values as calculated by Mandel & Agol, and the barycenter methods for a synthetic light curve with one missing point. The *x*-axis presents the rank of missing points in light curve.

Table 3. Parameters of the LHS 6343 system according to Johnson et al. (2011).

Parameter	Value
M_A (solar mass)	0.370 ± 0.009
M_B (solar mass)	0.30 ± 0.01
M_C (Jupiter mass)	62.7 ± 2.4
a_{AB} (AU)	20.130 ± 0.605
a_{AC} (AU)	0.0804 ± 0.0006
P_C (days)	12.71382 ± 0.00004

model of Mandel & Agol (2002). We then removed one point from the light-curve and calculated the time of mid-transit using both the barycenter method and the method of Mandel & Agol (2002). As shown in Fig. 7, and in agreement with Csizmadia et al. (2010), the results obtained by both methods show large deviations when the missing point was in ingress or egress (deviation ∼500 s). On the other hand, both methods become less sensitive when the missing point is close to the bottom of the light curve. This experiment suggested that both the barycenter and the Mandel & Agol methods require the full coverage of observation data in transit, and a missing point in the observation data may cause a large offset in the results.

We also examined the applicability of the barycenter method to the long integration time of *Kepler*'s long cadence observations (29.42 min) (Kipping 2010). Using the algorithm by Mandel & Agol (2002), we generated an artificial light-curve with bins of long integration times (we chose a point every 6 s and used the mean of 270 of those points as the observed flux). We changed the beginning time of each binning and studied the variations of mid-transit times as determined by the barycenter method. Results point to a deviation of no more than 4 s for the mid-transit times.

4. The LHS 6343 system and its transit timing

LHS 6343 is a close, M+M binary system with a separation of ∼20 AU. The primary of this binary, LHS 6343 A (KIC 10002261, RA = $19^h10^m14.33^s$, Dec = $46°57'25.50''$), has a

mass of 0.37 $M_\odot$ and the mass of the secondary, LHS 6343 B, is approximately 0.30 $M_\odot$ (see Table 3). The publicly available Q0 and Q1 data sets from *Kepler* revealed four deep transits in the light-curve of this system. By analyzing these data, Johnson et al. (2011) showed that these transits are produced by a third object, LHS 6343 C, which orbits LHS 6343 A every 12.71 days. As determined by these authors, LHS 6343 C is a brown dwarf

Table 4. Transit timing of LHS 6343, as measured by the barycenter method and O–C values in days were calculated according to the new linear ephemeris.

Transit number	T_0 (days) (The barycenter Method)	T_0 (days) (Calculated)	O–C (Sec) (TTV)
1	54957.216473 ± 0.000133	54957.216535	–5.4 ± 11.5
2	54969.930434 ± 0.000154	54969.930354	6.9 ± 13.3
4	54995.358025 ± 0.000135	54995.357992	2.9 ± 11.7
6	55020.785698 ± 0.000120	55020.785630	5.9 ± 10.4
7	55033.499199 ± 0.000147	55033.499449	–21.6 ± 12.7
9	55058.927144 ± 0.000136	55058.927087	4.9 ± 11.8
10	55071.641056 ± 0.000173	55071.640906	13.0 ± 15.0
11	55084.354626 ± 0.000156	55084.354725	–8.6 ± 13.5
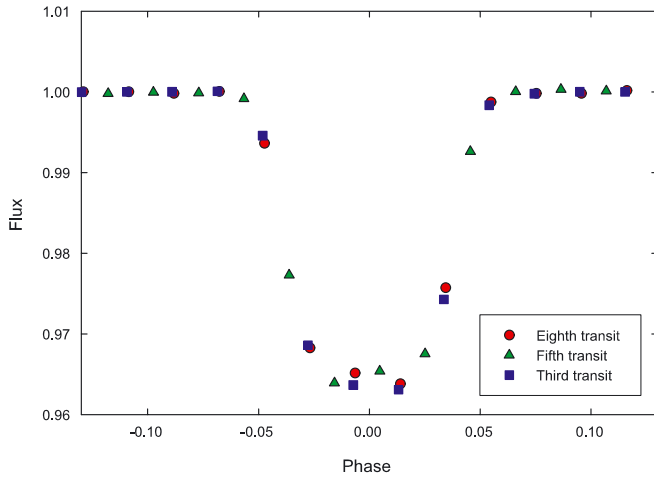
Fig. 8. Strange non-symmetric shape of third (blue square), fifth (green triangle), and eighth (red circle) transit of LHS 6343.

Fig. 9. Residual of the best fit of the Mandel & Agol method to all transits of LHS 6343 (just inside transit).

with a mass of ~63 M_J and is located at a distance 0.08 AU from LHS 6343 A.

In preparation for applying the barycenter method to the light-curve of LHS 6343, we analyzed each transit of this system separately. Our initial analysis of the light-curve of LHS 6343 at the time of the release of Q0 and Q1 data sets pointed to a non-symmetric transit (transit number 3) among the initial four transits of this system. We recall that the barycenter method is based on the symmetry of the shape of a transit. The release of the Q2 data set provided us with seven more transits, of which our analysis identified transits number 5 and 8 as asymmetric. Figure 8 shows these non-symmetric transits. We note that these anomalies may be caused by starspots. To better portray the anomalies in the shapes of these transits, we used Mandel & Agol's methodology and obtained the best fit to all 11 transits of this system. Figure 9 shows the residuals of each single transit with respect to this best fit. As shown here, the residuals of the third, fifth, and eighth transits are larger than $1 - \sigma$ (closer to $2 - \sigma$) because of their anomalies inside their transits.

As mentioned for Kepler-9b, developing a model to explain these anomalies would require many observational points inside each transit and will depend on several parameters such as the size and latitude of starspots, their lifetimes, the rotational period of the star, and the orientation of the rotation axis of the star relative to the orbit of transiting brown dwarf. Although an interesting project on its own, developing such a model is beyond the scope of our study. Also, given that with the currently available

data, the number of points in each transit is limited to only 5 or 6, such a model may not even be entirely realistic. Therefore, because the basis of the barycenter method is on the symmetry of a transit, and also to restrain false positive TTVs, we decided to exclude the most asymmetric transits (i.e., transits 3, 5, and 8) from our analysis. Table 4 lists the times of the mid-transits of the remaining eight transits of the system calculated using the barycenter method. To estimate the corresponding errors of each mid-transit time, we used the bootstrap method (Wall & Jenkins 2003) and considered the standard deviation inside each transit as the initial uncertainty. Note that the standard deviation inside a transit may be larger than outside due to crossing over starspots. To check the validity of our error estimation, we also calculated the values of errors using Eq. (2) and the methodology used by Doyle & Deeg (2004). Our calculations showed that the values of the errors obtained from all three methods have the same order of magnitude.

To obtain the variations in the transit timing of the system, we applied a linear fit to the eight mid-transit times in Table 4. Results suggested a period of $P = 12.713815$ days, corresponding to a semimajor axis of 0.076–0.080 AU for the transiting body. These results closely agree with the results reported by Johnson et al. (2011).

Given that LHS 6343 is a binary system and the transiting object (LHS 6343 C) orbits the primary star, the three-body system of LHS 6343 AC-B forms a hierarchical three-body system. We examined the stability of LHS 6343 C in this system by numerically integrating its orbit. Results indicated that this

Fig. 10. Diagram of the transit-timing variations of LHS 6343.

Fig. 11. Values of LTTs of LHS 6343 for different values of the binary semimajor axis.

Fig. 12. Values of LTTs of LHS 6343 for different values of the binary eccentricity.

object is stable for long times. We refer the reader to a recent article by Borkovits et al. (2011) and references therein, where the authors have presented a detailed analysis of the dynamics and transit/eclipse timing variations of hierarchical tripe systems.

5. Analyzing the O–C diagram of LHS 6343

The times of mid-transits obtained from the barycenter method show small deviations from their linear fit. Figure 10 and the right column of Table 4 show these deviations and their corresponding uncertainties for each mid-transit time. In this section, we analyze these deviations from the linear fit of transit timings and discuss their implications for the possible existence of a second smaller object around the primary LHS 6343 A.

Because it is in a hierarchical tripe configuration, LHS 6343 C is continuously subject to the gravitational perturbation of the secondary star. These perturbations affect the orbit of this object and cause variations in the times of its transit (for a detailed analysis of TTVs in hierarchical tripe sy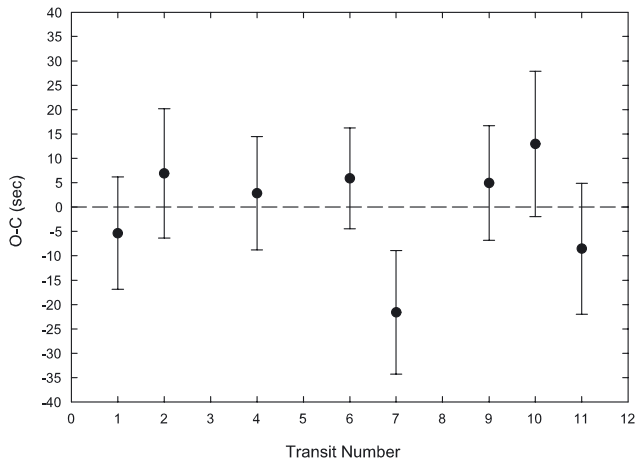stems we refer the reader to Borkovits et al. 2011). Given that the semimajor axis of the binary (∼20 AU) and its projected separation (19–21 AU) are much larger than the semimajor axis of LHS 6343 C, it would be important to determine to what degree the variations in the transit timing of this object have been caused by the binary's light-travel time (LTT) effect. To examine this possibility, we used the methodology presented by Montalto (2010) and calculated LTTs for different values of the semimajor axis and eccentricity of the binary. We changed the values of the projected separation of the binary using the distribution given by Duquennoy & Mayor (1991), and performed 10 000 LTT-calculations for randomly chosen values of the binary eccentricity between 0 and 0.9. In all our simulations, we considered the system to be coplanar. We identified the systems for which the value of LTT was between 1 s and 6 s. Figures 11 and 12 show the results for a timespan of three years (duration of *Kepler*'s primary mission). As shown here, systems with LTTs between 4.5 s and 5.5 s constitute the majority of the cases (we recall that the minimum reported value of TTV that can be detected by *Kepler* is ∼10 s, see Ford et al. 2011). Figure 13 shows the results of all our simulations for LTTs between 5 s and 6 s in more detail. As shown in this figure, the values of LTTs do not exceed 6 s, which implies that during the period spanned by the present public release of the *Kepler* observations data (∼144 days), the
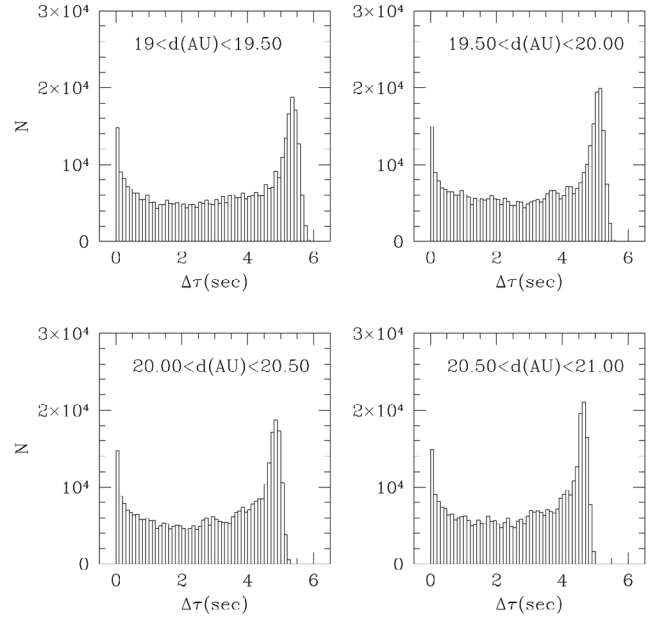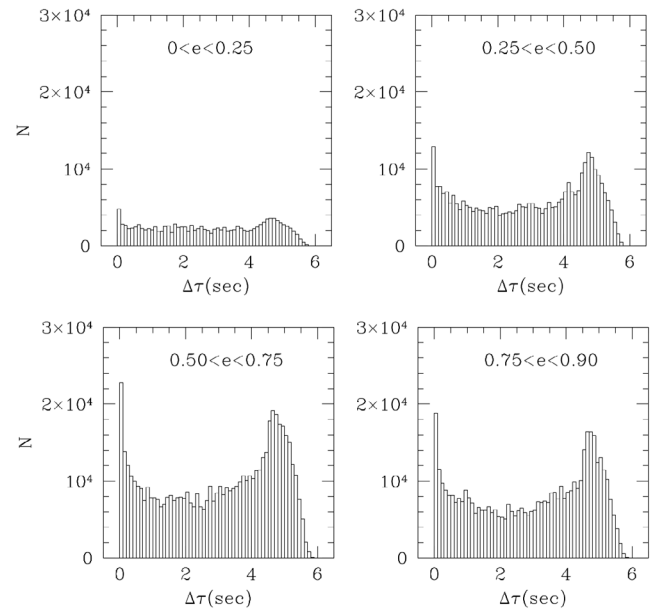
contribution of the binary LTT to the variations in the transit timing of LHS 6343 C is negligible.

The fact that the contribution of LTT to the O–C values, as listed in Table 4, is negligibly small implies that in modeling these deviations from the linear fit of transit timings, one can safely ignore the effect of the secondary star.

To examine whether these deviations could be caused by an additional body in the system, we considered the two-body system of LHS 6343 AC, and calculated the O–C values for different values of the mass, semimajor axis, and orbital eccentricity of a hypothetical perturber around the primary LHS 6343 A. To reduce the amount of calculations (which could be large because of the large size of the parameter-space), we limited our study to only circular and coplanar systems. Figure 14 shows the results
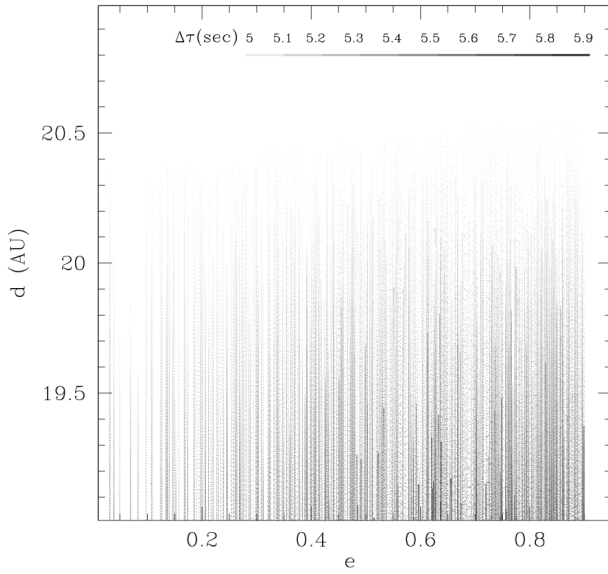
Fig. 13. Graph of LTTs between 5 s and 6 s for different values of the binary semimajor axis and eccentricity.

for different values of the initial angular position of the hypothetical third body. A comparison between these results and the values of the O–C in the right column of Table 4 suggests that a perturber with a mass ranging from 0.1 to 1 M_J may be able to produce these values when in an orbit with a period ranging from ~3.5 to 8P (where $P = 12.713815$ days is the orbital period of LHS 6343 C) around LHS 6343 A. To determine an upper limit for the mass of the perturber, we calculated the O–C values for different values of the mass and semimajor axis of this object, and compared the results with the values of O–C as shown in Fig. 10. Figure 15 shows the maximum values of the mass of the perturber for which the value of χ^2 between the O–C obtained from the model and those listed in Table 4 are lower than 3. As shown in this figure, the mass of the perturber cannot be larger than one Jupiter-mass.

6. Conclusion

We presented a technique called the barycenter method for calculating the time of the mid-transit in transit-timing studies. This method is based on the symmetry of the light-curve, and has the advantage that is independent of the parameters of the system. In other words, unlike other techniques for calculating the mid-transit timing, the results obtained from the barycenter method will not change by changing the assumption on the parameters of the central star. However, the fact that this method requires symmetry in the light-curve implies that when the transit curve is not perfectly symmetric (i.e., when observational points are missing, or because of starspots), large offsets may appear in the mid-transit timing measurements. The application of the barycenter method to several known transiting systems showed that the results obtained from this technique are comparable with those obtained from other methods. Our study indicates that for complete and symmetric transit lightcurves, the barycenter method achieves the same precision as in the model of Mandel & Agol (2002), but with fewer assumptions and much faster.

We used the barycenter method to calculate the times of mid-transits of the M+M binary star LHS 6343. Our results indicated
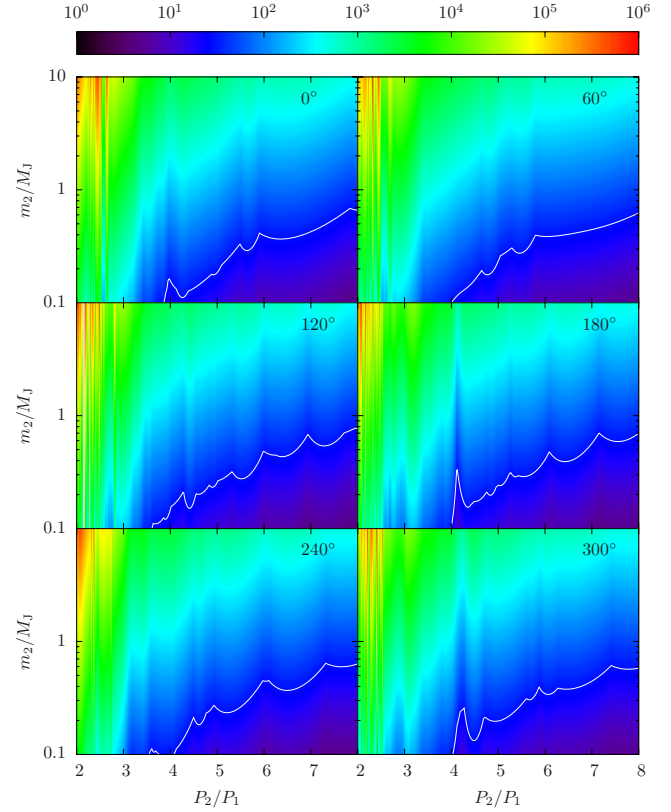
Fig. 14. Values of TTVs in the system of LHS 6343AC due to a hypothetical perturber. The system is assumed to be circular and coplanar. Each panel shows TTVs for a different value of the angular phase of the perturber. The units on the color scale are in seconds.
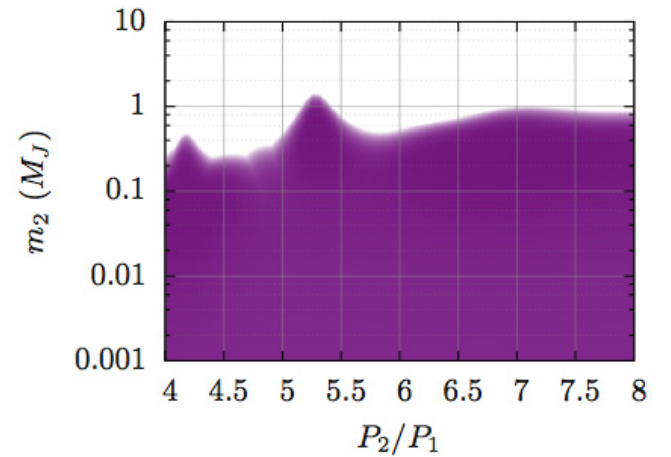
Fig. 15. Maximum mass of the perturber on circular orbit reproducing the TTVs as in Fig. 10, as a function of its orbital period.

that as suggested by Johnson et al. (2011), the primary of this system is host to a smaller object with a period of ~12.7 days. A study of the variations in the transit timing of this body (LHS 6343 C) points to the possibility that a small object with a mass no larger than 1 M_J may exist around LHS 6343 A, which can produce the O–C values lower than the upper values presented here. Whether such an object actually exists requires more transit data and more observations of this system.

References

Adams, E. R., López-Morales, M., Elliot, J. L., Seager, S., & Osip, D. J. 2010, ApJ, 714, 13

Adams, E. R., López-Morales, M., Elliot, J. L., Seager, S., & Osip, D. J. 2011, ApJ, 728, 125

Agol, E., & Steffen, J. H. 2007, MNRAS, 374, 941

Agol, E., Steffen, J., Sari, R., & Clarkson, W. 2005, MNRAS, 359, 567

Alonso, R., Alapini, A., Aigrain, S., et al. 2009, A&A, 506, 353

Ballard, S., Fabrycky, D., Fressin, F., et al. 2011, ApJ, 743, 200

Bean, J. L. 2009, A&A, 506, 369

Borkovits, T., Csizmadia, S., Forgács-Dajka, E., & Hegedüs, T. 2011, A&A, 528, A53

Csizmadia, S., Renner, S., Barge, P., et al. 2010, A&A, 510, A94

Deeg, H. J., Doyle, L. R., Kozhevnikov, V. P., et al. 2000, A&A, 358, L5

Deeg, H. J., Ocaña, B., Kozhevnikov, V. P., et al. 2008, A&A, 480, 563

Deming, D., Sada, P. V., Jackson, B., et al. 2011, ApJ, 740, 33

Doyle, L. R., & Deeg, H.-J. 2004, in Bioastronomy 2002: Life Among the Stars, ed. R. Norris, & F. Stootman, IAU Symp., 213, 80

Duquennoy, A., & Mayor, M. 1991, A&A, 248, 485

Ford, E. B., Rowe, J. F., Fabrycky, D. C., et al. 2011, ApJS, 197, 2

García-Melendo, E., & López-Morales, M. 2011, MNRAS, 417, L16

Haghighipour, N., Agol, E., Eastman, J. D., et al. 2009, astro2010: The Astronomy and Astrophysics Decadal Survey, 109

Haghighipour, N., & Kirste, S. 2011, Cel. Mech. Dyn. Astron., 111, 267

Holman, M. J., & Murray, N. W. 2005, Science, 307, 1288

Holman, M. J., Fabrycky, D. C., Ragozzine, D., et al. 2010, Science, 330, 51

Johnson, J. A., Apps, K., Gazak, J. Z., et al. 2011, ApJ, 730, 79

Kipping, D. M. 2009, MNRAS, 392, 181

Kipping, D. M. 2010, MNRAS, 408, 1758

Kipping, D. M. 2011, MNRAS, 416, 689

Kwee, K. K., & van Woerden, H. 1956, Bull. Astron. Inst. Netherlands, 12, 327

Lissauer, J. J., Fabrycky, D. C., Ford, E. B., et al. 2011, Nature, 470, 53

Maciejewski, G., Dimitrov, D., Neuhäuser, R., et al. 2010, MNRAS, 407, 2625

Maciejewski, G., Dimitrov, D., Neuhäuser, R., et al. 2011a, MNRAS, 411, 1204

Maciejewski, G., Errmann, R., Raetz, S., et al. 2011b, A&A, 528, A65

Mandel, K., & Agol, E. 2002, ApJ, 580, L171

Meschiari, S., & Laughlin, G. P. 2010, ApJ, 718, 543

Miralda-Escudé, J. 2002, ApJ, 564, 1019

Montalto, M. 2010, A&A, 521, A60

Nesvorný, D. 2009, ApJ, 701, 1116

Nesvorný, D., & Beaugé, C. 2010, ApJ, 709, L44

Nesvorný, D., & Morbidelli, A. 2008, ApJ, 688, 636

Nutzman, P. A., Fabrycky, D. C., & Fortney, J. J. 2011, ApJ, 740, L10

Rabus, M., Alonso, R., Belmonte, J. A., et al. 2009, A&A, 494, 391

Sanchis-Ojeda, R., & Winn, J. N. 2011, ApJ, 743, 61

Sanchis-Ojeda, R., Winn, J. N., Holman, M. J., et al. 2011, ApJ, 733, 127

Schwarz, R., Haghighipour, N., Eggl, S., Pilat-Lohinger, E., & Funk, B. 2011, MNRAS, 414, 2763

Silva-Valio, A. 2008, ApJ, 683, L179

Simon, A., Szatmáry, K., & Szabó, G. M. 2007, A&A, 470, 727

Steffen, J. H., Gaudi, B. S., Ford, E. B., Agol, E., & Holman, M. J. 2007 [arXiv:0704.0632]

Szabó, G. M., Szatmáry, K., Divéki, Z., & Simon, A. 2006, A&A, 450, 395

Wall, J. V., & Jenkins, C. R. 2003, Practical Statistics for Astronomers (Cambridge University Press)

Table 1. Transit timing of Kepler-1b - Kepler-9c, measured by both methods.

Number	T_0-Barycenter method(MJD-2 454 900)	T_0(MJD-2 454 900)
1.1	65.645006 ± 0.000054	65.645036 ± 0.000073
1.2	68.115621 ± 0.000051	68.115649 ± 0.000051
1.3	70.586201 ± 0.000051	70.586262 ± 0.000079
1.4	73.056852 ± 0.000055	73.056875 ± 0.000186
1.5	75.527497 ± 0.000051	75.527488 ± 0.000098
1.6	77.998120 ± 0.000054	77.998101 ± 0.000103
1.7	80.468596 ± 0.000052	80.468714 ± 0.000071
1.8	82.939301 ± 0.000051	82.939327 ± 0.000080
1.9	85.409937 ± 0.000050	85.409940 ± 0.000074
1.10	87.880533 ± 0.000051	87.880553 ± 0.000054
2.1	65.381504 ± 0.000085	65.381496 ± 0.000185
2.2	67.586213 ± 0.000087	67.586232 ± 0.000238
2.3	69.791026 ± 0.000090	69.790967 ± 0.000178
2.4	71.995973 ± 0.000088	71.995703 ± 0.000178
2.5	74.200488 ± 0.000113	74.200438 ± 0.000181
2.7	78.610067 ± 0.000089	78.609909 ± 0.000210
2.8	80.814614 ± 0.000086	80.814644 ± 0.000172
2.9	83.019473 ± 0.000086	83.019380 ± 0.000210
2.11	87.428970 ± 0.000086	87.428851 ± 0.000199
3.1	67.591623 ± 0.000181	67.587958 ± 0.000558
3.2	72.476370 ± 0.000096	72.475763 ± 0.000343
3.3	77.363887 ± 0.000111	77.363568 ± 0.000564
3.4	82.250995 ± 0.000114	82.251373 ± 0.000555
3.5	87.139357 ± 0.000103	87.139178 ± 0.000515
3.6	92.026855 ± 0.000108	92.026983 ± 0.000491
3.7	96.914806 ± 0.000094	96.914788 ± 0.000482
3.9	106.690806 ± 0.000096	106.690398 ± 0.000368
3.10	111.577701 ± 0.000096	111.578203 ± 0.000488
3.11	121.353559 ± 0.000097	121.353813 ± 0.000448
4.1	104.816415 ± 0.002636	104.815900 ± 0.002940
4.2	108.029416 ± 0.002417	108.029584 ± 0.002460
4.3	111.244774 ± 0.002342	111.243268 ± 0.003001
4.5	117.672537 ± 0.002587	117.670635 ± 0.002792
4.6	120.884243 ± 0.002438	120.884319 ± 0.002080
4.7	124.098430 ± 0.002747	124.098003 ± 0.002296
4.8	127.309430 ± 0.002302	127.311687 ± 0.002627
4.9	130.527792 ± 0.002522	130.525370 ± 0.003034
4.11	136.953717 ± 0.001792	136.952738 ± 0.002374
4.12	140.167899 ± 0.001699	140.166422 ± 0.002767
5.1	66.545846 ± 0.000776	66.546068 ± 0.000494
5.2	70.094334 ± 0.000582	70.094536 ± 0.000520
5.3	73.643932 ± 0.000517	73.643005 ± 0.000564
5.4	77.191271 ± 0.000503	77.191473 ± 0.000434
5.5	80.739494 ± 0.000514	80.739942 ± 0.000579
5.6	84.288634 ± 0.000449	84.288410 ± 0.000543
5.7	87.836005 ± 0.000510	87.836878 ± 0.000526
5.8	91.385478 ± 0.000587	91.385347 ± 0.000495
5.9	94.933849 ± 0.000492	94.933815 ± 0.000447
6.1	67.430812 ± 0.000408	67.424550 ± 0.000441
6.2	70.659594 ± 0.000359	70.659250 ± 0.000499
6.3	73.894048 ± 0.000406	73.893951 ± 0.000421
6.4	77.128802 ± 0.000352	77.128650 ± 0.000468
6.5	80.363963 ± 0.000403	80.363351 ± 0.000453
6.6	83.597843 ± 0.000355	83.598052 ± 0.000443
6.7	86.832717 ± 0.000359	86.832752 ± 0.000568
6.8	90.067911 ± 0.000355	90.067452 ± 0.000489
6.9	93.302393 ± 0.000410	93.302153 ± 0.000495
6.10	96.536655 ± 0.000356	96.536853 ± 0.000456
7.1	67.276389 ± 0.000429	67.276027 ± 0.000374
7.2	72.161758 ± 0.000406	72.161517 ± 0.000459
7.3	77.047387 ± 0.000407	77.047008 ± 0.000382
7.4	81.932553 ± 0.000332	81.932498 ± 0.000316
7.5	86.817611 ± 0.000410	86.817988 ± 0.000455
7.6	91.703986 ± 0.000412	91.703478 ± 0.000538
7.7	96.588905 ± 0.000367	96.588969 ± 0.002094

Table 1. continued.

Number	T_0-Barycenter method(MJD-2 454 900)	T_0(MJD-2 454 900)
8.1	64.685860 ± 0.000691	64.686046 ± 0.000472
8.2	68.208387 ± 0.000598	68.208545 ± 0.000345
8.3	71.731198 ± 0.000581	71.731044 ± 0.000385
8.4	75.253391 ± 0.000578	75.253544 ± 0.000447
8.5	78.776414 ± 0.000555	78.776043 ± 0.000628
8.7	85.821393 ± 0.000695	85.821041 ± 0.000602
8.8	89.343196 ± 0.000618	89.343540 ± 0.000630
8.9	92.866237 ± 0.000492	92.866039 ± 0.000644
8.10	96.388414 ± 0.000731	96.388538 ± 0.000712
9b.1	77.2484 ± 0.00086	77.24875 ± 0.00087
9b.2	96.48276 ± 0.00099	96.4824 ± 0.00092
9b.3	134.95455 ± 0.00122	134.95437 ± 0.00077
9b.4	154.18997 ± 0.00094	154.19058 ± 0.00077
9b.5	173.44199 ± 0.00116	173.43412 ± 0.00107
9b.6	211.92629 ± 0.00082	211.92589 ± 0.00074
9b.7	231.17112 ± 0.00082	231.17167 ± 0.00071
9b.8	250.42960 ± 0.00074	250.42951 ± 0.00071
9b.9	269.68043 ± 0.00071	269.68103 ± 0.00068
9c.1	69.30489 ± 0.00091	69.30577 ± 0.00127
9c.2	108.33019 ± 0.00133	108.33086 ± 0.00111
9c.3	147.33572 ± 0.00107	147.3356 ± 0.00105
9c.4	186.31434 ± 0.00120	186.31251 ± 0.00107
9c.5	225.26218 ± 0.00103	225.26284 ± 0.00096
9c.6	264.18192 ± 0.00099	264.18168 ± 0.00100

Notes. The first column is the number of transit, the second column lists mid-transits found by the barycenter method (MJD-2 454 900), and the third column lists mid-transits reported in Holman et al. (2010); Ford et al. (2011).

Chapter 4

SOAP-T

4.1 Modeling the anomalies inside the transit light-curve to remove them

Stellar spots, which are the most frequent manifestation of stellar activity, combined with the stellar rotation can mimic periodic RVs signal that may lead to a false positive detection of a planet (Boisse et al., 2011, 2009; Bonfils et al., 2007; Figueira et al., 2010; Huélamo et al., 2008; Queloz et al., 2001). Furthermore, the overlap of the planet and the stellar spots on the surface of a star can create anomalies inside the transit light-curve that cause difficulties in constraining the depth of transit and, subsequently the radius of the planet (Rabus et al., 2009). These anomalies can also influence the transit timing measurements which can lead to the false positive detection of non-transiting planets by the TTV method. For instance, as shown in Oshagh et al. (2012), for the case of LHS 6343 system, those anomalies inside the transit light-curves introduced a misleadingly high amplitude TTV signal, like in the case of HAT-P-11 system Sanchis-Ojeda et al. (2011) .

To deal with the issue of the anomalies generated by the overlap of a stellar spot and a transiting planet in a fitting process, most of authors assign a zero weight to the anomalous points of the light curve (see e.g. Sanchis-Ojeda & Winn, 2011). However, as shown by Barros et al. (2013), in the presence of red noise, this treatment to the stellar spot anomalies may not be the best approach since

4.1 Modeling the anomalies inside the transit light-curve to remove them

the missing points in the transit light-curve can significantly underestimate the transit time. Moreover, in the models which are based on the symmetric shape of the light curve, the missing points may break the light curve's symmetry, and as a result, the fitting routine may give more weight to the portion of the light curve that does not include the spot anomaly. This may causes a spurious variation in transit timing (shifting of the center of the light curve) and subsequently produces a measurable TTV signal (e.g., Gibson et al., 2009; Oshagh et al., 2012).

In my second paper during my PhD, entitled "SOAP-T: a tool to study the light curve and radial velocity of a system with a transiting planet and a rotating spotted star", we described a new tool for studying the systems consisting of a rotating star with active zones and a transiting planet. The code, named "SOAP-T" generates synthetic RV signal and synthetic transit light-curves for the system as functions of the stellar rotation phase. This tool is fast and as such can be utilized to simulate different possibilities for different initial configurations in order to find the best solution for inverse problems. We tested the capability of our code by comparing its results with both the result of theoretical models and real observations.

The SOAP-T code is able to reproduce the anomalies inside the transit light-curve, a crucial feature in order to model the observed anomalies inside the transits and subsequently remove the anomaly feature from the transit. By implementing this approach, instead of assigning a zero weight to the anomalous points of the light curve which means excluding those data points from the light curve, we merely eliminate the anomaly feature from the light curve and create a symmetric light curve. As a result, by studying the "clean" light curves, without anomalies, the true value of planetary parameters such as radius and transit time can be estimated.

4.2 Extract information on the planetary system from the anomalies inside transit light-curve

The stellar spots anomalies may also provide important information about the orbital configuration of the star's planetary system. One quantity that is particularly interesting is the angle of the stellar spin axis with respect to the planet orbital plane. There are two major techniques to estimate this spin-orbit angle: first one is the Rossiter-McLaughlin effect, which is based on the RV variations of the star during the planet's transit (e.g., Hébrard et al., 2008; Hirano et al., 2011; Narita et al., 2007; Ohta et al., 2005; Triaud et al., 2010, 2009; Winn et al., 2010, 2005), and the second one is based on the monitoring of the anomalies inside the transit light-curves. If long-term, high-precision, and continuous observations of a star in photometry are accessible (e.g., target stars of the *Kepler* telescope), we are able to follow the evolution of these anomalies inside transits and use them to determine the spin-orbit angle, inclination of the stellar spin axis, and the configuration of stellar spots on the surface of the star (longitude, latitude, and the filling factor) (Désert et al., 2011; Nutzman et al., 2011; Sanchis-Ojeda et al., 2012; Sanchis-Ojeda & Winn, 2011). Having an estimation on the spin-orbit angle and inclination of the stellar spin axis, and combining them with the inclination of planet orbital plane, allows us to estimate the true obliquity of the system. The true obliquity of the system is essential quantity in order to have a better understanding on the configuration of the planetary systems as well as its formation, dynamical evolution, and possible migration (e.g., Fabrycky & Winn, 2009; Hirano et al., 2012; Morton & Johnson, 2011; Ohta et al., 2005; Queloz et al., 2000; Triaud et al., 2010; Winn et al., 2005).

In my second paper as an application of SOAP-T tool, we applied it on the HAT-P-11 system to determine the misalignment angle of the planet in the system by using the anomalies inside its transit light curve. We demonstrated that when using the edge-on star scenario of HAT-P-11 proposed by Sanchis-Ojeda & Winn (2011), SOAP-T is capable of reproducing the same features as obtained from observations for outside of transits as well as the anomalies inside the transit

light-curves. We also found that the reconstruction of the large modulation of the outside transit of HAT-P-11 with the pole-on star model of Sanchis-Ojeda & Winn (2011) requires an assumption on the size of spot on the star which may not be realistic.

Astronomy & Astrophysics

SOAP-T*: a tool to study the light curve and radial velocity of a system with a transiting planet and a rotating spotted star

M. Oshagh[1,2], I. Boisse[1], G. Boué[1,3], M. Montalto[1], N. C. Santos[1,2], X. Bonfils[4], and N. Haghighipour[5]

[1] Centro de Astrofísica, Universidade do Porto, Rua das Estrelas, 4150-762 Porto, Portugal
e-mail: moshagh@astro.up.pt

[2] Departamento de Física e Astronomia, Faculdade de Ciências, Universidade do Porto, Rua do Campo Alegre, 4169-007 Porto, Portugal

[3] Astronomie et Systèmes Dynamiques, IMCCE-CNRS UMR 8028, Observatoire de Paris, UPMC, 77 Av. Denfert-Rochereau, 75014 Paris, France

[4] UJF-Grenoble 1/CNRS-INSU, Institut de Planétologie et d'Astrophysique de Grenoble (IPAG) UMR 5274, 38041 Grenoble, France

[5] Institute for Astronomy and NASA Astrobiology Institute, University of Hawaii-Manoa, 2680 Woodlawn Drive, Honolulu, HI 96822, USA

ABSTRACT

We present an improved version of SOAP named "SOAP-T", which can generate the radial velocity variations and light curves for systems consisting of a rotating spotted star with a transiting planet. This tool can be used to study the anomalies inside transit light curves and the Rossiter-McLaughlin effect, to better constrain the orbital configuration and properties of planetary systems and the active zones of their host stars. Tests of the code are presented to illustrate its performance and to validate its capability when compared with analytical models and real data. Finally, we apply SOAP-T to the active star, HAT-P-11, observed by the NASA *Kepler* space telescope and use this system to discuss the capability of this tool in analyzing light curves for the cases where the transiting planet overlaps with the star's spots.

Key words. planetary systems – methods: numerical – techniques: photometric – techniques: radial velocities – stars: activity

1. Introduction

Stellar spots and plages, combined with the rotation of the star, can mimic periodic radial velocity (RV) signals that may lead to false positives in detecting a planet (Queloz et al. 2001; Bonfils et al. 2007; Huélamo et al. 2008; Boisse et al. 2009, 2011). Furthermore, the overlap of the planet and the active zones on the surface of a star can create anomalies inside the transit light curve that cause difficulties in constraining the depth of transit and, as a result, the radius of the planet (Rabus et al. 2009). These anomalies can also lead to false positives in the detection of nontransiting planets by the transit timing variation method (Oshagh et al. 2012; Sanchis-Ojeda et al. 2011).

The stellar spots may provide important information about the orbital configuration of the star's planetary system. One quantity that is particularly interesting is the angle of stellar spin axis with respect to the orbital plane of the planet. There are two methods to measure this spin-orbit angle: the Rossiter-McLaughlin (RM) effect, which is based on the RV variations of the star during the planet's transit (e.g., Ohta et al. 2005; Winn et al. 2005; Narita et al. 2007; Hébrard et al. 2008; Triaud et al. 2009, 2010; Winn et al. 2010; Hirano et al. 2011), and the study of the anomalies inside the transit light curve due to an overlap of the transiting planet with an active zone of its host star. If long-term and continuous observations of a star in photometry are accessible (e.g., target stars of the *Kepler* telescope), we will be able to detect the evolution of these anomalies

inside transits and use them to determine the spin-orbit angle, inclination of the stellar spin axis, and the configuration of stellar spots on the surface of the star (longitude, latitude, and size) (Nutzman et al. 2011; Désert et al. 2011; Sanchis-Ojeda & Winn 2011; Sanchis-Ojeda et al. 2012). Measuring the angle between stellar spin axis and orbital plane can give us a better understanding of the configuration of the planetary system as well as its formation, dynamical evolution, and possible migration (e.g., Queloz et al. 2000; Ohta et al. 2005; Winn et al. 2005; Fabrycky & Winn 2009; Triaud et al. 2010; Morton & Johnson 2011; Hirano et al. 2012).

In this paper, we present a new tool for studying systems consisting of a rotating star with active zones and a transiting planet. The code, named "SOAP-T" generates synthetic radial velocity variations and produces light curves for the system as functions of the stellar rotation phase. This tool is fast and as such can be utilized to simulate different possibilities for different initial configuration in order to find the best solution for inverse problems.

We describe SOAP-T in Sect. 2. We explain its software platform, language, input parameters, methodology, implementation, and output quantities. In Sect. 3 we present several tests of this software to demonstrate its capabilities. Section 4 is concerned with applying SOAP-T to the particular case of HAT-P-11 and comparing its result with the result of Sanchis-Ojeda & Winn (2011). We use this comparison as a demonstration of the capability of SOAP-T in analyzing the case where the planet and spot overlap. In the last section, we discuss other possible applications of SOAP-T and conclude this study by presenting its future improvements.

---

* The tool's public interface is available at
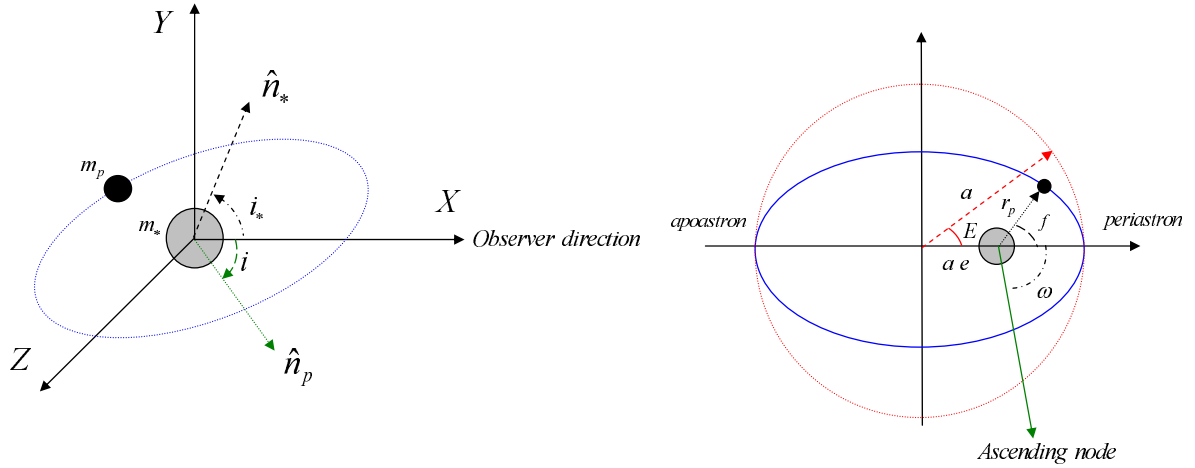http://www.astro.up.pt/resources/soap-t/

Fig. 1. *Left*: schematic configuration of the stellar spin axis and planetary orbital plane. The vector $\hat{n}_p$ is the normal unit vector of the planetary orbital plane, the vector $\hat{n}_*$ is the stellar spin axis, and i_* is the stellar inclination. We denote the angle between the projected stellar spin axis and the projected normal unit vector of the planetary orbital plane on the y-z plane with λ (not shown here). *Right*: schematic view of planetary orbit from above the orbital plane, the star is the gray circle and the planet is the black full circle. See Sect. 2 for more details on the symbols.

2. Software description

SOAP-T has been developed based on the already published code SOAP (Boisse et al. 2012)[1] that simulates spots and plages on the surface of a rotating star. We refer the reader to Boisse et al. (2012) for more details. The code in SOAP-T is written in Python with calls to functions written in C in order to make the code faster.

2.1. Inputs

The code requires initial conditions that can be assigned by the user in an input configuration file "driver.cfg". The details of the initial parameters for the rotating spotted star can be found in Boisse et al. (2012). Here we explain the extra parameters that are required by SOAP-T.

Stellar parameters: one new feature of SOAP-T compared to SOAP is the implementation of the quadratic limb darkening (Mandel & Agol 2002, SOAP considered the linear limb darkening for the star)

$$I(r) = 1 - \gamma_1(1-\mu) - \gamma_2(1-\mu)^2, \qquad \gamma_1 + \gamma_2 < 1. \qquad (1)$$

In this equation, r is the normalized radial coordinate on the disk of the star, $I(r)$ is the specific intensity defined to reach its maximum 1 at the center of the star ($r = 0$) and its minimum at the star's limb, and $\mu = \cos\theta = (1 - r^2)^{1/2}$ where θ is the angle between the normal to the surface and the observer. As shown by Eq. (1), the input parameters require two coefficients of quadratic limb darkening (γ_1 and γ_2).

Spot parameters: the number of spots is another important parameter. Unlike in SOAP where the number of spots could approach four, it is possible to choose up to ten spots in SOAP-T.

Planet parameters: users are able to set the initial orbital configuration of the planet by selecting the following quantities: initial value of the planet's orbital period ($P_{\rm orb}$), the time of its periastron passage (T_0), its initial orbital phase (PS_0), eccentricity (e), semimajor axis (a), argument of periastron (ω), inclination with respect to the line of sight (i), as well as the planet's

---

[1] http://www.astro.up.pt/soap/

radius ($R_{\rm planet}$) and the angle between the stellar spin axis and the normal to the orbit of the planet projected on the y-z plane. We denote this angle by λ.

2.2. Detailed description of computation

We restate here from Boisse et al. (2012) that the rotating spotted star is centered on a grid of $grid \times grid$ cells on a y-z plane. The cells take their y and z values between –1 and 1, normalized to the stellar radius. Each grid cell (p_y, p_z) contains a flux value and a CCF (cross correlation function). Our goal in this section is to describe 1) how we add a planet to the rotating spotted star; 2) how we compute its impact in photometry and in RV; and 3) how we incorporate the overlap between the stellar inhomogeneities and the planet.

To determine the effect of a planet on the RV and flux of an unspotted star in each phase step, the code first checks whether the planet is in the foreground or the background with respect to the star. For that reason, in the first step, SOAP-T calculates the position of the planet for each time step. Since the output of the code is in the stellar rotational phase, the code uses the following equation to convert stellar rotation phase into time

$$T = (PS + PS_0) \times P_{\rm rot}. \qquad (2)$$

The quantity PS is the stellar rotation phase, which can be between 0 and 1; PS_0 is the planet's orbital initial phase, which defines the initial position of the planet; and $P_{\rm rot}$ is the stellar rotation period in days. This equation is only valid for stellar rotation periods longer than the orbital period of the planet, which should be true for most of the cases of transiting extrasolar planetary systems.

To determine the planet's position, the code has to calculate λ. As explained above, λ is the angle between the stellar spin axis (denoted by $\hat{n}_*$) projected on the y-z plane and the unit vector normal to the plane of the planet's orbit (shown by $\hat{n}_p$ in Fig. 1) also projected on the same plane. The coordinates of vector $\hat{n}_*$ are determined using

$$\hat{n}_* = R_x(\psi_*)R_y(i_*)\begin{pmatrix} 1 \\ 0 \\ 0 \end{pmatrix} = \begin{pmatrix} \cos i_* \\ \sin i_* \sin \psi_* \\ -\sin i_* \cos \psi_* \end{pmatrix}, \qquad (3)$$

where (ψ_*) is the longitude of stellar spin, (i_*) is the star's inclination, and R_x and R_y are the rotation matrices around the x and y axes. The coordinates of the normal vector $\hat{n}_p$ are also determined in the same fashion using the planet's longitude of ascending node (Ω) and orbital inclination (i) as

$$\hat{n}_p = R_x(\Omega)R_y(i) \begin{pmatrix} 1 \\ 0 \\ 0 \end{pmatrix} = \begin{pmatrix} \cos i \\ \sin i \sin \Omega \\ -\sin i \cos \Omega \end{pmatrix}. \tag{4}$$

The angle λ is then calculated using $\lambda = \Omega - \psi_*$. The code subsequently aligns the projected stellar spin axis with the z direction by setting $\psi_* = 180°$ and uses the longitude of the ascending node of the planet $\Omega = 180 + \lambda$ to calculate the coordinates of its position vector (see Sect. 4 and Eqs. (53)–(55) in Murray & Correia 2011, for more details). At each stellar phase step, the position vector of the planet (D) is given by

$$D = r_p \begin{pmatrix} \sin i \sin(\omega + f) \\ -\cos \lambda \cos(\omega + f) + \sin \lambda \cos i \sin(\omega + f) \\ -\sin \lambda \cos(\omega + f) - \cos \lambda \cos i \sin(\omega + f) \end{pmatrix}. \tag{5}$$

In Eq. (5)

$$r_p = \frac{a(1 - e^2)}{1 + e \cos f}, \tag{6}$$

where r_p is the distance between the stellar center and the center of planet, and

$$f = 2 \tan^{-1} \left[\left(\frac{1 + e}{1 - e} \right)^{1/2} \tan \left(\frac{E}{2} \right) \right] \tag{7}$$

is the true anomaly of the planet. To calculate f, for small eccentricity, the code uses Kepler's equation

$$E = M + \frac{e \sin M - M}{1 - e \cos M}, \tag{8}$$

where $M = 2\pi(T - T_0)/P_{orb}$ is the mean-anomaly of the planet's orbit (e.g. Ohta et al. 2005; Murray & Correia 2011, see Fig. 1, a schematic view of a planetary system).

If the planet is in the foreground ($D_x > 0$), the code checks that the planet is inside the stellar disk or outside by comparing the projected distance of the planet's center to the stellar center with the radius of star ($|D| < R_*$). If the planet is inside, the code resolves the area of the grid where the planet is located and establishes an area around the planet where it will focus the subsequent calculations. This area is then scanned to determine whether each grid cell is located inside or outside the stellar disk (especially in the case where the planet is on the stellar limb), and if this grid cell belongs to the planet's disk, the code determines the location by calculating the distance of the grid cell to the center of planet and comparing it with planet's radius. Assuming that a grid cell is located inside the stellar disk and also belongs to the planet's disk, its CCF is modeled by a Gaussian with a width and amplitude given by the input parameters and doppler-shifted according to the projected stellar rotation velocity weighted by the quadratic limb-darkening law. This CCF value will then be removed from the total CCF of the rotating unspotted star. For the same grid cell, the values of the flux can be calculated using only on the quadratic limb-darkening law. The code also removes the flux value of that cell from the total flux of the rotating spotted star.

In the next step, the code adds a planet to the rotating spotted star in order to calculate the effect of both the planet and the spots
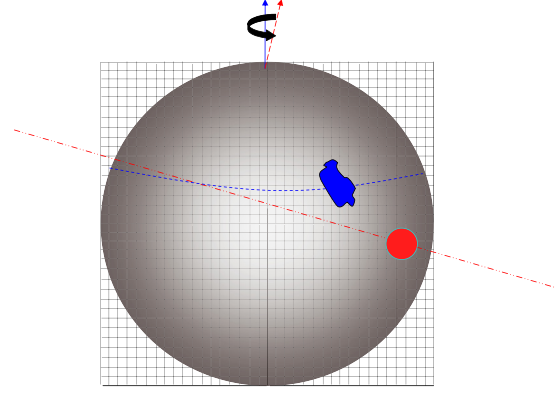

Fig. 2. Schematic view of stellar spot and the transiting planet in simulations by SOAP-T.

on the RV and flux at the same time. In the case that the spot is not partly covered by the planet, the procedure is as explained below. The code

- determines the position of the spot;
- determines the position of the planet;
- applies inverse rotation to the spot to bring it along the line of sight;
- scans the region of the spot's position to identify the grid cells that belong to the spot's disk area;
- sums up the CCF and flux of all cells inside the spot and removes them from the total flux and CCF of the unspotted star (see Fig. 4 of Boisse et al. 2012 for the inverse rotation and also for more details on spot calculation);
- scans the region of the planet's position to determine the grid cells that are inside the disk of the planet;
- calculates the sum of the CCF and flux for those grid cells inside the transiting planet and removes them from the total flux and CCF of the spotted star.

The complexity arises from the overlapping of the transiting planet with a spot on the surface of the star. In this case, the code considers those parts of the spot whose distances to the center of the planet are smaller than the planet's radius as the overlapped area. Those points will not be scanned during the spot-scanning process. As a consequence, they will skip the rest of procedure for CCF and flux of spot and removal from total CCF and flux. This procedure is able to produce those positive "bump" anomalies inside the transit light curve that are due to the reduction in the loss of light. The schematic view of the system that is simulated by SOAP-T is shown in Fig. 2.

2.3. Outputs

The code returns the results of its simulation into the output file "output.dat". The output file contains four columns that represent stellar phase, flux, RV, and BIS (the bisector span), respectively. These quantities can be plotted directly by SOAP-T as functions of the stellar rotation phase. Similar to SOAP, the stellar phase step can be chosen in two ways, either by selecting the constant fraction of the phase between 0 to 1, or by uploading the wanted phase values in the *ph_in* file. The flux values correspond to the photometry of the system (the total flux of system), and they are normalized to the maximum value of total flux during the stellar rotation phase. The RV values are obtained by fitting a Gaussian function to each total CCF (see more details in Boisse et al. 2012). We note here that each total CCF is also
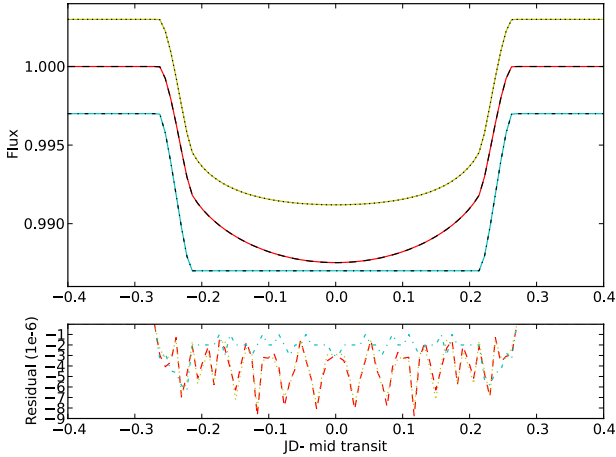
Fig. 3. Comparing the photometric results of SOAP-T and the theoretical model of a transiting planet over an unspotted star (Mandel & Agol 2002). The cyan, red, and yellow lines show SOAP-T's results for a star without limb darkening, a star with linear limb darkening ($\gamma_1 = 0.6$), and a star with quadratic limb darkening ($\gamma_1 = 0.29$ and $\gamma_2 = 0.34$), respectively. The dash-dotted, dashed, and the dotted lines show the corresponding results using the mechanism by Mandel & Agol (2002).

normalized to its maximal value. We refer the reader to Queloz et al. (2001) for details on BIS calculations.

3. Tests

To check the capability of SOAP-T and the validity of its result, we preformed several tests to compare its outcome with theoretical models and real observations. Tests related to the effects of spots on the RV and flux signals have been presented and explained in Boisse et al. (2011, 2012). In this section, we test the validity of the results for the photometry and RV with a transiting planet around both an unspotted and a spotted star.

To begin with, we consider a system consisting of an unspotted star with a transiting planet. The purpose of this test is to determine whether the code can reproduce the light curve of a star with a transiting planet as obtained from the theoretical model of Mandel & Agol (2002). We select various initial conditions including a star without any limb darkening, or with linear or quadratic limb darkening. As shown in Fig. 3, the results obtained from SOAP-T agree strongly with the results obtained from the theoretical model based on the formalism presented by Mandel & Agol (2002). The latter implies that SOAP-T can be used reliably to characterize the light curve of a transiting planetary system.

In a second test, we examined the RVs obtained using SOAP-T during the transit of a planet in front of an unspotted star. We applied SOAP-T to the system of WASP-3, which is known to harbor a planet with a misalignment between its orbital plane and stellar spin axis (see the parameters of WASP-3 system in Table 1). The RV observation data of WASP-3 during its transits were taken from Simpson et al. (2010). Observations were made using the SOPHIE spectrograph at Haute-Provence Observatory. We fitted the RVs produced by SOAP-T to the observational data and compared the results with those of Simpson et al. (2010). We only allowed stellar rotation velocity ($v \sin i$) and misalignment angle (λ) to vary as free parameters, and kept all other parameters constant and equal to their values reported by Gibson et al. (2008) and Simpson et al. (2010) (see Table 1).

Table 1. Stellar and planet's parameters of the WASP-3 system (Gibson et al. 2008; Simpson et al. 2010).

| Parameter	Value	Uncertainty
Stellar parameters		
$R_\star (R_\odot)$	1.31	$\pm^{0.05}_{0.07}$
Linear limb darkening coefficient	0.69	–
Stellar inclination (deg)	90	–
Spectroscopic stellar rotation velocity $v \sin i$ (km s^{-1})	13.4	± 1.5
Planet parameters		
Planet-to-star radius ratio (R_p/R_*)	0.1013	$\pm^{0.0014}_{0.0013}$
Period (days)	1.846835	± 0.000002
Eccentricity	0	–
Scaled semimajor axis (a/R_*)	5.173	$\pm^{0.246}_{0.162}$
Orbital inclination (deg)	84.93	$\pm^{1.32}_{0.78}$
Projected spin-orbit misalignment angle (deg)	13	$\pm^{9}_{7}$
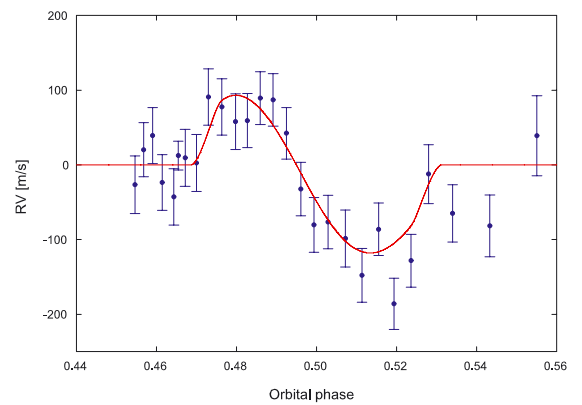
Fig. 4. RV observations of WASP-3 during transit of WASP-3b (RM effect) minus Keplerian motion, which are blue dots (Simpson et al. 2010), overplotted with the best fit of RV signals obtained from SOAP-T, which is a red line.

The best fit result obtained using SOAP-T corresponds to $\lambda = 20.0° \pm 3.3°$ and $v \sin i = 13.31 \pm 0.45$ km s^{-1} with $\chi^2_{\rm red} = 0.9308$. We obtained the error bars of these measurements using the bootstrap method (Wall & Jenkins 2003). The value of the misalignment angle (λ) is consistent with the value reported by Simpson et al. (2010) ($13°\pm^{9°}_{7°}$) within 1σ. The error bars obtained with SOAP-T are more than twice smaller than those derived by Simpson et al. (2010). We assume that this could be due to the smaller number of free parameters in our fitting procedure. Otherwise it might also be because SOAP-T has been developed to reproduce the analysis routine of RV measurements exactly, and is thus closer to the observations when compared to the result of the analytical formula used by Simpson et al. (2010) (Boué et al. 2012). Indeed, we also obtained better agreement between the projected stellar rotation velocity ($v \sin i$) and the value obtained by spectroscopic broadening measurements (13.4 ± 1.5 km s^{-1}). For comparison, Simpson et al. (2010) obtained $v \sin i = 19.6 \pm^{2.2}_{2.1}$ km s^{-1}. Figure 4 shows the result of the best SOAP-T RV's fit and the observation of RM effect of WASP-3.

Finally, since there is no theoretical model for the case where a transiting planet and star spots overlap, to evaluate the performance of SOAP-T in this case, we compared the photometric result of SOAP-T with the results reported in the literature for the real observation of HAT-P-11 by the *Kepler* space telescope. We explain this test and its applications in the next section.

Table 2. Stellar and planet's parameters of the HAT-P-11 system (Bakos et al. 2010; Sanchis-Ojeda & Winn 2011).

Parameter	Value	Uncertainty
Star parameters		
$M_\star (M_\odot)$	0.81	$\pm^{0.02}_{0.03}$
$R_\star (R_\odot)$	0.75	± 0.02
Stellar rotation period (days)	30.5	$\pm^{4.1}_{3.2}$
Age (Gyr)	6.5	$\pm^{5.9}_{4.1}$
Distance (pc)	38.0	± 1.3
Linear limb darkening coefficient	0.599	± 0.015
Quadratic limb darkening coefficient	0.073	± 0.016
Planet parameters		
$M_P (M_{Jup})$	0.081	± 0.009
Planet to star radius ratio ($R_p/R_\star$)	0.05862	± 0.00026
Orbital period (days)	4.8878049	± 0.0000013
Scaled semimajor axis ($a/R_\star$)	15.6	± 1.5
Eccentricity	0.198	± 0.046

**Table 3.** Parameters of the HAT-P-11 system for different solutions reported by Sanchis-Ojeda & Winn (2011).

Parameter	Value	Uncertainty
Edge-on solution		
Projected spin-orbit misalignment angle λ (deg)	106	+15/–12
Stellar inclination i_s (deg)	80	+4/–3
Latitude of active zone (deg)	19.7	+1.5/–2.2
Half-width of active zone (deg)	4.8	+1.5/–1.8
Pole-on solution		
Projected spin-orbit misalignment angle λ (deg)	121	+24/–21
Stellar inclination i_s (deg)	168	+2/–5
Latitude of active zone (deg)	67	+2/–4
Half-width of active zone (deg)	4.5	+1.6/–1.9

4. Application of SOAP-T to HAT-P-11

HAT-P-11 is a 6.5 Gyr bright ($V = 9.6$) K4 star with a mass of 0.81 $M_\odot$ and radius of 0.75 $R_\odot$. At a distance of 38 pc, this star hosts a transiting Neptune-sized planet with a mass of 0.081 M_{Jup} and radius of 0.422 R_{Jup} (Bakos et al. 2010). HAT-P-11b has a period of 4.887 days and revolves around its central star in an orbit with a semimajor axis of 0.053 AU and an eccentricity of $e = 0.198$. More details of the parameters of this planet and its host star can be found in Table 2.

Studies of the HAT-P-11 planetary system have shown extreme misalignment of the projected angle between the stellar spin axis and the planet's orbital plane ($\lambda = 103° \pm^{26°}_{10°}$) through the RM effect (Winn et al. 2010).

HAT-P-11 (KOI-3) was used as one of the calibration target stars for the *Kepler* space telescope and has been observed throughout *Kepler*'s mission in both short and long cadences. The high-precision photometry of this star has revealed some features inside its transit light curve and has also shown a large modulation outside of transits. The anomalies inside the transit light curve of HAT-P-11 can be attributed to the overlapping of the transiting planet with active zones on the surface of the star (Sanchis-Ojeda & Winn 2011). The recurrence (or not) of these anomalies can be used to put an upper limit on the stellar obliquity. Recently Sanchis-Ojeda & Winn (2011) carried out a purely photometric study of this system based on the observation of photometric anomalies inside the transit light curve using
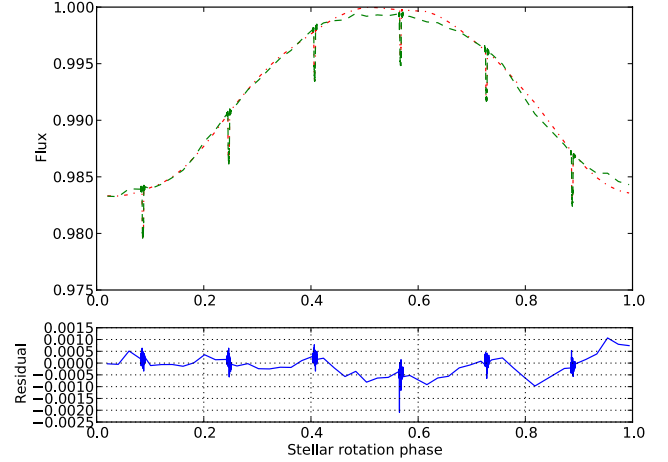
Fig. 5. Comparing the best fit model to the transit photometry of HAT-P-11 using SOAP-T and the *Kepler* observation of HAT-P-11 for one period of stellar rotation. Red (dash-dotted) line shows SOAP-T's photometric result for an edge-on solution and green (dashed) line correspond to HAT-P-11 observation. The blue (solid) line in the bottom panel shows the residual.

the *Kepler* public data Q0-Q2 and showed that no recurrence of anomalies exists in two closely spaced transits in the *Kepler* data of HAT-P-11. They considered this result as evidence of the misalignment of the stellar spin axis with respect to the orbital plane. Fortunately, these authors were able to detect a feature with two peaks in the folded light curve of 26 transits of this star which could be interpreted as evidence for the existence of two long-lived spot belt regions on the star. By using a simple geometric model, these authors arrived at two solutions for the stellar obliquity; an edge-on solution that is in good agreement with the result of Winn et al. (2010) through the RM study, and an alternative solution in which the star is seen almost pole-on. The method used by Sanchis-Ojeda & Winn (2011) also allowed these authors to put some constraints on the position (latitude) and size of the active zones on the surface of star (see details of parameters for two solutions in Table 3).

Here we present the results of the application of SOAP-T to HAT-P-11 reproducing the light curve of this star over one stellar rotation. The rotation period of this star contains six transits.

Since the inside transit anomalies carry more information about the configuration of a planetary system, we decided to give more weight to these points in our study. We, therefore, performed a regular sampling to reduce the number of points outside of the transit light curve. One point was taken from each 300 points in the light curve outside the transit. This process reduced the running time of the code significantly.

4.1. HAT-P-11 edge-on solution

In this section, we consider the system to be edged-on and choose all initial parameters of the star, planet, and spots (except the number of spots and their longitude) from the values reported by Sanchis-Ojeda & Winn (2011). The spots' brightness is fixed to zero. The details of initial conditions are listed in Table 3. To reproduce all the features in the light curve, both inside and outside the transit, we limited the latitude and the size of the spots to the range reported by Sanchis-Ojeda & Winn (2011). The spots' radii are equal to the half-width of the active zone and correspond to $R_{spot} = 0.08 R_\star$. However, we allowed
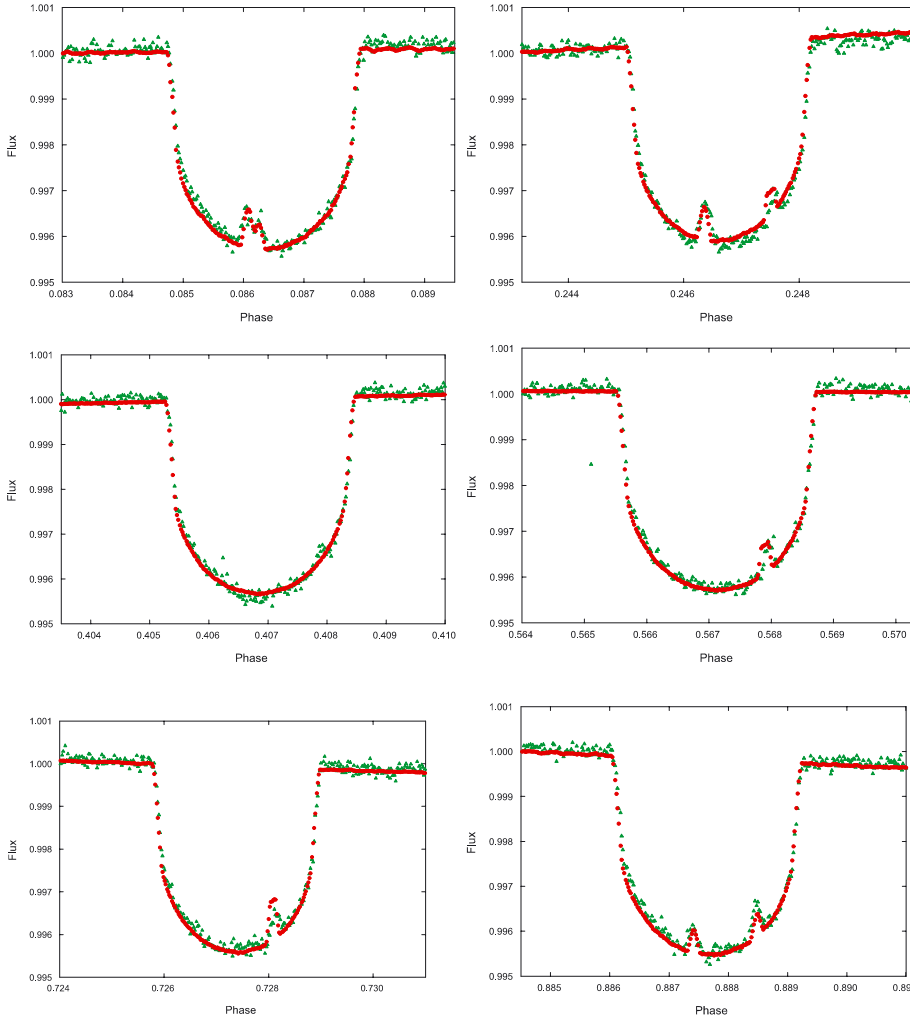
Fig. 6. Zoom on the six transits of HAT-P-11 in Fig. 5. The flux values are normalized to one for both observation and SOAP-T. Red dots represent the SOAP-T photometric result and green triangles are observed flux of HAT-P-11.

the number of spots and their longitudes to vary as free parameters between 0–10 and 0°–360°, respectively. The best fit to the observations ($\chi^2_{\rm red} = 7.356$) was obtained with eight spots on the surface of the star. Figure 5 shows the best result of SOAP-T photometry overplotted with the real observation of HAT-P-11 during one stellar period. Figure 6 shows more details of the inside of each transit and the results obtained from SOAP-T after normalizing both flux values to one. As shown in both figures, SOAP-T could manage to reproduce all the inside transit anomalies and also the outside transit variation. We note here that the results of Sanchis-Ojeda & Winn (2011) were obtained by considering the inside transit anomalies. These authors did not consider the outside features of the light curve. However, using SOAP-T we were able to study the entire light curve, both inside transit and outside, at the same time. We note that here we do not intend to confirm the results of Sanchis-Ojeda & Winn (2011). We only use the similarities between the results obtained from SOAP-T photometry (e.g. position and size of spots, stellar inclination, and spin-orbit misalignment angle) and the results by these authors as a proof of the validity of SOAP-T's capability in simulating the case of spot and planet overlapping.

4.2. HAT-P-11 pole-on solution

In this section, we examine the pole-on model for the system proposed by Sanchis-Ojeda & Winn (2011). We note that here we explore which configuration of spot on the surface of the star

would be able to generate the out of transits variation, and we did not attempt to reproduce the inside transit features. We generated the light curve of HAT-P-11 using SOAP-T photometry and the parameters of the pole-on model given by these authors. (see the details of parameters in Table 3). Since the pole-on solution presented by Sanchis-Ojeda & Winn (2011) is only nearly pole-on (i.e., the angle of misalignment is ~168°), some spots located close to the equator of the star can produce large variations outside the transit by disappearing from the view for a small part of the rotation period. We investigated the effect of different possible sizes of the spots that were located in different latitudes. Our analysis showed that the optimized result, whose outside-transit profile is similar to that from the observation, has to have a spot on 20° or 60° latitude with a size equal to 0.2 R_* (see Fig. 7). Since the brightness of spot is fixed to zero, it is the minimal size of the spot. For a star with a similar spectral type as HAT-P-11 (i.e., K), this is a very large spot. Although spots with very large sizes have been detected on K stars (Strassmeier 1999), this situation is unlikely for HAT-P-11.

5. Conclusion and perspective

In this paper, we introduced a new software package that can be used to produce the photometric and RV signals of a system consisting of a rotating spotted star and a transiting planet where the spots and planet overlap. We tested the capability of our code by comparing its results with theoretical models and the results of
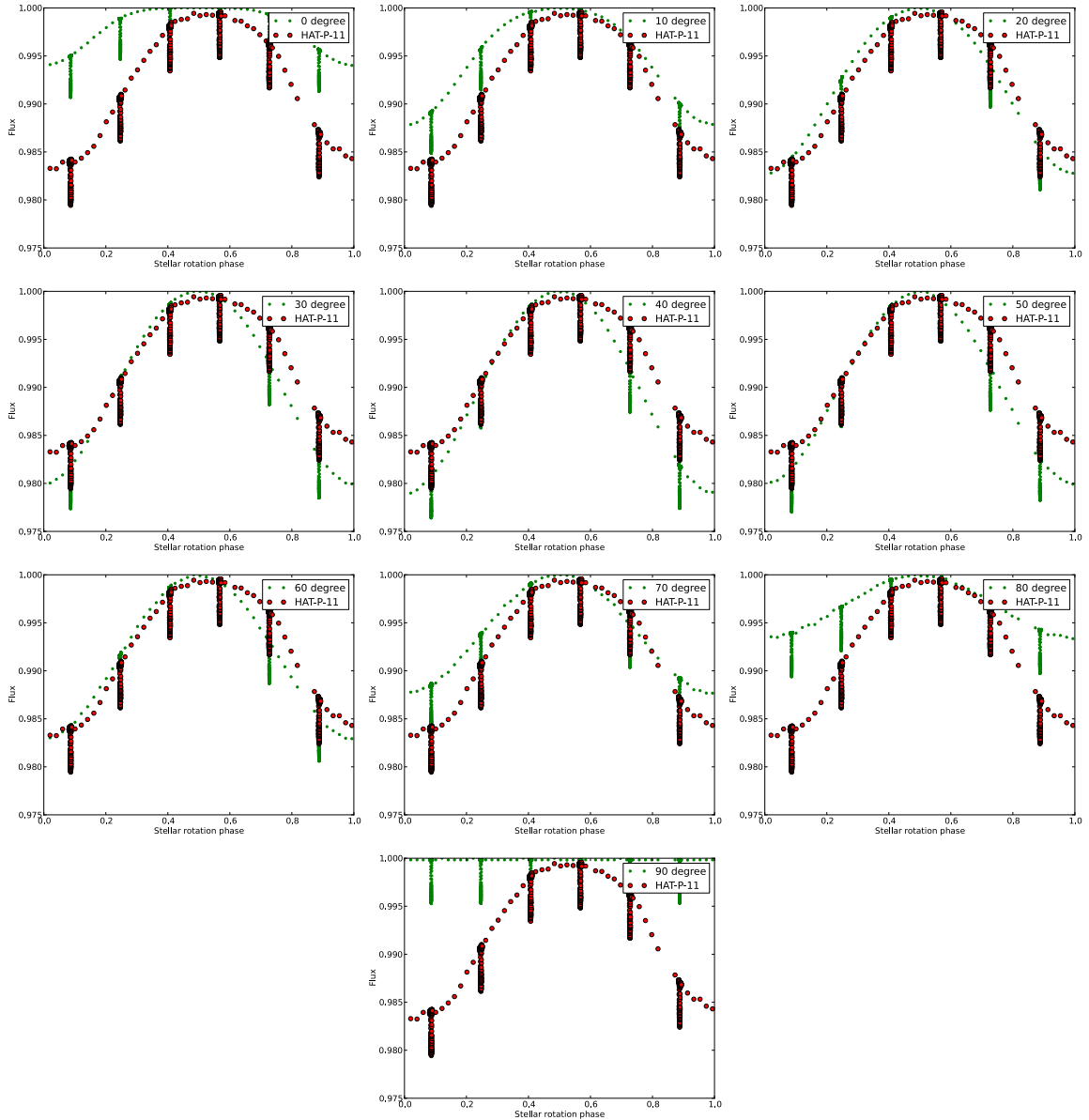
Fig. 7. Comparing SOAP-T's photometric result with the observation of HAT-P-11 for the pole-on model of Sanchis-Ojeda & Winn (2011). Each panel shows different values for the latitude of one spot with the size of 0.2 radius of star. Green dot is the SOAP-T photometric result and red circle is the observation of HAT-P-11.

observations. We used the HAT-P-11 system and demonstrated that when using the edge-on model of Sanchis-Ojeda & Winn (2011), SOAP-T is capable of reproducing the same features as obtained from observations for the outside of transits, as well as the anomalies inside the transits. We also showed that the reconstruction of the large modulation of the outside transit of HAT-P-11 with the pole-on model of Sanchis-Ojeda & Winn (2011) requires an assumption on the size of spot on the star, which may not be realistic.

In using SOAP-T, the number of free parameters of a system that can be chosen by the user is large. In general, for a system consisting of a rotating star with one spot and a planet transiting, there are 18 free parameters. As a result, for a system where parameters are not constrained (e.g., by observation), finding the best solution that fits real observation becomes a complicated task. The minimization of the reduced chi-squared (the indicator of goodness of the fit) in this case requires the exploration of a large parameter space. A simple griding of this space turns

the calculations into a time-consuming process that may result in finding local minima instead of a global minimum. Efforts are currently underway to investigate different optimization strategies that can lead to faster and more secure determination of a global minimum.

References

Bakos, G. Á., Torres, G., Pál, A., et al. 2010, ApJ, 710, 1724
Boisse, I., Moutou, C., Vidal-Madjar, A., et al. 2009, A&A, 495, 959
Boisse, I., Bouchy, F., Hébrard, G., et al. 2011, A&A, 528, A4
Boisse, I., Bonfils, X., & Santos, N. C. 2012, A&A, 545, A109
Bonfils, X., Mayor, M., Delfosse, X., et al. 2007, A&A, 474, 293
Boué, G., Montalto, M., Boisse, I., Oshagh, M., & Santos, N. 2012, A&A, accepted [arXiv:1211.3310]
Désert, J.-M., Charbonneau, D., Demory, B.-O., et al. 2011, ApJS, 197, 14
Fabrycky, D. C., & Winn, J. N. 2009, ApJ, 696, 1230
Gibson, N. P., Pollacco, D., Simpson, E. K., et al. 2008, A&A, 492, 603
Hébrard, G., Bouchy, F., Pont, F., et al. 2008, A&A, 488, 763
Hirano, T., Suto, Y., Winn, J. N., et al. 2011, ApJ, 742, 69
Hirano, T., Sanchis-Ojeda, R., Takeda, Y., et al. 2012, ApJ, 756, 66
Huélamo, N., Figueira, P., Bonfils, X., et al. 2008, A&A, 489, L9
Mandel, K., & Agol, E. 2002, ApJ, 580, L171
Morton, T. D., & Johnson, J. A. 2011, ApJ, 729, 138
Murray, C. D., & Correia, A. C. M. 2011, Keplerian Orbits and Dynamics of Exoplanets, ed. S. Piper, 15

Narita, N., Enya, K., Sato, B., et al. 2007, PASJ, 59, 763
Nutzman, P. A., Fabrycky, D. C., & Fortney, J. J. 2011, ApJ, 740, L10
Ohta, Y., Taruya, A., & Suto, Y. 2005, ApJ, 622, 1118
Oshagh, M., Boué, G., Haghighipour, N., et al. 2012, A&A, 540, A62
Queloz, D., Eggenberger, A., Mayor, M., et al. 2000, A&A, 359, L13
Queloz, D., Henry, G. W., Sivan, J. P., et al. 2001, A&A, 379, 279
Rabus, M., Alonso, R., Belmonte, J. A., et al. 2009, A&A, 494, 391
Sanchis-Ojeda, R., & Winn, J. N. 2011, ApJ, 743, 61
Sanchis-Ojeda, R., Winn, J. N., Holman, M. J., et al. 2011, ApJ, 733, 127
Sanchis-Ojeda, R., Fabrycky, D. C., Winn, J. N., et al. 2012, Nature, 487, 449
Simpson, E. K., Pollacco, D., Hébrard, G., et al. 2010, MNRAS, 405, 1867
Strassmeier, K. G. 1999, A&A, 347, 225
Triaud, A. H. M. J., Queloz, D., Bouchy, F., et al. 2009, A&A, 506, 377
Triaud, A. H. M. J., Collier Cameron, A., Queloz, D., et al. 2010, A&A, 524, A25
Wall, J. V., & Jenkins, C. R. 2003, Practical Statistics for Astronomers (Cambridge University Press)
Winn, J. N., Noyes, R. W., Holman, M. J., et al. 2005, ApJ, 631, 1215
Winn, J. N., Johnson, J. A., Howard, A. W., et al. 2010, ApJ, 723, L223

Chapter 5

Quantifying the effect of stellar spots

In Chapter 4, we assumed that all the anomalous features inside the transit light-curve were corrected before applying the analysis tools on the light curve to extract the information from it (such as an estimation of the planet radius, inclination, limb darkening coefficients, and the transit timings). However, in reality most studies done in the transit field were performed without considering those corrections. In my third paper, named "Effect of stellar spots on the high-precision transit light-curve", we investigated the impact of those stellar spot anomalies on the planetary parameters estimations. We managed to carry a quantitative study on the effect of those anomalies.

We obtained that spot anomalies in the transit light-curves can lead to an underestimation of a planet radius that 4%. Likewise, the transit duration may be estimated to be about 4% longer or shorter. Depending on the size and distribution of spots, anomalies can also produce transit-timing variations (TTVs) with significant amplitudes. For instance, TTVs with signal amplitudes of 200 seconds can be produced by a dark spot as large as the largest Sunspot. Such a large TTV is similar to that induced by an Earth-mass planet in a mean-motion resonance with a Jovian type body transiting a solar-mass star in a three-day orbit (e.g., Boué et al. (2012)), or by an Earth-mass exomoon on a Neptune mass transiting planet (Kipping, 2009).

Astronomy & Astrophysics

Effect of stellar spots on high-precision transit light-curve

M. Oshagh[1,2], N. C. Santos[1,2], I. Boisse[1], G. Boué[3], M. Montalto[1], X. Dumusque[4], and N. Haghighipour[5]

[1] Centro de Astrofísica, Universidade do Porto, Rua das Estrelas, 4150-762 Porto, Portugal
e-mail: moshagh@astro.up.pt
[2] Departamento de Física e Astronomia, Faculdade de Ciências, Universidade do Porto, Rua do Campo Alegre, 4169-007 Porto, Portugal
[3] Department of Astronomy and Astrophysics, University of Chicago, 5640 South Ellis Avenue, Chicago, IL 60637, USA
[4] Observatoire de Genève, Université de Genève, 51 chemin des Maillettes, 1290 Sauverny, Switzerland
[5] Institute for Astronomy and NASA Astrobiology Institute, University of Hawaii-Manoa, 2680 Woodlawn Drive, Honolulu, HI 96822, USA

ABSTRACT

Stellar-activity features such as spots can complicate the determination of planetary parameters through spectroscopic and photometric observations. The overlap of a transiting planet and a stellar spot, for instance, can produce anomalies in the transit light-curves that may lead to an inaccurate estimation of the transit duration, depth, and timing. These inaccuracies can for instance affect the precise derivation of the planet radius. We present the results of a quantitative study on the effects of stellar spots on high-precision transit light-curves. We show that spot anomalies can lead to an estimate of a planet radius that is 4% smaller than the real value. Likewise, the transit duration may be estimated about 4%, longer or shorter. Depending on the size and distribution of spots, anomalies can also produce transit-timing variations (TTVs) with significant amplitudes. For instance, TTVs with signal amplitudes of 200 s can be produced when the spot is completely dark and has the size of the largest Sun spot. Our study also indicates that the smallest size of a stellar spot that still has detectable effects on a high-precision transit light-curve is around 0.03 time the stellar radius for typical *Kepler* Telescope precision. We also show that the strategy of including more free parameters (such as transit depth and duration) in the fitting procedure to measure the transit time of each individual transit will not produce accurate results for active stars.

Key words. planets and satellites: detection – planetary systems – methods: numerical – stars: activity – techniques: photometric

1. Introduction

A survey of the currently known extrasolar planets indicates that many of these objects orbit stars that show high levels of activity. Among the stars in the field of view of the *Kepler* Space Telescope, for instance, a quarter to a third are more active than the Sun (Basri et al. 2013). Active stars may also harbor spots. Indeed, spots on the stellar disk are a clear evidence of stellar activity. In general, stellar spots are larger than Sun spots (Berdyugina 2005). The largest observed stellar spots are on the giant stars HD 12545 and II Peg (O'Neal et al. 1998; Strassmeier 1999; Tas & Evren 2000). The spots on the surface of these stars may cover up to half of their stellar disks.

Stellar spots can have profound effects on the detection and characterization of planets through both photometry and spectroscopy (see e.g. Boisse et al. 2009, 2011; Ballerini et al. 2012). In photometric observations, stellar spots that are not occulted by a transiting planet can produce outside-transit light-curve variations that can lead to a wrong estimation of planet parameters such as its radius (Pont et al. 2008). The overlap of a transiting planet and stellar spots can produce anomalies in the transit light-curve that may also lead to an incorrect determination of planetary parameters, such as the planet radius and the limb-darkening coefficients of the host star (Pont et al. 2007; Czesla et al. 2009; Berta et al. 2011; Désert et al. 2011; Ballerini et al. 2012). Stellar spot anomalies can also cause offsets in the transit-timing measurement that can lead to a false-positive detection of a non-transiting planet by transit-timing variation (TTV) method (Alonso et al. 2009; Sanchis-Ojeda et al. 2011; Sanchis-Ojeda & Winn 2011; Oshagh et al. 2012).

To account for the anomalies generated by the overlap of a stellar spot and a transiting planet in a fitting process, some authors assigned a zero weight to the anomalous points of the light curve (see e.g. Sanchis-Ojeda & Winn 2011). However, as shown by Barros et al. (2013), in the presence of red noise, this treatment of stellar spot anomalies may not be the best approach since the missing points in the transit light-curve can significantly underestimate the transit time. Moreover, in models that are based on the symmetry of the light curve, the missing points may break the light curve's symmetry, and as a result, the fitting routine may give more weight to the portion of the light curve that does not include the spot anomaly. This may cause variations in transit timing (shifting of the center of the light curve) and subsequently produce a TTV signal (e.g., Gibson et al. 2009; Oshagh et al. 2012).

In this paper, we present the results of a quantitative study on the effects of stellar spots on high-precision photometry observations. In Sect. 2, we describe the details of our models and initial conditions used in our simulations. Some of these require selection criteria that we also explain in this section. In Sect. 3, we present the results of the simulations for different cases and discuss possible interpretations. We also determine the detectable limits on the size of a spot considering the best precision of *Kepler* light curves. In Sect. 4, we conclude our study by summarizing the results and discussing their implications.

2. Models

We considered a system consisting of a late spectral-type star (e.g., FGKM), and a Jupiter- or Saturn-sized transiting planet.

We chose these stars because they form more than 70% of the stars in the solar neighborhood (Henry et al. 1997), and because they are routinely chosen as targets of transit photometry surveys (e.g., MEarth survey Charbonneau et al. 2008, and the *Kepler* Space Telescope). These combinations of planetary sizes and late spectral-type stars result in three values for the ratio of the planet-to-star radius, $R_p/R_* = 0.15, 0.1$, and 0.05. We also assumed the central star to have quadratic limb-darkening coefficients of $u1 = 0.29$ and $u2 = 0.34$, which corresponds to a stellar temperature close to that of the Sun ($\sim$5800 K) (Sing 2010; Claret & Bloemen 2011). Similar coefficients have been considered for the star HD 209458 in the wavelength range of 582−638 nm (Brown et al. 2001). In Sect. 4.3, we study the effect of other limb-darkening coefficients on our results.

Since we are interested in studying the maximum effect of a stellar spot, we assumed that the transiting planet and spot completely overlap and that the spot has no brightness. This model is able to produce a light curve that is close to a real one obtained from observations with the spot's anomaly inside the transit light-curve. Again in Sect. 4.3 we examine the effect of a stellar spot with non-zero brightness, as well. For the fitting purpose, we also determined the light curve of the star excluding the effect of the overlap between the planet and the stellar spot.

We assumed that the planet is in a three-day circular and edge-on orbit, and that the spot is located on zero latitude corresponding to the stellar equator. We varied the filling factor of this spot defined as

$$f = (R_{\mathrm{spot}}/R_*)^2 \qquad (1)$$

in the range of 0.01% to 1%. The upper limit of this range corresponds to the largest size of a Sun spot (Solanki 2003) (R_{spot} and R_* are the radii of the spot and star, respectively, and f is defined for the visible stellar disk). The sampling time of the observation was chosen to be 60 s, which is equal to the short-cadence integration time of the *Kepler* Space Telescope.

3. Simulations and results

To study the effects of stellar spots in the light curves of our models, we used the publicly available tool "SOAP-T"[1]. The code is explained in detail in Boisse et al. (2012) and Oshagh et al. (2013). This code produces the expected light curve and the radial velocity signal of a system consisting of a rotating spotted star with a transiting planet. SOAP-T is also able to reproduce the *positive bump* anomaly in the transit light-curve generated by a planet-spot overlap.

3.1. Amplitude of anomaly

We considered a rotating late-type star with a rotational period of nine days. We assumed that the star has a dark spot on its surface with a filling factor of 1%, and that it hosts a transiting planet with a radius of $R_p/R_* = 0.15$. We started our simulation by considering the spot to be on the longitude and overlap with the planet while on the limb of the star. In this case, the anomaly is produced in the egress of the transit light-curve. For the sake of comparison and fitting purposes, we also generated a synthesis transit light-curve with the same initial conditions without considering the overlap between the spot and planet. The residual between the light curve of this system and the previous one where the spot and planet overlap can be used to determine the
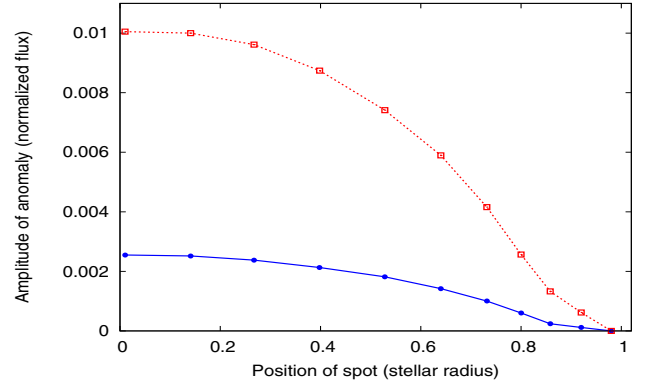
[1] http://www.astro.up.pt/resources/soap-t/

Fig. 1. Amplitude of the anomaly in the transit light-curve as a function of the position of planet-spot overlap (0 on *x*-axis means overlap occurs while the spot is at the center of stellar disk). The values of the amplitude have been normalized to the flux value. The red dotted line and the blue solid line correspond to transit light-curves of a transiting planet with a radius of $R_p/R_* = 0.15$ and a spot with a filling a factor of 1% and 0.25%, respectively.

amplitude of the anomaly. We repeated this process for different values of the spot's longitude and determined the magnitude of the amplitude of the transit light-curve anomaly as a function of the position of the spot on the disk of the star. As shown in Fig. 1, the amplitude of the anomaly increases as the position of the overlap between the planet and spot progresses toward the center of the stellar disk. When the overlap occurs while the spot is on the limb of star, the amplitude of the anomaly becomes smaller than when the spot and planet overlap at the center of the stellar disk. We note that the maximum amplitude of the anomaly is a function of the spot's filling factor. We repeated the same analysis with a spot with a filling factor equal to 0.25%. As shown in Fig. 1, the amplitudes of the anomalies corresponding to the two filling factors show the same behavior as a function of the position of the planet-spot overlap, but they have different magnitudes.

3.2. Effect of the stellar spot on the time, depth, and duration of the transit

In this section, we examine the effect of stellar spots on the transit light-curve and its corresponding planetary parameters. For this purpose, we generated a large number of transit light-curves for a system with a spotted star (as in Sect. 3.1), and to understand how the spot affects the parameters of the planet, we fit these light curves with the light curve of a system in which the effect of the spot-planet overlap was not taken into account. In the fitting procedure, we allowed the depth, duration, and time of the transit to vary as free parameters, keeping other parameters of the system constant to their values given in Sect. 3.1. The best fit of the no-anomaly light curve to each simulated transit light-curve with anomaly will give the best value for the ratio of the planet to the stellar radius, and the time and duration of its transit. To study the effects of the planet size and the spot filling factor, we considered the radius of the planet to be $R_p/R_* = 0.1$ and $R_p/R_* = 0.05$, and generated light curves in the spot-harboring system for a zero-brightness dark spot with a filling factor of 0.25% and 1%. We then fit again as explained above. Figure 2 shows some of the results: in simulations for which the position of the spot anomaly is toward the middle of the transit light-curve (i.e., the location of the planet-spot overlap is farther from the limb and is closer to the center of the stellar
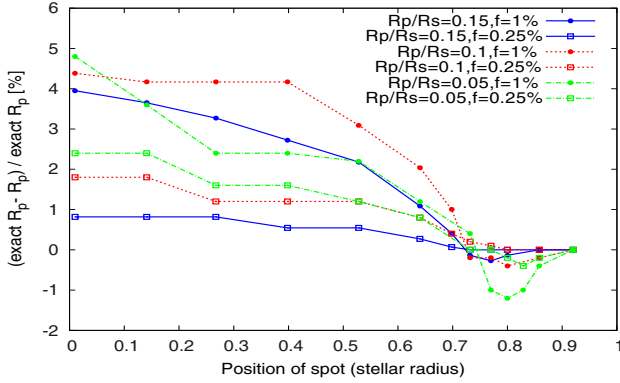
Fig. 2. Deviation of the fitted value of the planet radius from its exact value as a function of the position of planet-spot overlap. Different colors correspond to different combinations of the planet-to-star-radius ratio as well as the spot filling factor.
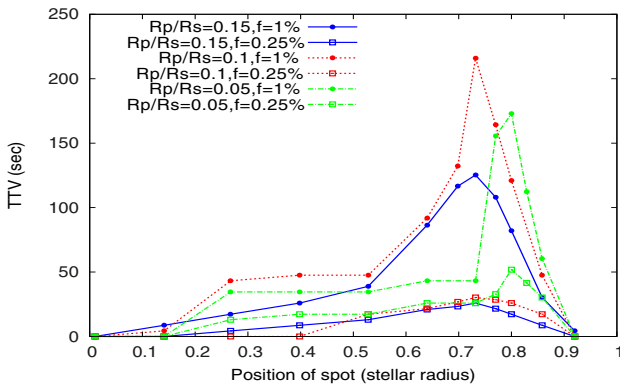

Fig. 3. Amplitude of the transit-timing variations as a function of the position of the planet-spot overlap, and for different combinations of the planet-to-star-radius ratio and the spot filling factor.

Fig. 4. Deviations of the fitted value of the transit duration from its exact value as a function of the planet-spot overlap for different combinations of the planet-to-star-radius ratio and spot filling factor.

disk), the fitted value of the transit depth (that is used to derive the radius of the planet in the units of stellar radius) becomes lower. For instance, in a system where the transiting planet has a radius of $R_p/R_* = 0.05$ and the spot filling factor is 1%, the anomaly in the light curve causes the estimate of the planet radius to be 4% smaller than its actual value. This significant effect in the size-estimates of exoplanets matches the values reported for active stars and transiting planets such as the CoRoT-2 system (3%, see Czesla et al. 2009) and the system of WASP-10 (2%), as reported by Barros et al. (2013).

Figure 3 shows the connection between the induced TTV and the position of the planet-spot overlap. The TTVs were obtained by calculating the difference between the transit timing in the best-fit model and its known values. Interestingly, the TTV amplitudes show a different behavior from that of the transit anomaly amplitude in term of its location. As shown in the figure, significant TTVs may be produced as a result of the spot anomaly in the transit light-curve even when the amplitude of the anomaly is not so significant. Our simulations show that the highest TTV value is reached when the position of the overlap between the planet and the spot is at 0.7 stellar radii from the center of the star. This result agrees with results presented by Barros et al. (2013). This indicates that when studying the effects of spot anomalies on variations in transit timing, one can only focus on this area where the TTV has its highest value. Figure 3 also shows that for a transiting planet with $R_p/R_* = 0.1$ overlapping a spot with a filling factor of 1%, the highest TTV value
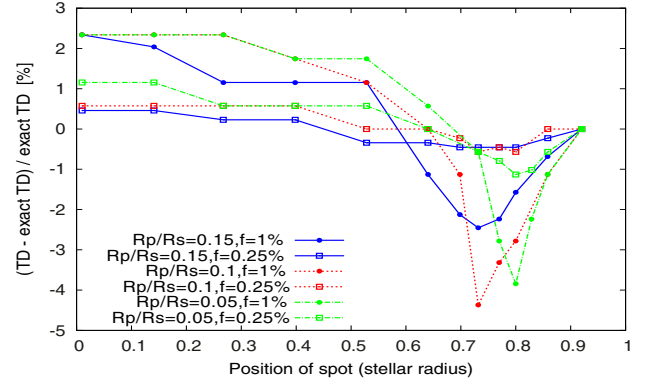
can exceed 200 s. Such a large TTV is similar to that induced by an Earth-mass planet in a mean-motion resonance with a Jovian-type body transiting a solar-mass star in a three-day orbit (e.g., Boué et al. 2012), or by an Earth-mass exomoon on a Neptune-mass transiting planet (Kipping 2009).

The connection between an induced spot anomaly in a transit light-curve and the duration of the transit is shown in Fig. 4. The transit duration can become shorter or longer, depending on where the anomaly appears. The results shown here agree with those reported by Barros et al. (2013) for the WASP-10 system. Figure 4 also shows that in extreme cases, transit durations can be under- or overestimated by about 4%. This can be seen, for instance, for planets with $R_p/R_* = 0.1$ and a spot filling factor of 1%.

3.3. Probing the effect of different limb-darkening coefficients and a non-zero-brightness spot

To probe the sensitivity of our results to the stellar spot brightness and also to quadratic limb-darkening coefficients, we examined their influence in cases where the maximum effect on TTVs were obtained.

To assess the effect of the choice of the quadratic limb-darkening coefficients, we considered the system with the highest TTV. In this system, the stellar spot was taken to have zero-brightness, its filling factor was 1%, and the ratio of the radius of the planet to that of the star was $R_p/R_* = 0.1$. We considered two extreme cases of stellar temperatures for this system. According to the Claret 2011 catalog (Claret & Bloemen 2011), these extreme temperatures correspond to extreme values for the limb-darkening coefficients. For a cool star with a temperature of 4000 K, the coefficients of the quadratic limb-darkening are $u1 = 0.6$ and $u2 = 0.16$, and for a hot star with a temperature of 7500 K, these coefficients are $u1 = 0.38$ and $u2 = 0.37$. Figures 5 to 7 show the effects of these extreme quadratic limb-darkening coefficients on the depth, as well as the amplitude of the TTV, and the transit duration. Apparently, the results are not sensitive to the choice of the two extreme cases considered here. This, however, cannot be reliable because we did not consider other possibilities. Studies similar to that of Csizmadia et al. (2013) are needed to fully explore the effect of varying the limb-darkening coefficients on the measurements of planetary parameters.

To study the effect of a stellar spot with a non-zero-brightness, we considered the brightness of the spot to be 50% of that of the star. We also increased its size by a factor 1.4 to
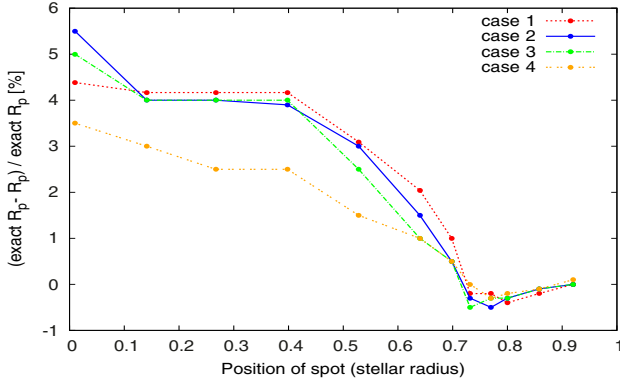
Fig. 5. Deviation of the fitted value of the planet radius and its exact value as a function of the planet-spot overlap. In cases 1 to 3, the transiting planet has a radius of $R_p/R_* = 0.1$, the spot has zero-brightness and a filling factor of 1%, and the limb-darkening coefficients are $(u_1, u_2) = (0.29, 0.34)$, $(0.38, 0.37)$, and $(0.6, 0.16)$, respectively. Case 4 is similar to case 1 with the brightness of the stellar spot increased to 50%.
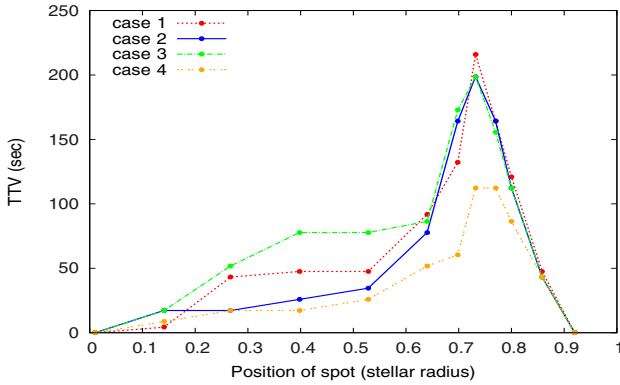

Fig. 6. Amplitude of transit-timing variation as a function of the position of the planet-spot overlap for the same cases as in Fig. 5.
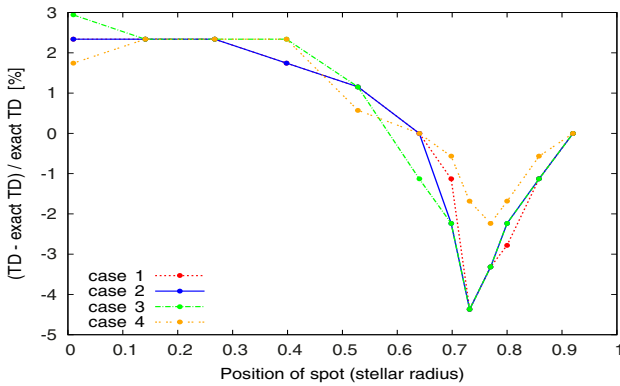

Fig. 7. Deviation of the fitted value of the transit duration from its exact value as a function of the position of the planet-spot overlap for the same cases as in Fig. 5.

compensate for the change in its brightness. This is equivalent to fixing the spot filling factor to 0.1%. As expected and similar to a zero-brightness spot, the spot with a non-zero brightness causes variations in the time, depth, and duration of the transit, but with smaller amplitudes (Figs. 5–7). This is an expected result because the occultation of the non-zero-brightness spot by the transiting planet produces an anomaly that has a smaller amplitude than that produced by a zero-brightness spot.
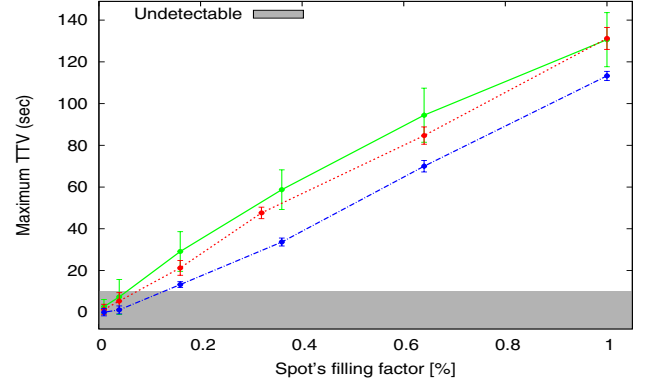
Fig. 8. Highest TTV value as a function of spot filling factor. The green, dotted red, and blue dotted-dashed lines correspond to a planet radius of $R_p/R_* = 0.05$, 0.1, and 0.15, respectively.

3.4. Estimating the spot size using its induced TTV

In this section, we estimate the maximum size of a stellar spot that will have no significant effect on a high-precision photometric observation (e.g. *Kepler*). The result of this study can be used to determine the minimum detectable size of a stellar spot by using the best accessible photometric facility.

We defined the minimum size of a stellar spot as the limit for which the corresponding anomaly in the transit light-curve cannot be identified visually and will only be detectable by its effect on transit-timing measurements. We considered a system with a transiting planet with a size of $R_p/R_* = 0.05$, 0.1, and 0.15 in a three-day orbit around a late-type spotted star. We assumed that the orbit of the planet is edge-on and circular. We assigned values of $u1 = 0.29$ and $u2 = 0.34$ to the star quadratic limb-darkening coefficients, and considered its rotational period to be nine days. We placed a dark stellar spot with a zero-brightness and filling factor of 1% on the longitude, which corresponds to 0.7 stellar radius in the time of overlap of planet and spot. To make the simulation closer to the real observation, we added a random Gaussian noise to each data point of the simulated light curve. The standard deviation of the Gaussian was chosen as the best standard deviation of a *Kepler* short-cadence observation for one of its brightest target stars ($\sigma = 0.00017$). We allowed the transit timing to vary as a free parameter and fit to this system a synthetic transit light-curve that was obtained without considering the effect of the overlap between the planet and the spot. The TTV values were obtained from the best-fit model. We note that we only used the TTVs generated by the spot anomaly in the transit light-curve as an indicator of the existence of a spot. Since a random noise was added to the simulation, we repeated this process 100 times and obtained the mean value and standard deviations (shown as error bars in Fig. 8) of the TTVs. We then reduced the filling factor of the spot and determined the TTV value. Figure 8 shows the behavior of the highest TTV value as a function of spot filling factor.

To determine the minimum size of a stellar spot, we progressively reduced the spot size until the amplitude of the TTV signal reached the *Kepler* detection limit. Following Kipping & Bakos (2011), we considered this limit to be about 10 s. As shown in Fig. 8, the minimum detectable size is obtained for a filling factor of 0.08%, which corresponds to a spot radius of 0.028 of the stellar radius. We would like to note that because we assumed that the overlap between planet and spot occurs at 0.7 stellar radii (where the amplitude of the effect is highest), the limit obtained
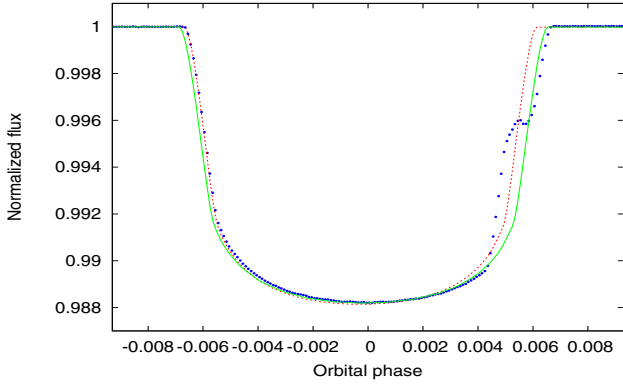
Fig. 9. Transit light-curve of a star with a spot anomaly shown as a blue dot and a transiting planet with a radius of $R_p/R_* = 0.1$. Overplotted is the best fit allowing transit duration, depth, and time to vary as free parameters (red dotted line), and the best fit obtained by holding the transit duration and depth constant and allowing only the transit timing to vary (green line).

from our analysis is in fact a lower limit. Any other positions of the same spot can also produce undetectable TTV signals.

A linear fit to the highest values of TTVs obtained for different values of the planet size and stellar spot filling factor indicates that the amplitude of TTVs caused by the stellar spot can be approximated by

$$ AMP = \begin{cases} 139 \times f & \text{if } R_p/R_* = 0.05 \\ 132 \times f & \text{if } R_p/R_* = 0.10 \\ 110 \times f & \text{if } R_p/R_* = 0.15, \end{cases} \tag{2} $$

where AMP is the maximum amplitude of TTV in units of seconds, and f is the stellar spot filling factor in percent.

The results of our simulations show that when transit duration and depth are held constant and equal to their known values, the TTV amplitude is smaller than when these parameters are let free. For a transit light-curve with stellar spot anomalies in egress or ingress, if in the fitting procedure we allow the transit duration, depth, and time to vary all as free parameters, the chi-square of the fit becomes smaller, but will not correspond to the best fit. As shown in Fig. 9, allowing the transit duration, depth, and time to be free parameters, the best fit may pass through the anomaly by reducing the transit duration and producing a very strong TTV signal. However, if the transit duration and depth are held constant, contrary to what is expected that more free parameters in the fitting process will result in more realistic planetary parameters (e.g. Mazeh et al. 2013), and allowing for variations in the transit timing will result in TTVs with smaller amplitudes.

4. Conclusions

We presented a quantifying analysis of the effect of stellar spots on a high-precision transit light-curve. We showed that light-curve anomalies caused by the overlap of a transiting planet and the star spot can have strong effects on the estimate of the planet parameters. These effects can lead to an underestimation of a the planet radius by about 4%. They can also affect the transit duration and make it 4% longer or shorter than its actual value. More importantly, depending on the size of the spot and its location, an anomaly can produce transit-timing variations with an amplitudes of about 200 s for a typical Sun-like spot. We also

found for an active star that allowing more free parameters (e.g., transit depth and duration) during transit fitting may lead to an erroneous estimation of the transit timing in comparison to the case where the transit depth and duration are held constant.

Because we considered only a few cases with different values of limb-darkening coefficients, we cannot conclude that our result are applicable to all values and combinations of these quantities. We have examined the reliability of our result for extreme cases of limb-darkening related to extreme stellar temperatures because it is reasonable to assume that if there is going to be any significant effect from limb-darkening, it will be from the extreme values of its coefficients. We did not, however, find any significant effects from those values in our study.

This study can be used to properly account for the difficulties arising from stellar activities in planet characterizations using the transit method. It also enables us to constrain the size of stellar spot using indirect techniques.

References

Alonso, R., Aigrain, S., Pont, F., Mazeh, T., & CoRoT Exoplanet Science Team. 2009, in IAU Symp. 253, eds. F. Pont, D. Sasselov, & M. J. Holman, 91
Ballerini, P., Micela, G., Lanza, A. F., & Pagano, I. 2012, A&A, 539, A140
Barros, S. C. C., Boué, G., Gibson, N. P., et al. 2013, MNRAS, 430, 3032
Basri, G., Walkowicz, L. M., & Reiners, A. 2013, ApJ, 769, 37
Berdyugina, S. V. 2005, Liv. Rev. Sol. Phys., 2, 8
Berta, Z. K., Charbonneau, D., Bean, J., et al. 2011, ApJ, 736, 12
Boisse, I., Moutou, C., Vidal-Madjar, A., et al. 2009, A&A, 495, 959
Boisse, I., Bouchy, F., Hébrard, G., et al. 2011, A&A, 528, A4
Boisse, I., Bonfils, X., & Santos, N. C. 2012, A&A, 545, A109
Boué, G., Oshagh, M., Montalto, M., & Santos, N. C. 2012, MNRAS, 422, L57
Brown, T. M., Charbonneau, D., Gilliland, R. L., Noyes, R. W., & Burrows, A. 2001, ApJ, 552, 699
Charbonneau, D., Irwin, J., Nutzman, P., & Falco, E. E. 2008, in BAAS, 40, Am. Astron. Soc. Meet. Abstr. #212, 242
Claret, A., & Bloemen, S. 2011, VizieR Online Data Catalog: J/A&A/529/A75
Csizmadia, S., Pasternacki, T., Dreyer, C., et al. 2013, A&A, 549, A9
Czesla, S., Huber, K. F., Wolter, U., Schröter, S., & Schmitt, J. H. M. M. 2009, A&A, 505, 1277
Désert, J.-M., Charbonneau, D., Demory, B.-O., et al. 2011, ApJS, 197, 14
Gibson, N. P., Pollacco, D., Simpson, E. K., et al. 2009, ApJ, 700, 1078
Henry, T. J., Ianna, P. A., Kirkpatrick, J. D., & Jahreiss, H. 1997, AJ, 114, 388
Kipping, D. M. 2009, MNRAS, 392, 181
Kipping, D., & Bakos, G. 2011, ApJ, 733, 36
Mazeh, T., Nachmani, G., Holczer, T., et al. 2013, ApJ, submitted [arXiv:1301.5499]
O'Neal, D., Saar, S. M., & Neff, J. E. 1998, ApJ, 501, L73
Oshagh, M., Boué, G., Haghighipour, N., et al. 2012, A&A, 540, A62
Oshagh, M., Boisse, I., Boué, G., et al. 2013, A&A, 549, A35
Pont, F., Gilliland, R. L., Moutou, C., et al. 2007, A&A, 476, 1347
Pont, F., Knutson, H., Gilliland, R. L., Moutou, C., & Charbonneau, D. 2008, MNRAS, 385, 109
Sanchis-Ojeda, R., & Winn, J. N. 2011, ApJ, 743, 61
Sanchis-Ojeda, R., Winn, J. N., Holman, M. J., et al. 2011, ApJ, 733, 127
Sing, D. K. 2010, A&A, 510, A21
Solanki, S. K. 2003, A&ARv, 11, 153
Strassmeier, K. G. 1999, A&A, 347, 225
Tas, G., & Evren, S. 2000, Information Bulletin on Variable Stars, 4992, 1

Impact of the occultation of stellar active regions on transmission spectra

Most of the attempts to characterize exoplanetary atmospheres have been performed through the use of transmission spectroscopy (multiband photometry) of transiting exoplanets. The transmission spectroscopy is based on the observations of the planetary transit in different wavelengths and determining the planet-to-star radius ratio as a function of wavelength. Then the planet-to-star radius ratio wavelength variations can then be interpreted as a presence of planetary atmosphere.

In most transmission spectroscopy studies, however, the impact of stellar activity on the estimate of the planetary radius has not been taken into account. Only in a few cases the influence of activity features has been discussed but only the impact of non-occulted stellar spots (spots that are not occulted by the planet during the transit) was examined.

In my fourth paper, we examine the possible impact of the occultation of stellar activity features, such as spots and plages, on transmission spectra. In this paper for the first time, we explore the impact of the presence of plages (plage is a bright region in the stellar chromosphere). We find that the anomalies inside the transit light curve , due to occulation of stellar spot/plage by the transiting planet, can lead to a significant underestimation or overestimation of the planet-to-star radius ratio as a function of wavelength. At short wavelengths, the effect

can reach up to a maximum difference of 10% in the planet-to-star radius ratio, mimicking the signature of light scattering in the planetary atmosphere.

To demonstrate the application of our idea, we showed that the transmission spectroscopy measurements of the active stars HD 189733b and GJ 3470b, and especially their excess of the planet radius in the bluer part of the spectra, can almost exactly be reproduced by assuming the occultation of the HD 189733b and GJ 3470b with the active region (plage) of their host star.

Astronomy & Astrophysics

Impact of occultations of stellar active regions on transmission spectra

Can occultation of a plage mimic the signature of a blue sky?

M. Oshagh[1,2,3], N. C. Santos[1,2,3], D. Ehrenreich[4], N. Haghighipour[5], P. Figueira[1,3], A. Santerne[1,3], and M. Montalto[1,3]

[1] Centro de Astrofísica, Universidade do Porto, Rua das Estrelas, 4150-762 Porto, Portugal
e-mail: moshagh@astro.up.pt
[2] Instituto de Astrofísica e Ciências do Espaço, Universidade do Porto, CAUP, Rua das Estrelas, 4150-762 Porto, Portugal
[3] Departamento de Física e Astronomia, Faculdade de Ciências, Universidade do Porto, Rua do Campo Alegre, 4169-007 Porto, Portugal
[4] Observatoire de Genève, Université de Genève, 51 chemin des Maillettes, 1290 Sauverny, Switzerland
[5] Institute for Astronomy and NASA Astrobiology Institute, University of Hawaii-Manoa, 2680 Woodlawn Drive, Honolulu HI 96822, USA

ABSTRACT

Transmission spectroscopy during planetary transits, which is based on the measurements of the variations of the planet-to-star radius ratio as a function of wavelength, is a powerful technique to study the atmospheric properties of transiting planets. One of the main limitations of this technique is the effects of stellar activity, which up until now, have been taken into account only by assessing the effect of non-occulted stellar spots on the estimates of the planet-to-star radius ratio. In this paper, we study the impact of the occultation of a stellar spot and plage on the transmission spectra of transiting exoplanets for the first time. We simulated this effect by generating a large number of transit light curves for different transiting planets, stellar spectral types, and different wavelengths. Results of our simulations indicate that the anomalies inside the transit light curve can lead to a significant underestimation or overestimation of the planet-to-star radius ratio as a function of wavelength. At short wavelengths, the effect can reach to a difference of up to 10% in the planet-to-star radius ratio, mimicking the signature of light scattering in the planetary atmosphere. Atmospheric scattering has been proposed to interpret the increasing slopes of transmission spectra toward blue for exoplanets HD 189733b and GJ 3470b. Here, we show that these signatures can be alternatively interpreted by the occultation of stellar plages. Results also suggest that the best strategy to identify and quantify the effects of stellar activities on the transmission spectrum of a planet is to perform several observations during the transit epoch at the same wavelength. This will allow for identifying the possible variations in transit depth as a function of time due to stellar activity variability.

Key words. planets and satellites: atmospheres – techniques: photometric – methods: data analysis – methods: numerical – stars: activity

1. Introduction

Most attempts in characterizing exoplanetary atmospheres have been made by using the transmission spectroscopy (multiband photometry) of transiting exoplanets. In this approach, observations of planetary transits in different wavelengths are used to determine planet-to-star radius ratio, $R_p/R_* = k(\lambda)$, as a function of color. The inferred wavelength dependence of this quantity is the result of differential absorption in the planetary atmosphere (Seager & Sasselov 2000; Brown et al. 2001; Charbonneau et al. 2002) which has been used to constrain different atmospheric composition models: for example GJ 3470b (Demory et al. 2013; Fukui et al. 2013; Nascimbeni et al. 2013; Crossfield et al. 2013), GJ 1214b (Kreidberg et al. 2014), HD 209458b (Désert et al. 2008), and HD 189733b (Pont et al. 2007, 2008, 2013; Ehrenreich et al. 2007; Sing et al. 2009, 2011).

Although the magnitude of the planet-to-star radius ratio is strongly affected by the activity of the central star and its corresponding surface features (Czesla et al. 2009; Oshagh et al. 2013a), except for the systems of GJ436, GJ3470, and HD 189733 (Pont et al. 2007, 2013; Knutson et al. 2011; Sing et al. 2011; Nascimbeni et al. 2013), in most studies using

transmission spectroscopy, the impact of stellar features has not been taken into account. Even in the cases of GJ436 and GJ3470, only the impact of non-occulted stellar spots has been discussed. The system of HD 189733 is the only case in which the effect of the occulted stellar spot inside the transit has been taken into account.

The main objective of this paper is to examine the possible impact of the occultation of stellar activity features (such as spots and plages) by transiting planets, on transmission spectra. In particular and for the first time, we explore the impact of the occultation of plages (bright regions in the stellar chromosphere). We perform a large number of simulations to quantify the impact of this effect on the transit depth measurements in different wavelengths and for various physical configurations. To demonstrate the application of our results, we apply our methodology to the planetary systems of two active stars HD 189733 and GJ 3470. Due to their low density and large planet-to-star radius ratio, these systems are among the most favorable targets for atmospheric characterization purposes. The measurements of planet radii in these systems have shown an excess in the short wavelength regime of 300–800 nm. Several studies of the entire transmission spectra of these two planets have contributed those

observed excesses to Rayleigh scattering processes in the planets' atmospheres. In this paper, we investigate the possibility of explaining these excesses features by taking the effects of stellar spots and plages occultation into account.

In Sect. 2, we present the details of our models that are used to produce light curves of a system which has a planet transiting plages and spots on the surface of its host star. In Sect. 3, we apply our models to different configurations of stars with different spectral types, stellar activity features, and for planet radii corresponding to wavelengths ranging from 400 nm to 4500 nm. In Sect. 4 we reanalyze the transmission spectra of HD 189733b as reported by Pont et al. (2013) and GJ 3470b as reported by Nascimbeni et al. (2013), and explore possible scenarios which could reproduce the same transmission spectra by invoking only occultation of stellar plages. In Sect. 5, we conclude our study by summarizing the results and discussing their implications.

2. Description of the model

We considered a transiting system with a planet in a 3 day orbit. We chose the central star to be of spectral types M and G and took the planet to be of Jupiter (J) and Neptune (N) sizes. The G star was chosen to be Sun-like and the radius of the M star was taken to be 0.7 solar-radii. Both stars have a rotational period of 9 days. The planet-to-star radius ratios in these systems are 0.035, 0.1, 0.05, and 0.15 for the NG, JG, NM, and JM systems, respectively. We chose these systems because the large values of their planet-to-star radius ratio make them favorable for planet atmosphere studies.

To study the effects of spots and plages, we assigned them a filling factor defined as

$$f = \frac{A_s}{A_*} = \left(\frac{R_s}{R_*}\right)^2. \tag{1}$$

In this equation, A_s is the area of the stellar activity feature, R_s is its radius, and A_* is the area of the stellar disk. In applying Eq. (1) to spots, we considered f to be 0.25% and 1% where 1% is the largest filling factor of a Sun spot (Solanki 2003; Meunier et al. 2010). For plages, we considered f = 0.25%, 1%, and 6.25%, in which the maximum value coincides with the maximum filling factor of a Sun's plage (Meunier et al. 2010). At the time of the overlap between the transiting planet and the stellar activity feature, we assumed that the feature is on the star's equator and at a longitude equal to 0.5 stellar radii. As shown by Oshagh et al. (2013a), the maximum underestimation of the planet radius in the transit light curve with a spot anomaly inside the transit occurs when the spot anomaly appears in the center of the transit light curve.

2.1. Generating light curves

To generate the light curves of our system, we used the publicly available software SOAP-T (Oshagh et al. 2013b). This software has the capability of producing light curves of systems where a transiting planet orbits a rotating star with activity features in the form of stellar spots or plages. The three wavelength-dependent stellar parameters in this software, namely the coefficients of quadratic stellar limb darkening (u_1 and u_2) and the relative brightness of stellar active regions (b) enable one to produce light curves for different values of wavelength. Table 1 shows the values of u_1 and u_2 adopted from the catalog by Claret & Bloemen (2011) for the values of the wavelength used in our

Table 1. Quadratic limb darkening coefficients for M and G stars in different wavelength (Claret & Bloemen 2011).

λ(nm)	400	800	1500	3000	4500
M-dwarf					
u_1	0.45	0.43	0.40	0.05	0.05
u_2	0.36	0.34	0.36	0.20	0.18
G-dwarf					
u_1	0.70	0.30	0.10	0.07	0.05
u_2	0.18	0.30	0.32	0.14	0.12

simulations. These wavelengths have been chosen to cover the entire visible spectrum and the near- and mid-infrared ranges.

To determine the value of b, we note that this quantity can be written as

$$b(\lambda) = \frac{\exp[hc/\lambda K_B T_*] - 1}{\exp[hc/\lambda K_B T_s] - 1} \tag{2}$$

to the first-order of approximation. In this equation, h is the Planck constant, c is the speed of light, K_B is the Boltzmann constant, T_* is the stellar temperature, and T_s denotes the temperature of the activity feature. We considered $T_* = 5780$ K and 3000 K for our G and M stars, respectively. For any star with a temperature within this range, the amplitude of the effect of the occultation of its active region is between that of these two stars (Fig. 3).

To obtain the value of T_s for a stellar spot, we used Fig. 7 of Berdyugina (2005), where the observed temperature of spots for stars with different spectral types is presented. For plages, this temperature has only been measured for the Sun (Worden et al. 1998; Unruh et al. 1999; Meunier et al. 2010), which showed the maximum temperature contrast of 300 K for a plage at the Sun's limb and the minimum of 100 K at the center of the Sun. We note that the spots on the surface of the Sun show a limb-darkening effect. That is, a Sun spot at the center of the Sun's disk shows a higher contrast compared to the one on the Sun's limb (Unruh et al. 1999; Meunier et al. 2010). On the contrary, a Sun plage shows a limb brightening behavior, which means that a Sun plage on the Sun's limb displays higher contrast compared to that on the center of the Sun's disk (Meunier et al. 2010). The values for the temperature of spots and plages in this study have been chosen by considering this opposite behavior of the spot's limb darkening and the plage's limb brightening. This enabled us to consider the impact of the position of a stellar spot/plage on its maximum temperature-contrast when simulating our systems. For instance, a stellar spot in the center of the stellar disk could reach the maximum possible temperature-contrast with the stellar photosphere, whereas a plage in that location would reach only a third of the maximum possible plage temperature-contrast. By taking into account that in our simulations, we consider that the plages are located at the center of the stellar disk, therefore, we use a 100 K temperature contrast for a plage on the surface of our G star, and by assuming that on an M star, a plage at its maximum temperature contrast will have a similar temperature-difference. Table 2 shows the values of T_s for all our models. The variations of $b(\lambda)$ as a function of the wavelength is shown in Fig. 1.
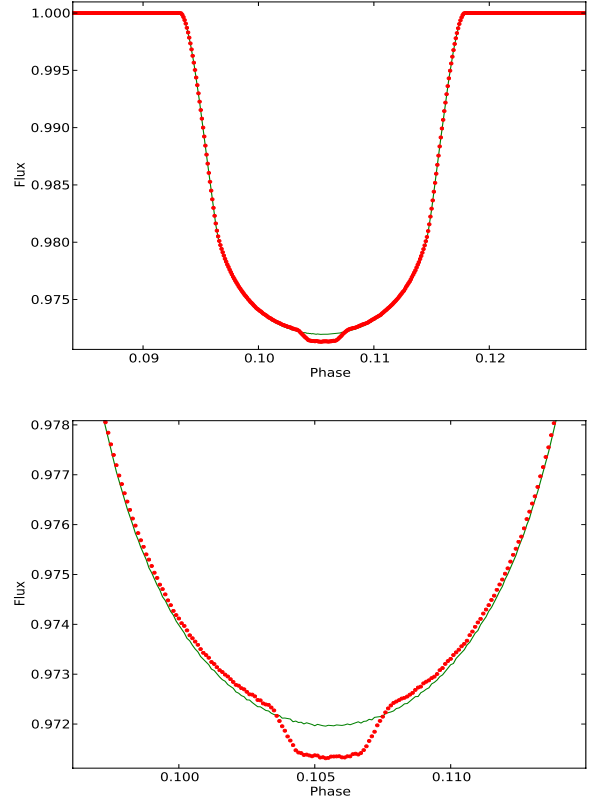
3. Results of simulations

We generated a large number of mock transit light curves for our G and M stars by considering transiting planets with radii equal to those of Neptune and Jupiter. As we are interested in

Table 2. Detailed parameters of our models.

Model number	T_*	T_s	f	R_p/R_*
G dwarf+ spot				
1	5780	4000	0.25%	0.035
2	5780	4000	0.25%	0.1
3	5780	4000	1%	0.035
4	5780	4000	1%	0.1
G dwarf+ plage				
5	5780	5880	0.25%	0.035
6	5780	5880	0.25%	0.1
7	5780	5880	1%	0.035
8	5780	5880	1%	0.1
9	5780	5880	6.25%	0.035
10	5780	5880	6.25%	0.1
M dwarf + spot				
11	3000	2500	0.25%	0.05
12	3000	2500	0.25%	0.15
13	3000	2500	1%	0.05
14	3000	2500	1%	0.15
M dwarf + plage				
15	3000	3100	0.25%	0.05
16	3000	3100	0.25%	0.15
17	3000	3100	1%	0.05
18	3000	3100	1%	0.15
19	3000	3100	6.25%	0.05
20	3000	3100	6.25%	0.15
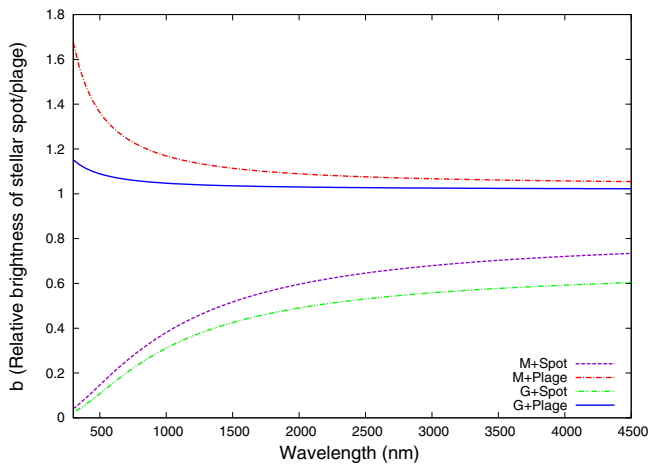
Fig. 1. Relative brightness of stellar spots and plages on M and G stars as a function of wavelength. The details of the parameters of spots, plage, and stars are listed in Table 2.

Fig. 2. *Top*: a sample light curve of our simulations. The system consists of an M star with a 9 day rotational period with a Jupiter-sized planet ($R_p/R_* = 0.15$) in a 3 day orbit. We considered a plage with a filling factor of 0.25% on the surface of the star. The red curve corresponds to the case when the transiting planet occults the plage. The green curve shows the best fit transit light curve without considering the occultation. *Bottom*: zoomed-in at the bottom of light curve.

determining the impact of the occultation of stellar active regions on the estimates of the radius of the transiting planet, we considered our stars to contain plages or spots and generated light curves for different values of wavelength (see Table 1). As a result, all the generated mock light curves exhibited anomalies in their transit parts. To examine the effects of these anomalies on the estimates of the planet radius, we fit all these mock light curves with transit light curve models corresponding to systems in which the planet does not occult the stellar active region. In each fitted model, we set all the parameters equal to those used to generate the system's initial mock light curve, except for the planet's radius, which we allowed to vary freely. In general, the latter curves show the exact same behavior as those with anomalies, except for inside the transit where the spot/plage occulted anomalies exist. Figure 2 shows a sample of our fitting results (model 16 in Table 2). The light curve in red corresponds to the

system in which the planet occulted a stellar plage. The green curve represents the best-fitted transit without the occultation of that plage.

It is important to mention that during the fitting procedure, we allow the depth of the transit to vary as a free parameter, while holding other parameters of the system constant. In that case the best fit anomaly-free light curve is used to determine the best planet-to-star radius ratio for each light curve with inside transit anomalies. It should be noted that only part of the spot/plage would be covered by the planet in systems where the planet radius is smaller than the radius of the stellar active region (for instance, model 3 in Table 2) and as a result, the remaining fraction of the spot/plage will affect the out-of-transit light curve similar to an un-occulted spot/plage. However, as explained above, in our simulations, the only difference between the light curve containing an anomaly and the anomaly-free light curve is only inside their transits, this out-of-transit light will not affect the results of our fitting.

Figure 3 shows the relative error in the estimate of the planetary radius obtained from the anomaly-free fitting procedure compared to the radius of the planet that is used in generating the mock light curves (i.e., Neptune or Jupiter radii). As shown here, the underestimation or overestimation of the planet-to-star radius ratio can be quite high (~10%), particularly on the blue side of the spectrum where the stellar active regions show higher contrast. These results also suggest that the stellar spot/plage filling factor seems to play an important role in the estimate of the planet's radius. For instance, the maximum effect appears for
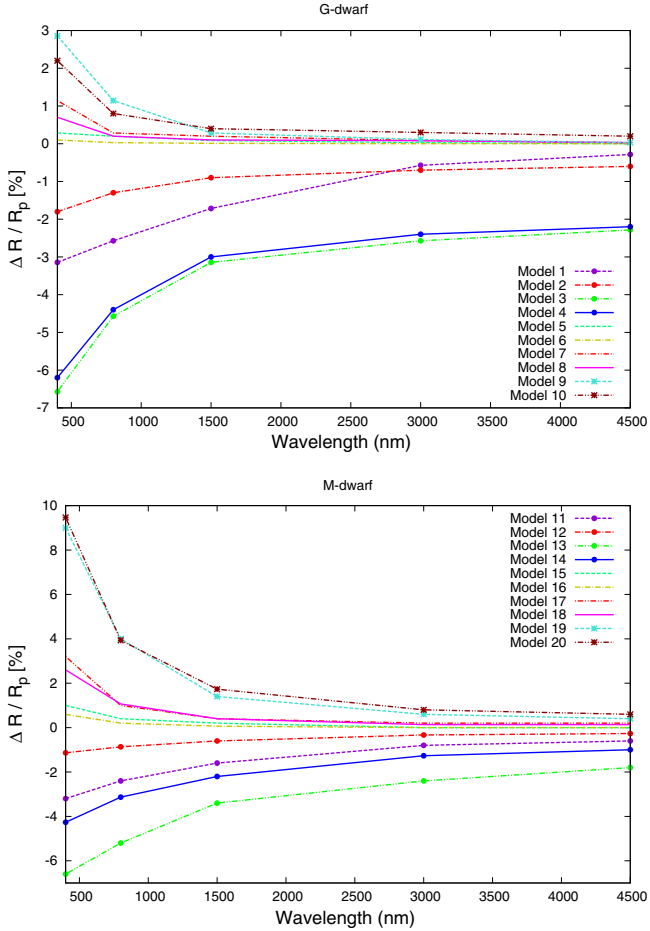
Fig. 3. Relative error in the estimate of the radius of a transiting planet as a function of wavelength calculated by comparing the value of the planet radius obtained from the best-fitted anomaly-free light curve with that obtained from the light curve by taking the effects of stellar spots and plages occultation into account. Different colors correspond to different models, as described in Table 2.

the largest filling factors corresponding to models 3, 4, 9 and 10 in the models where a Jupiter- or Neptune-sized planet orbit a G-dwarf (see Table 2). It should be noted that the temperature contrast between a stellar active region and its surrounding area and the value of the filling factor impose a strong degeneracy to the estimate of the planet's radius. That is, a variation in the temperature contrast of a spot or plage can be compensated by a properly chosen value of the filling factor, such that different combinations of temperature contras/filling factor produce the same value for the planet's radius.

As we noted earlier in all our simulations, we assumed that the stellar rotation axis is parallel to the plane of sky, the orbit of the transiting planet is edge-on, and the occultation of a spot/plage occurs when this feature is on the center of the star's disk. As a result of these assumptions, the values presented here are upper limits.

4. Reanalyzing HD 189733b and GJ 3470b: Do they have blue skies?

4.1. HD 189733b

HD 189733 is a K-dwarf with an effective temperature of 5050 K, surface gravity of $\log g = 4.53$, and brightness of $V \simeq 7.7$ (Sing et al. 2011). The short-period planet of this star,
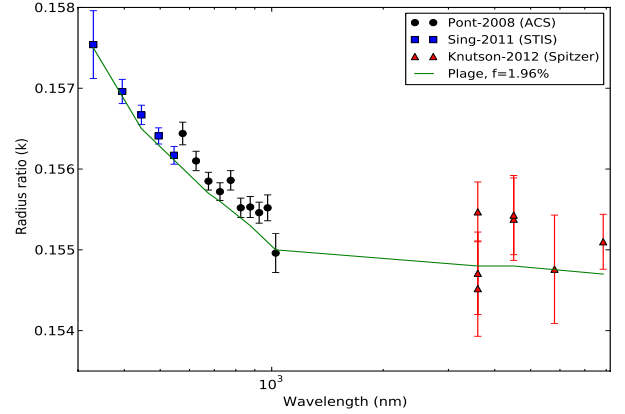
Fig. 4. Observed transmission spectrum of HD 189733b and reconstructed transmission spectrum by assuming the planet overlapping a stellar plage. The excess in the estimate of the planet radius-ratio in the blue side of spectrum can be reproduced by presuming a plage on the surface of HD 189733. See text for more details.

HD 189733b, is a Jupiter-like body in a 2.2 day orbit with a scaled semimajor axis of $a/R_* = 8.92$ (Pont et al. 2007). The ratio of the radius of HD 189733b to that of its host star is 0.155. The large atmospheric scale height of HD 189733b has made this planet one of the best studied systems in the studies of exoplanetary atmospheres (e.g., Lecavelier Des Etangs et al. 2008; Pont et al. 2008, 2013; Sing et al. 2011). As reported by Sing et al. (2011) and Pont et al. (2013), HD 189733b shows an excess in its radius in the entire visual band (300−800 nm), which can be attributed to Rayleigh scattering in the planet's atmosphere.

The star HD 189733 is a highly active star. It has a strong X-ray emission and intense chromospheric Ca II H and K lines, which suggest a high level of activity on the surface of this star (Knutson et al. 2010; Poppenhaeger et al. 2013). During its 12 day stellar rotation, HD 189733 also shows photometric modulation (Photo$_{var}$) of up to $\simeq 2\%$ in the mean b and y Strömgren bands (510 nm) (Boisse et al. 2009; Sing et al. 2011). Sing et al. (2011) have shown that the light curve of HD 189733 carries clear signatures of stellar spot occultation inside its transit. These authors and, more recently, Pont et al. (2013) studied the effects of occulted and non-occulted stellar spots on the estimates of the radius of HD 189733b and found that these anomalies have significant effects on the accurate measurements of the planet's radius.

We examined the possible influences of stellar plages on the spectra of HD 189733b and the measurement of its radius. Following the procedure described in Sect. 3, we generated mock light curves of HD 189733 for different values of wavelength by considering an overlap between a plage and the transiting planet. We then fitted these mock light curves with models in which the planet/plage occultation was not taken into account. Results of our analysis indicated that the observed transmission spectrum of HD 189733b can be reproduced by considering the planet that occults a stellar plage with a filling factor of 1.96% and a temperature-contrast of 100 K. As shown in Fig. 4, the observed excess in the planet radius in the bluer part of spectrum is also well matched by the predictions of the plage-occultation scenario.

By considering the above filling factor and the relative brightness of a plage as obtained from Eq. (2), we found that the amplitude of the photometric modulations of HD 189733 is approximately 0.4% at 510 nm wavelength, which is noticeably smaller than the ~2% value obtained from observation.

This suggests that our proposed scenario (i.e., the occultation of a plage on the surface of the star) is physically viable. We note here that as explained before, determining the plage's temperature and filling factor introduce a strong degeneracy in the modeling process. For instance, if we considered a temperature ratio of ∼0.87 for HD 189733 compared to the Sun and used this ratio to estimate the temperature contrast of a plage on the surface of HD 189733 (∼65 K), the required plage's filling factor for reproducing the transmission spectra of HD 189733b would be around 2.89%.

4.2. GJ 3470b

The star GJ 3470 is an M-star with a temperature of 3600 K and surface gravity of $\log g = 4.658$ (Demory et al. 2013). This star is host to a Uranus-mass planet (GJ 3470b) in a 3.34 day orbit with a scaled semimajor axis of $a/R_* = 14.02$ (Fukui et al. 2013) and a planet-to-star radius ratio of 0.078. The planet GJ 3470b was first discovered with the radial velocity technique using the HARPS spectrograph. The transits of this planet were later detected through ground-based follow-up observation by Bonfils et al. (2012). Recently, several attempts were made to characterize the atmosphere of GJ 3470b using ground- and space-based facilities (Fukui et al. 2013; Demory et al. 2013; Crossfield et al. 2013; Nascimbeni et al. 2013; Ehrenreich et al. 2014). These observations indicated that the planet's atmosphere has a flat infrared spectrum between 1 and 5 μm, suggesting an increase in slope toward the blue side of spectrum ($\lambda \sim 360$ nm), which was interpreted by Nascimbeni et al. (2013) to be the result of Rayleigh scattering in the atmosphere.

As suggested by Bonfils et al. (2012) GJ 3470 may not be a very active star because of its slow rotation. Fukui et al. (2013) confirmed this finding by using photometric observations and stated that thus star may not be very active, although GJ 3470 showed photometric variability of approximately $\text{Phot}_{\text{var}} \simeq 1\%$ at Ic-band (786.5 nm), during the course of their 60-day observations. Those variabilities can be explained by assuming that GJ 3470 harbors a spot with a filling factor of 1%. The latter motivated Nascimbeni et al. (2013) to study the possible contribution of a non-occulted stellar spot on the spectrum of GJ 3470b, and they concluded that their results are not affected by that effect. In this section, we examine whether an occulted stellar plage can affect the results.

We generated synthetic transit light curves of GJ 3470b by considering plage occultation anomalies inside the transit for different values of wavelength. We found that the observed excess in the planet's radius in short wavelengths can be explained by the overlap of this planet with a plage with a filling factor of 2.56% and temperature contrast of 100 K (Fig. 5). The size and relative brightness of such a plage results in photometric variations of about 1.3% at 786 nm wavelength, which is compatible with the observed value 1%.

In larger wavelengths, however, our plage occultation scenario was not able to properly model the results reported by Nascimbeni et al. (2013) (at the wavelength of 963 nm) and the values reported by Ehrenreich et al. (2014) for wavelengths between 1170 and 1650 nm. One explanation is that the obtained planet radius was systemically offset toward a large value causing no significant decrements to be observed in the planet radius in the range of 963−1650 nm during two successive transits of the planet at 4520 nm detected by Demory et al. (2013). To examine this possibility, we assumed that the actual planet-to-star radius ratio is smaller than the reported value (0.077) and
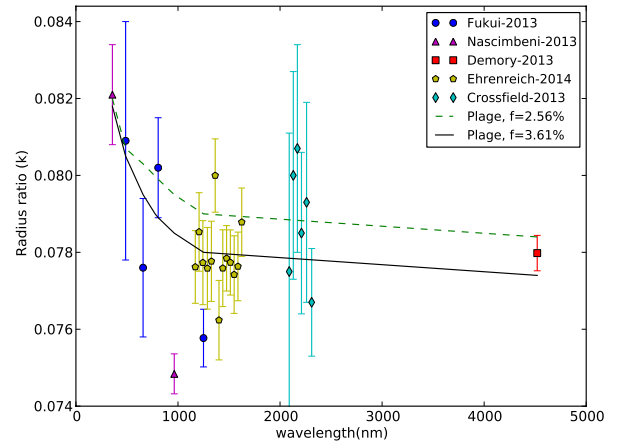

Fig. 5. Observed transmission spectrum of GJ 3470b and reconstructed transmission spectrum by assuming the planet overlapping a stellar plage. The excess in the estimate of the planet radius-ratio in the blue side of spectrum can be reproduced by presuming a plage on the surface of GJ 3470. See text for more details.

obtained in this case, the minimum required plage's filling factor is ∼3.61% with a temperature contrast of 100 K (Fig. 5).

We note that these values for the plage's temperature and filling factor strongly depend on the choice of the temperature contrast. For instance, if we use a temperature ratio of GJ 3470 to that of the Sun (∼0.62) to estimate the temperature contrast of a plage on the surface of GJ 3470 (∼45 K), the plage's filling factors of 2.56% and 3.61% increase to 7.29% and 9%, respectively.

5. Discussion and conclusions

For the first time, we present the results of a study on the effect of the occultation of a stellar plages and spots on the transmission spectroscopy measurements of a planet. We carried out simulations by considering transiting systems with G or M stars, Jupiter- or Neptune-sized planets, and different values of a spot/plage's filling factor in different wavelength. Results indicated that there could be significant underestimation or overestimation of the planet-to-star radius ratio as a function of the wavelength. The maximum overestimation of the planet radius (10%) may occur for the occultation of a plage by a planet that transits an M-dwarf in the short wavelength regime. Application of our calculations to the systems of the stars, HD 189733 and GJ 3470, indicated that the transmission spectroscopy measurements of the planets of these stars, and especially the reported excess in their planet-to-star radius ratio in the bluer part of the spectra, which were interpreted as the signature of blue sky, can almost exactly be reproduced by assuming that the planet occults a plage on the surface of these stars.

The results of our study strongly suggest that it is crucially important to rule out the possible contamination in the measurements due to effects of stellar activities (both occulted and non-occulted active regions) prior to interpreting the values obtained for the radius of a transiting planet in different wavelengths and attempting to set constrains on the planet's atmospheric models. The best strategy for doing so is to carry out several observations of a transit in a given wavelength and use the variations of transit depth as a function of time to assess the impact of potential stellar spot/plage occultation. In case of a very active star, which always harbors stellar spots or plages, all transits could be affected by the occultation. In that case, the alternative strategy would be to carry out simultaneous multiband photometric observations
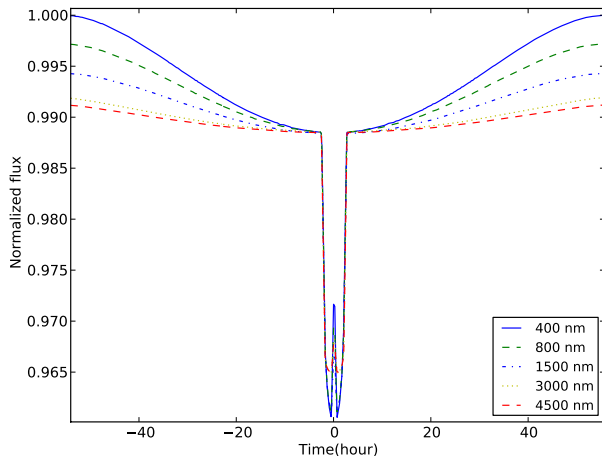
Fig. 6. Out-of-transit light curves for different wavelengths in a system with a stellar spot.

for several hours, which can correspond to half of the stellar rotation period before and after the transit. These observations will allow us to diagnose the presence of stellar spots/plages during the transit and can also provide information about the parameters of these regions, such as their sizes and temperature contrasts. Figure 6 shows an example of the distinct behavior of an out-of-transit light curve in different wavelengths in the present of a stellar spot. The system depicted here consists of a Jupiter-sized planet with $R_p/R_* = 0.15$, which orbits in a 3-day orbit around an M-dwarf. The M-dwarf has a rotation period of 9 days and harbors a spot with 1% filling factor.

We note that the results presented here are based on simple assumptions. For instance, we always assumed that the transiting planet would occult the same plage at each epoch. This could be true in the case of a very active star, such as HD 189733. Our simulations were done by assuming a circular spot and plage which might affect the determination of spot/plage's filling factor. We also considered a constant temperature contrast of 100 K between a plage and its surrounding region on the star's photosphere. However, this value could be different for different stars. Larger or smaller temperature contrasts will result in lower or higher values for the filling factor. Finally, we assumed that the plage occultation anomalies appear in the middle of transit light curve, so that it would have the maximum impact on planet radius estimations. However, if these anomalies appear in other locations in the transit light curve, different values of the filling factor and/or plage-photosphere temperature contrast are required to account for the observed transmission spectroscopic properties of the system.

References

Berdyugina, S. V. 2005, Liv. Rev. Sol. Phys., 2, 8
Boisse, I., Moutou, C., Vidal-Madjar, A., et al. 2009, A&A, 495, 959
Bonfils, X., Gillon, M., Udry, S., et al. 2012, A&A, 546, A27
Brown, T. M., Charbonneau, D., Gilliland, R. L., Noyes, R. W., & Burrows, A. 2001, ApJ, 552, 699
Charbonneau, D., Brown, T. M., Noyes, R. W., & Gilliland, R. L. 2002, ApJ, 568, 377
Claret, A., & Bloemen, S. 2011, VizieR Online Data Catalog, 352, 99075
Crossfield, I. J. M., Barman, T., Hansen, B. M. S., & Howard, A. W. 2013, A&A, 559, A33
Czesla, S., Huber, K. F., Wolter, U., Schröter, S., & Schmitt, J. H. M. M. 2009, A&A, 505, 1277
Demory, B.-O., Torres, G., Neves, V., et al. 2013, ApJ, 768, 154
Désert, J.-M., Vidal-Madjar, A., Lecavelier Des Etangs, A., et al. 2008, A&A, 492, 585
Ehrenreich, D., Hébrard, G., Lecavelier des Etangs, A., et al. 2007, ApJ, 668, L179
Ehrenreich, D., Bonfils, X., Lovis, C., et al. 2014, A&A, in press,
    DOI: 10.1051/0004-6361/201423809
Fukui, A., Narita, N., Kurosaki, K., et al. 2013, ApJ, 770, 95
Knutson, H. A., Howard, A. W., & Isaacson, H. 2010, ApJ, 720, 1569
Knutson, H. A., Madhusudhan, N., Cowan, N. B., et al. 2011, ApJ, 735, 27
Kreidberg, L., Bean, J. L., Désert, J.-M., et al. 2014, Nature, 505, 69
Lecavelier Des Etangs, A., Pont, F., Vidal-Madjar, A., & Sing, D. 2008, A&A, 481, L83
Meunier, N., Desort, M., & Lagrange, A.-M. 2010, A&A, 512, A39
Nascimbeni, V., Piotto, G., Pagano, I., et al. 2013, A&A, 559, A32
Oshagh, M., Santos, N. C., Boisse, I., et al. 2013a, A&A, 556, A19
Oshagh, M., Boisse, I., Boué, G., et al. 2013b, A&A, 549, A35
Pont, F., Gilliland, R. L., Moutou, C., et al. 2007, A&A, 476, 1347
Pont, F., Knutson, H., Gilliland, R. L., Moutou, C., & Charbonneau, D. 2008, MNRAS, 385, 109
Pont, F., Sing, D. K., Gibson, N. P., et al. 2013, MNRAS, 432, 2917
Poppenhaeger, K., Schmitt, J. H. M. M., & Wolk, S. J. 2013, ApJ, 773, 62
Seager, S., & Sasselov, D. D. 2000, ApJ, 537, 916
Sing, D. K., Désert, J.-M., Lecavelier Des Etangs, A., et al. 2009, A&A, 505, 891
Sing, D. K., Pont, F., Aigrain, S., et al. 2011, MNRAS, 416, 1443
Solanki, S. K. 2003, A&ARv, 11, 153
Unruh, Y. C., Solanki, S. K., & Fligge, M. 1999, A&A, 345, 635
Worden, J. R., White, O. R., & Woods, T. N. 1998, ApJ, 496, 998

Chapter 7

Conclusions and future works

7.1   Conclusions

The main objective of my PhD project was to learn how to deal with long-term high-precision photomeric observations (such as the *Kepler* space telescope observation), especially in the presence of stellar activity noise, in order to accurately detect and precisely characterize the transiting and also non-transiting exoplanets.

At the beginning, we were more interested in precise determinations of the transit timing of already known transiting planets in the *Kepler* planet candidates list. By having such precision transit time measurements we would be able to obtain the TTV signal which can be used to detect and characterize non-transiting planets through their gravitational perturbation into transiting planet. To provide a method which can determine the mid-transit time with high-precision, we proposed a technique called the *barycenter* method. The idea of this method is only based on the symmetry of the transit light-curve, and as a consequence it has a remarkable advantage when compared to other methods, which are all model-dependent. In other words, unlike other techniques for calculating the mid-transit times, the results obtained from the *barycenter* method will not be influenced by changing the assumed parameters of the system. Our study indicates that for complete and symmetric transit light-curves, the *barycenter* method results are in strong agreement with other method's results, and it reaches better precision

on the transit timing than the method of Mandel & Agol (2002), with fewer assumptions and much faster running time. The *barycenter* description, its test, and its application were presented in my first paper published during PhD (Oshagh et al., 2012). It is important to note here that this method and all other methods of transit timing measurement require symmetric transit light-curve, and thus imply that when the transit light-curve is not perfectly symmetric large offsets may appear in all the mid-transit timing measurements. For instance, missing the data points in the transit light-curve due to observational error or anomalies inside the transit light-curve can break its symmetry.

A survey on currently known extrasolar planets has revealed that many of these orbit stars that show high levels of activity. For instance, among the stars in the field of view of the *Kepler* Space Telescope, a quarter to a third are more active than the Sun (Basri et al., 2013). Active stars are expected to harbor stellar spots. As a result, most of the transit light-curves might show out of transit variations due to appearance and disappearance of the stellar spots caused by the stellar rotation, and in the addition inside transit light-curve anomalies due to the occultation of the transiting planet with the stellar spots. Those inside anomalies break the symmetry of transit light-curve and lead to an incorrect determination of the transit time, and in addition may lead to underestimation of planetary parameters, such as the planet radius, the orbital inclination and the limb darkening coefficients of the host star. To tackle the issues caused by those anomalies, we developed a new software package, named SOAP-T, that can reproduce the photometric and RV signals of a system consisting of a rotating spotted star and a transiting planet where the spots and planet overlap, thus SOAP-T can reproduce the inside transit anomalies features. We tested the capability of our tool by comparing its results with theoretical model's results and the result of observations. The description of the SOAP-T code, its test and application were presented in my second paper during my PhD which published in a refereed journal publication (Oshagh et al., 2013a).

The most important application of the SOAP-T tool is the modeling of observed anomalies inside the transits and subsequently removing the anomaly features from the transit light-curve. By implementing this approach, instead of

assigning a zero weight to the anomalous points of the light curve, which means deleting those data points from the transit light-curve, we cam eliminate the anomaly feature and make the light curve symmetric. Therefore, by studying the clean light curve, without any anomalies inside, the actual value of planetary parameters such as its radius, inclination, and transit timing can be derived precisely.

The anomalies inside the transit light-curve may carry extra information about the architecture of the planetary systems, such as the angle of stellar spin axis with respect to the orbital plane of the planet and also with respect to the observer. The combination of known value for the misalignment angle of spin-orbit, the inclination of stellar spin axis, and the planet orbital inclination provide an estimation on the true value of obliquity of the system. Considering the long-term, high-precision and continuous photometric observations of a star (e.g., target stars of the *Kepler* telescope), allows us to detect the evolution of the anomalies inside transits and extract information on the spin-orbit angle, the inclination of the stellar spin axis, and also the configuration of stellar spots on the surface of the star (longitude, latitude, and size).

For instance, we applied the SOAP-T tool on the HAT-P-11 system, which is a known active star harboring a transiting planet, to determine the misalignment angle of the planet in the system by using the anomalies inside its transit light curve. We demonstrated that by considering the edge-on star model which was proposed by Sanchis-Ojeda & Winn (2011), the SOAP-T program is capable of reproducing the same features as obtained from observations for the outside of transits as well as the anomalies inside the transits. We also obtained that the reconstruction of the large modulation of the outside transit of HAT-P-11 with the pole-on star model of Sanchis-Ojeda & Winn (2011) requires an assumption on the size of spot on the stellar surface which may not be a realistic assumption. These results for the case of the HAT-P-11 system are also presented in my second paper (Oshagh et al., 2013a).

Taking into account the fact that in large surveys of transiting planets, and especially in the TTV studies of those surveys the stellar activity have been assumed to be negligible, we thus decided to perform a quantitative study to estimate by how much the estimations on the planetary parameters can be underestimated or

overestimated. This issue has never been explored. We presented our quantitative analysis of the effect of stellar spots on a high-precision transit light-curve in my third published paper (Oshagh et al., 2013b). We demonstrated that the inside transit light-curve anomalies can have strong effects on the estimate of planetary parameters. These effects can lead to an underestimation of a the planet radius by about 4%. Likewise, they can also affect the transit duration and make it 4% longer or shorter than its actual value. Furthermore, depending on the size of the spot and its location, an anomaly can produce transit-timing variations with an amplitudes of about 200 seconds for a typical Sun-like spot. Such a large TTV is similar to that induced by an Earth-mass planet in a mean-motion resonance with a Jovian type body transiting a solar-mass star in a three-day orbit (e.g., Boué et al. (2012)), or by an Earth-mass exomoon on a Neptune mass transiting planet (Kipping, 2009). We also found for an active star, allowing more free parameters (e.g., transit depth and duration) during transit fitting procedure may lead to an erroneous estimation of the transit timing in comparison to the case where the transit depth and duration are held constant. Furthermore, we have also examined the sensitivity of our result for extreme cases of limb-darkening values related to extreme stellar temperatures, we did not find any significant effects from those extreme values in our study.

Considering that transmission spectroscopy (multiband photometry), which is the most used technique to explore exoplanetary atmospheres, is based on the transit observations of the planetary at different wavelengths, thus it may encounter limitations due to stellar activity. Only in a few cases the influence of non-occulted stellar spots on transmission spectroscopy measurements has been discussed. Therefore, we decided to study possible influences of occultation of stellar active regions, such as stellar spots or plages, by a transiting planet on the transmission spectroscopy's measurements. The results of large number of simulations of twenty different configurations, with different planet, star, and active regions parameters indicate significant underestimation or overestimation on the planet to star radius ratio as a function of wavelength. The maximum overestimation of the planet radius ratio (10%) may occur for the occultation of a transiting planet and a plage on M-dwarf on the short wavelength regime. We demonstrated that transmission spectroscopy measurements of the active stars

HD 189733b and GJ 3470b, and especially their excess of the planet radius in the bluer part of the spectra, can almost exactly be reproduced by assuming the occultation of the HD 189733b and GJ 3470b with the active region (plage) of their host star.

7.2 Future works

7.2.1 The effect of star-spots on the Rossiter-McLaughlin (RM) effect

Since SOAP-T is able to generate the RM effect of a transiting planet over a rotating spotted star, we will be able to perform a quantitative numerical study on the impact of the overlap of the transiting planet and the stellar spots on the RM measurements . This issue has never been explored. We will thus quantify the propagated effect on our estimation on the misalignment angle and the stellar rotation velocity ($v \sin i$). We will also check RM observations which are publicly available in e.g. the ESO and Keck archives to explore any possible sign of the planet-spot overlap anomalies in the RM signal.

7.2.2 Simultaneous photometric and RM observation

The combination of the information from the transit light-curve anomalies and the RM measurements, which are affected by the planet-spot overlap, might break the degeneracies which sometimes arise. For example, the size of the stellar spot(s), their exact position on the surface of star and their temperature can be unambiguously determined with simultaneous observations. For this purpose, we will need strictly simultaneous high-precision photometric and high-precision RV observations. In order to probe this case, we will analyze simultaneous photometric and RV observations independently and also the combination. For high-precision RV we will consider observing with the SOPHIE, HARPS, HARPS-N and in near future ESPRESSO at VLT. For high-precision photometric observations we
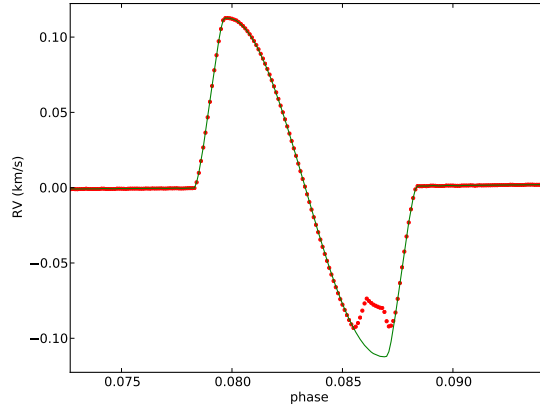
Figure 7.1: The preliminary simulation with SOAP-T which shows the clear impact the occultation of a stellar spot by the transiting planet on the RM effect measurements.

should consider using space missions such as the MOST, TESS, and CHEOPS and also in near future ground base facilities such as NGTS, ExTra.

7.2.3   Additional perturbing planets in the system?

The Kepler TTV candidates catalogue (Mazeh et al., 2013) includes 150 Weak TTV objects: Kepler Objects of Interest (KOIs) which show TTV signals with amplitude less than 200 s; these may be produced by the stellar activity. I will study an active sub-sample of these which show out of transit variation due stellar-rotational modulation in star spot visibility. I will carefully examine the transit light-curves of this Active Weak TTV sub-sample, identifying anomalies due to the overlap of the transiting planet and a stellar spot. Then by using SOAP-T, I will reproduce synthetic transit light-curves containing the same anomalies. Using the synthetic light-curve I will correct the observed transit light-curves. Therefore, I will then measure the transit times of the corrected transit light-curves and recalculate the TTVs. If TTVs persist, it indicates that the TTV signal is real and it has be caused by gravitational perturbation of an additional

non-transiting planet(s). Conversely, if the TTV signal disappears after removing the stellar activity noise from the light-curve, we can discard the KOI from the TTV catalog. Kepler data for this work are public and immediately accessible; I will also study other brighter objects which are observed with ground based facilities which also show weak TTV signals e.g. WASP-12 (Haswell et al. (2012); Maciejewski et al. (2013).

Appendix A

Bootstrap

In this section we are describing the Bootstrap method which we have used several times in this thesis in order to estimate the uncertainty on the estimated value of parameters from the fitting producer.

Consider a sample of N data points which we are using to estimate the value of parameters of our models from them (for instance, we observed N points in the transit light curve, and we want to estimate the transit depth of a transit light-curve). In order to obtain the error on the parameters which are estimated, the following procedure should be performed. This method is known as the bootstrap method which was presented for the first time by Efron (1982). First, we determine the value of the parameters by using all the data points. Then, we have to go through the following steps,

- Should put label on each data points such as $a_1, a_2, ..., a_N$.

- Add a random-number generator to each data points. The random-generator should be a Gaussian random generator with the mean at zero and the width equal to the average of error of all the data points.

- Recalculate the value of the parameter

- Repeat the above process for a large number ($\dot{\iota}1000$)

The standard deviation of distribution of the recalculated parameter give the uncertainty on the measured value for the parameter.

Appendix B

TOPCAT

TOPCAT is a interactive graphical software based on the Java language, and a very suitable tool to work with the catalogs and huge tables. TOPCAT can be run on most of the operating systems and the only requirement is installation of Java Runtime Environment (JRE). The *Kepler* team suggested the TOPCAT as the most convenient, and powerful and useful software to be used for inspection of *Kepler* light curve files [1]. *Kepler* data are provided for each star in the quarters (Qs), in the binary FITS format. Each file contains the time, Barycenter corrected time, raw fluxes, corrected fluxes, astrometric measurements, and also the quality flag of the data.

The TOPCAT software can be obtained through its website[2]. After installing the program, and running the software, user can load the data through the "FILE" option. In the "FILE" option there is the "LOAD TABLE " option which allows user to import different formats of data including the FITS, ASCII, txt, and CSV. After selecting the format of the input data or leave it to its default option which is "AUTO", user can use "FILE STORE BROWSER" in order to search in different directories to reach the desired file. After importing the data file, the file name will appear on the left side panel of the software. If the user

---

[1] http://keplerscience.arc.nasa.gov/DataAnalysisTools.shtml
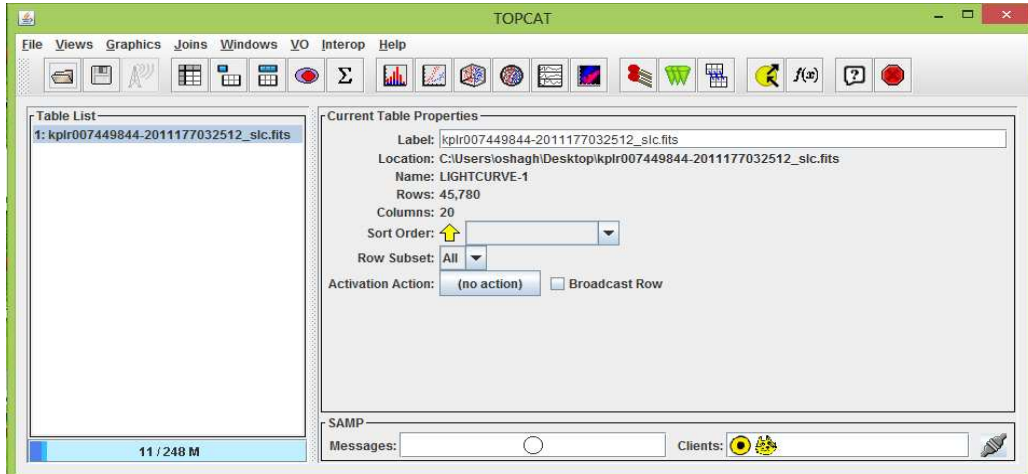
[2] http://www.star.bris.ac.uk/ mbt/topcat/

Figure B.1: The main window of TOPCAT. Data Input and Output is possible through File option. The left panel lists opened files; on the right information about the currently selected file is shown.

load more than one data files, in this panel by clicking the desired one can chosen. By clicking on the "DISPLAY DATA CELL TABLE" bottom (fourth icon from the left), users are able to see the details of each data table in different columns, such as time, SAP_FLUX, etc. In the "DISPLAY COLUMN METADATA" (sixth icon from the left) there are more details on each columns, such as their units, etc. By using the "DISPLAY COLUMN METADATA", the user also can select a sub-sample of the columns of data which are needed for user's research. In the option of "DISPLAY STATISTICS FOR EACH COLUMN" (eighth icon from the left) some statistics about the data of each column are presented, such as the mean, standard deviation, maximum, and minimum. The data can be converted to other format using the "SAVE TABLES" in the "FILE" option.

In order to plot the the data, user has to use the "SCATTER PLOT" option (tenth icon from the left). In the new window, the column which has to be used for plotting as X, and Y axis can be adjusted. The are boxes for plotting axis in

log scales. By selecting any area on the plot, there is possibility of zooming on that area. There is also possibility to define new sub-sample for the zoomed area (icon number 10). Re-scaling is possible by using the arrow icons. The plot can be saved as pdf by using icon number 4.
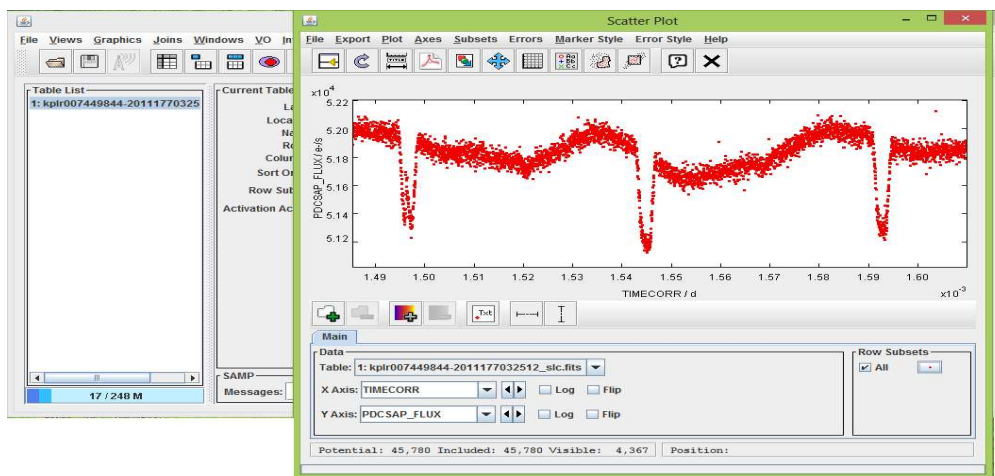

Figure B.2: TOPCAT plot of TIMECORR in days vs $PDCSAP - FLUX$.

Bibliography

Agol, E., Steffen, J., Sari, R., & Clarkson, W. 2005, MNRAS, 359, 567 22, 23

Albrecht, S., Winn, J. N., Johnson, J. A., et al. 2012, ApJ, 757, 18 16

Alibert, Y., Mordasini, C., & Benz, W. 2011, A&A, 526, A63 2

Alibert, Y., Mordasini, C., Benz, W., & Winisdoerffer, C. 2005, A&A, 434, 343 1

Alonso, R., Brown, T. M., Torres, G., et al. 2004, ApJ, 613, L153 12

Appenzeller, I., Fricke, K., Fürtig, W., et al. 1998, The Messenger, 94, 1 31

Baglin, A., Auvergne, M., Boisnard, L., et al. 2006, in COSPAR Meeting, Vol. 36, 36th COSPAR Scientific Assembly, 3749 12

Bakos, G., Noyes, R. W., Kovács, G., et al. 2004, PASP, 116, 266 12

Ballard, S., Fabrycky, D., Fressin, F., et al. 2011, ArXiv 1109.1561 23, 24

Ballerini, P., Micela, G., Lanza, A. F., & Pagano, I. 2012, A&A, 539, A140 13

Baranne, A., Queloz, D., Mayor, M., et al. 1996, A&AS, 119, 373 13, 14

Barclay, T., Rowe, J. F., Lissauer, J. J., et al. 2013, Nature, 494, 452 25

Barros, S. C. C., Boué, G., Gibson, N. P., et al. 2013, MNRAS, 430, 3032 55

Basri, G., Walkowicz, L. M., Batalha, N., et al. 2010, ApJ, 713, L155 28

Basri, G., Walkowicz, L. M., & Reiners, A. 2013, ApJ, 769, 37 27, 82

Batalha, N. M., Rowe, J. F., Bryson, S. T., et al. 2013, ApJS, 204, 24 24

Berdyugina, S. V. 2002, Astronomische Nachrichten, 323, 192 28

Berdyugina, S. V. 2005, Living Reviews in Solar Physics, 2, 8 29, 36, 37, 38, 39

Berdyugina, S. V., Berdyugin, A. V., Ilyin, I., & Tuominen, I. 1999, A&A, 350, 626 40

Berdyugina, S. V. & Henry, G. W. 2007, ApJ, 659, L157 40

Berta, Z. K., Charbonneau, D., Bean, J., et al. 2011, ApJ, 736, 12 13

Beuzit, J.-L., Feldt, M., Dohlen, K., et al. 2008, in Society of Photo-Optical Instrumentation Engineers (SPIE) Conference Series, Vol. 7014, Society of Photo-Optical Instrumentation Engineers (SPIE) Conference Series 21

Bogdan, T. J., Gilman, P. A., Lerche, I., & Howard, R. 1988, ApJ, 327, 451 33, 34

Boisse, I., Bouchy, F., Hébrard, G., et al. 2011, A&A, 528, A4 55

Boisse, I., Moutou, C., Vidal-Madjar, A., et al. 2009, A&A, 495, 959 55

Bond, I. A., Rattenbury, N. J., Skuljan, J., et al. 2002, MNRAS, 333, 71 18

Bonfils, X., Forveille, T., Delfosse, X., et al. 2005, A&A, 443, L15 6

Bonfils, X., Mayor, M., Delfosse, X., et al. 2007, A&A, 474, 293 55

Borucki, W. J., Agol, E., Fressin, F., et al. 2013, Science, 340, 587 25

Borucki, W. J., Koch, D., Basri, G., et al. 2010, Science, 327, 977 12, 24, 28

Boss, A. P. 1998, ApJ, 503, 923 1

Boué, G., Montalto, M., Boisse, I., Oshagh, M., & Santos, N. C. 2013, A&A, 550, A53 13

Boué, G., Oshagh, M., Montalto, M., & Santos, N. C. 2012, MNRAS, 422, L57 23, 67, 84

Bray, R. J. & Loughhead, R. E. 1964, Sunspots 33

Butler, R. P., Marcy, G. W., Williams, E., et al. 1996, PASP, 108, 500 14

Casertano, S., Lattanzi, M. G., Sozzetti, A., et al. 2008, A&A, 482, 699 17

Charbonneau, D., Brown, T. M., Latham, D. W., & Mayor, M. 2000, ApJ, 529, L45 12

Charbonneau, D., Irwin, J., Nutzman, P., & Falco, E. E. 2008, in Bulletin of the American Astronomical Society, Vol. 40, American Astronomical Society Meeting Abstracts #212, 242 12

Claret, A. 2000, A&A, 363, 1081 11

Collier Cameron, A. 1992, in Lecture Notes in Physics, Berlin Springer Verlag, Vol. 397, Surface Inhomogeneities on Late-Type Stars, ed. P. B. Byrne & D. J. Mullan, 33 28, 30, 36

Collier Cameron, A., Donati, J.-F., & Semel, M. 2002, MNRAS, 330, 699 41

Csizmadia, S., Pasternacki, T., Dreyer, C., et al. 2013, A&A, 549, A9 13

Czesla, S., Huber, K. F., Wolter, U., Schröter, S., & Schmitt, J. H. M. M. 2009, A&A, 505, 1277 13

Désert, J.-M., Charbonneau, D., Demory, B.-O., et al. 2011, ApJS, 197, 14 13, 57

Donati, J.-F. 1999, MNRAS, 302, 457 40

Donati, J.-F. & Collier Cameron, A. 1997, MNRAS, 291, 1 41

Donati, J.-F., Semel, M., Carter, B. D., Rees, D. E., & Collier Cameron, A. 1997, MNRAS, 291, 658 28

Dumusque, X., Pepe, F., Lovis, C., et al. 2012, Nature, 491, 207 1, 7

Efron, B. 1982, The Jackknife, the Bootstrap and other resampling plans 88

Einstein, A. 1936, Science, 84, 506 17, 32

Endl, M., MacQueen, P. J., Cochran, W. D., et al. 2011, ApJS, 197, 13 8

Fabrycky, D. C. & Winn, J. N. 2009, ApJ, 696, 1230 57

Fekel, F. C., Quigley, R., Gillies, K., & Africano, J. L. 1987, AJ, 94, 726 27

Fields, D. L., Albrow, M. D., An, J., et al. 2003, ApJ, 596, 1305 32

Figueira, P., Marmier, M., Bonfils, X., et al. 2010, A&A, 513, L8 55

García, R. A., Hekker, S., Stello, D., et al. 2011, MNRAS, 414, L6 26

Gaudi, B. S. & Winn, J. N. 2007, ApJ, 655, 550 15

Gibson, N. P., Pollacco, D., Simpson, E. K., et al. 2009, ApJ, 700, 1078 56

Gilliland, R. L., Jenkins, J. M., Borucki, W. J., et al. 2010, ApJ, 713, L160 25

Gizon, L. 2002, Astronomische Nachrichten, 323, 251 32

Gizon, L. & Solanki, S. K. 2004, Solar Physics, 220, 169 33, 41

Gray, D. F. 2005, The Observation and Analysis of Stellar Photospheres 11, 13

Gray, D. F. & Johanson, H. L. 1991, PASP, 103, 439 36

Hall, D. S. 1991a, ApJ, 380, L85 42

Hall, D. S. 1991b, in Lecture Notes in Physics, Berlin Springer Verlag, Vol. 380, IAU Colloq. 130: The Sun and Cool Stars. Activity, Magnetism, Dynamos, ed. I. Tuominen, D. Moss, & G. Rüdiger, 353 41

Hall, D. S. & Henry, G. W. 1994, International Amateur-Professional Photoelectric Photometry Communications, 55, 51 39

Hébrard, G., Bouchy, F., Pont, F., et al. 2008, A&A, 488, 763 16, 57

Henry, G. W., Eaton, J. A., Hamer, J., & Hall, D. S. 1995, ApJS, 97, 513 42

Henry, G. W., Marcy, G. W., Butler, R. P., & Vogt, S. S. 2000, ApJ, 529, L41 12

Hilditch, R. W. 2001, An Introduction to Close Binary Stars 17

Hinz, P. M., Solheid, E., Durney, O., & Hoffmann, W. F. 2008, in Society of Photo-Optical Instrumentation Engineers (SPIE) Conference Series, Vol. 7013, Society of Photo-Optical Instrumentation Engineers (SPIE) Conference Series 21

Hirano, T., Sanchis-Ojeda, R., Takeda, Y., et al. 2012, ApJ, 756, 66 57

Hirano, T., Suto, Y., Winn, J. N., et al. 2011, ApJ, 742, 69 13, 14, 16, 57

Holman, M. J., Fabrycky, D. C., Ragozzine, D., et al. 2010, Science, 330, 51 23

Holman, M. J. & Murray, N. W. 2005, Science, 307, 1288 22

Huélamo, N., Figueira, P., Bonfils, X., et al. 2008, A&A, 489, L9 55

Kalas, P., Graham, J. R., & Clampin, M. 2005, Nature, 435, 1067 21

Kipping, D. M. 2009, MNRAS, 392, 181 67, 84

Kron, G. E. 1947, PASP, 59, 261 29

Lanza, A. F. & Rodonò, M. 2002, Astronomische Nachrichten, 323, 424 33

Lanza, A. F., Rodono, M., & Zappala, R. A. 1993, A&A, 269, 351 41

Laureijs, R. J., Duvet, L., Escudero Sanz, I., et al. 2010, in Society of Photo-Optical Instrumentation Engineers (SPIE) Conference Series, Vol. 7731, Society of Photo-Optical Instrumentation Engineers (SPIE) Conference Series 18

Libbrecht, K. G. & Woodard, M. F. 1990, Nature, 345, 779 32

Lin, D. N. C., Bodenheimer, P., & Richardson, D. C. 1996, Nature, 380, 606 1

Lissauer, J. J., Fabrycky, D. C., Ford, E. B., et al. 2011, Nature, 470, 53 23, 25

Livingston, W. 2002, Solar Physics, 207, 41 38

Lovis, C. & Fischer, D. 2011, Radial Velocity Techniques for Exoplanets, ed.
   S. Seager, 27–53 5

Maciejewski, G., Dimitrov, D., Neuhäuser, R., et al. 2010, MNRAS, 407, 2625 23

Maciejewski, G., Dimitrov, D., Neuhäuser, R., et al. 2011a, MNRAS, 411, 1204
   23

Maciejewski, G., Errmann, R., Raetz, S., et al. 2011b, A&A, 528, A65+ 23

Macintosh, B. A., Graham, J. R., Palmer, D. W., et al. 2008, in Society of
   Photo-Optical Instrumentation Engineers (SPIE) Conference Series, Vol. 7015,
   Society of Photo-Optical Instrumentation Engineers (SPIE) Conference Series
   21

Mandel, K. & Agol, E. 2002, ApJ, 580, L171 12, 43, 44, 82

Marois, C., Macintosh, B., Barman, T., et al. 2008, Science, 322, 1348 21

Marois, C., Zuckerman, B., Konopacky, Q. M., Macintosh, B., & Barman, T.
   2010, Nature, 468, 1080 20

Mayor, M. & Queloz, D. 1995, Nature, 378, 355 1

Mazeh, T., Nachmani, G., Holczer, T., et al. 2013, ArXiv 1301.5499 86

McLaughlin, D. B. 1924, ApJ, 60, 22 13

Mekkaden, M. V. 1985, Ap&SS, 117, 381 27

Messina, S. & Guinan, E. F. 2003, A&A, 409, 1017 42

Meunier, N., Desort, M., & Lagrange, A.-M. 2010, A&A, 512, A39 33, 34

Mordasini, C., Alibert, Y., & Benz, W. 2009, A&A, 501, 1139 1

Mordasini, C., Alibert, Y., Benz, W., Klahr, H., & Henning, T. 2012, A&A, 541, A97 2

Morton, T. D. & Johnson, J. A. 2011, ApJ, 729, 138 57

Murphy, S. J. 2012, MNRAS, 422, 665 26

Narita, N., Enya, K., Sato, B., et al. 2007, PASJ, 59, 763 57

Nutzman, P. A., Fabrycky, D. C., & Fortney, J. J. 2011, ApJ, 740, L10 57

Ohta, Y., Taruya, A., & Suto, Y. 2005, ApJ, 622, 1118 13, 14, 57

O'Neal, D., Neff, J. E., Saar, S. H., & Cuntz, M. 2004, AJ, 128, 1802 36

O'Neal, D., Saar, S. H., & Neff, J. E. 1996, ApJ, 463, 766 35

O'Neal, D., Saar, S. M., & Neff, J. E. 1998, ApJ, 501, L73 35

Oshagh, M., Boisse, I., Boué, G., et al. 2013a, A&A, 549, A35 82, 83

Oshagh, M., Boué, G., Haghighipour, N., et al. 2012, A&A, 540, A62 23, 55, 56, 82

Oshagh, M., Santos, N. C., Boisse, I., et al. 2013b, A&A, 556, A19 24, 84

Ossendrijver, M. 2003, A&A Rev., 11, 287 27

Oswalt, T. D., ed. 2003, Astrophysics and Space Science Library, Vol. 288, The Future of Small Telescopes In The New Millennium. Volume II - The Telescopes We Use 20

Pallavicini, R., Golub, L., Rosner, R., et al. 1981, ApJ, 248, 279 27

Pepe, F., Mayor, M., Galland, F., et al. 2002, A&A, 388, 632 14

Pepe, F. A., Cristiani, S., Rebolo Lopez, R., et al. 2010, in Society of Photo-Optical Instrumentation Engineers (SPIE) Conference Series, Vol. 7735, Society of Photo-Optical Instrumentation Engineers (SPIE) Conference Series 7

Perryman, M. 2011, The Exoplanet Handbook 4

Perryman, M. 2013, ArXiv e-prints 16

Petrovay, K. & van Driel-Gesztelyi, L. 1997, Solar Physics, 176, 249 39

Poe, C. H. & Eaton, J. A. 1985, ApJ, 289, 644 35, 36

Pollacco, D. L., Skillen, I., Collier Cameron, A., et al. 2006, PASP, 118, 1407 12

Pollack, J. B., Hubickyj, O., Bodenheimer, P., et al. 1996, Icarus, 124, 62 1

Pont, F., Gilliland, R. L., Moutou, C., et al. 2007, A&A, 476, 1347 13

Pont, F., Knutson, H., Gilliland, R. L., Moutou, C., & Charbonneau, D. 2008, MNRAS, 385, 109 12

Queloz, D., Eggenberger, A., Mayor, M., et al. 2000, A&A, 359, L13 57

Queloz, D., Henry, G. W., Sivan, J. P., et al. 2001, A&A, 379, 279 55

Quintana, E. V., Barclay, T., Raymond, S. N., et al. 2014, Science, 344, 277 1

Rabus, M., Alonso, R., Belmonte, J. A., et al. 2009, A&A, 494, 391 55

Reiners, A. & Schmitt, J. H. M. M. 2002, A&A, 384, 155 41

Rice, J. B. & Strassmeier, K. G. 2000, A&AS, 147, 151 28

Robinson, Jr., R. D. 1980, ApJ, 239, 961 37

Rossiter, R. A. 1924, ApJ, 60, 15 13

Rousselet-Perraut, K., Stehlé, C., Lanz, T., et al. 2004, A&A, 422, 193 32

Saar, S. H. 1988, ApJ, 324, 441 37

Sanchis-Ojeda, R., Fabrycky, D. C., Winn, J. N., et al. 2012, Nature, 487, 449 57

Sanchis-Ojeda, R. & Winn, J. N. 2011, ApJ, 743, 61 55, 57, 58, 83

Sanchis-Ojeda, R., Winn, J. N., Holman, M. J., et al. 2011, ApJ, 733, 127 55

Santos, N. C. 2008, New A Rev., 52, 154 5

Seager, S. 2011, Exoplanets 9, 10

Shporer, A. & Brown, T. 2011, ApJ, 733, 30 14

Simpson, E. K., Pollacco, D., Hébrard, G., et al. 2010, MNRAS, 405, 1867 16

Skumanich, A. 1972, ApJ, 171, 565 27

Solanki, S. K. 2003, A&A Rev., 11, 153 33, 34, 35

Sozzetti, A. 2011, in EAS Publications Series, Vol. 45, EAS Publications Series, 273–278 17

Stenflo, J. O. 2013, A&A Rev., 21, 66 31

Strassmeier, K. G. 1999, A&A, 347, 225 34, 35, 36, 40

Strassmeier, K. G. 2009, A&A Rev., 17, 251 31

Strassmeier, K. G. & Bartus, J. 2000, A&A, 354, 537 40

Strassmeier, K. G., Pallavicini, R., Rice, J. B., & Andersen, M. I. 2004, Astronomische Nachrichten, 325, 278 31

Sumi, T., Kamiya, K., Bennett, D. P., et al. 2011, Nature, 473, 349 18

Szabó, G. M., Szatmáry, K., Divéki, Z., & Simon, A. 2006, A&A, 450, 395 43

Tas, G. & Evren, S. 2000, Information Bulletin on Variable Stars, 4992, 1 34

Telting, J. H., Avila, G., Buchhave, L., et al. 2014, Astronomische Nachrichten, 335, 41 6

Triaud, A. H. M. J., Collier Cameron, A., Queloz, D., et al. 2010, A&A, 524, A25 16, 57

Triaud, A. H. M. J., Queloz, D., Bouchy, F., et al. 2009, A&A, 506, 377 16, 57

Udalski, A., Szymanski, M., Kaluzny, J., Kubiak, M., & Mateo, M. 1992, Acta Astronomica, 42, 253 12, 18

Udalski, A., Szymanski, M., Kaluzny, J., et al. 1995, Acta Astronomica, 45, 1 32

Udry, S. & Santos, N. C. 2007, Annual Review of Astronomy & Astrophysics, 45, 397 2

Valenti, J. A. & Fischer, D. A. 2005, ApJS, 159, 141 14

Valenti, J. A. & Fischer, D. A. 2008, Physica Scripta Volume T, 130, 014003 2

Valenti, J. A. & Johns-Krull, C. 2001, in Astronomical Society of the Pacific Conference Series, Vol. 248, Magnetic Fields Across the Hertzsprung-Russell Diagram, ed. G. Mathys, S. K. Solanki, & D. T. Wickramasinghe, 179 37

Vogt, S. S., Allen, S. L., Bigelow, B. C., et al. 1994, in Society of Photo-Optical Instrumentation Engineers (SPIE) Conference Series, Vol. 2198, Instrumentation in Astronomy VIII, ed. D. L. Crawford & E. R. Craine, 362 6

Vogt, S. S., Hatzes, A. P., Misch, A. A., & Kürster, M. 1999, ApJS, 121, 547 40

Vogt, S. S. & Penrod, G. D. 1983, ApJ, 275, 661 30

Vogt, S. S., Penrod, G. D., & Hatzes, A. P. 1987, ApJ, 321, 496 28

Waldmeier, M. 1955, Ergebnisse und Probleme der Sonnenforschung. 39

Walker, G., Matthews, J., Kuschnig, R., et al. 2003, PASP, 115, 1023 12

Walter, F. M. & Bowyer, S. 1981, ApJ, 245, 671 27

Winn, J. N. 2010, ArXiv e-prints 8

Winn, J. N., Holman, M. J., Torres, G., et al. 2008, ApJ, 683, 1076 14

Winn, J. N., Johnson, J. A., Fabrycky, D., et al. 2009, ApJ, 700, 302 16

Winn, J. N., Johnson, J. A., Howard, A. W., et al. 2010, ApJ, 723, L223 16, 57

Winn, J. N., Noyes, R. W., Holman, M. J., et al. 2005, ApJ, 631, 1215 57

Wittkowski, M., Schöller, M., Hubrig, S., Posselt, B., & von der Lühe, O. 2002, Astronomische Nachrichten, 323, 241 32

Wolszczan, A. & Frail, D. A. 1992, Nature, 355, 145 19

Publication list

Mahmoudreza Oshagh

Publications

Peer reviewed

Figueira, P.; **Oshagh, M.**; Adibekyan, V. Zh.; Santos, N. C., "Revisiting the correlation between stellar activity and planetary surface gravity", Astronomy & Astrophysics, Volume 572, id.A51, 9 pp, 2014.

Oshagh, M.; Santos, N. C.; Ehrenreich, D.; Haghighipour, N.; Figueira, P.; Santerne, A.; Montalto, M. "Impact of occultations of stellar active regions on transmission spectra: Can occultation of a plage mimic the signature of a blue sky?", Astronomy & Astrophysics, Volume 568, id.A99, 6 pp, 2014.

Santos, N. C.; Mortier, A.; Faria, J. P.; Dumusque, X.; Adibekyan, V. Zh.; Delgado-Mena, E.; Figueira, P.; Benamati, L.; Boisse, I.; Cunha, D.; Gomes da Silva, J.; Lo Curto, G.; Lovis, C.; Martins, J. H. C.; Mayor, M.; Melo, C.; **Oshagh, M.**; Pepe, F.; Queloz, D.; Santerne, A.; SÃ'gransan, D.; Sozzetti, A.; Sousa, S. G.; Udry, S., "The HARPS search for southern extra-solar planets.? XXXV. The interesting case of HD41248: stellar activity, no planets?", Astronomy & Astrophysics, Volume 566, id.A35, 14 pp, 2014.

Montalto, M.; BouÃ', G.; **Oshagh, M.**; Boisse, I.; Bruno, G.; Santos, N. C., "Improvements on analytic modelling of stellar spot", Monthly Notices of the Royal Astronomical Society, Volume 444, Issue 2, p.1721-1728, 2014.

Rauer, H. et al (including **Oshagh , M.**), "The PLATO 2.0 Mission", *Experimental Astronomy*, 2014.

Oshagh, M.; Boué,G.; Figueira, P.; Santos, N. C.; Haghighipour,N. "Probing the gravitational microlensing effect on the Rossiter-McLaughlin effect measurements", *Astronomy & Astrophysics*, Volume 558, id.A65, 5 pp, 2013.

Oshagh, M.; Santos, N. C.; I. Boisse,I.; Boué,G.; Montalto,M.; Dumusque, X.; Haghighipour,N."The effect of stellar spots on the high precision transit light curve", *Astronomy & Astrophysics*, Volume 556, id.A19, 5 pp, 2013.

Oshagh, M.; Boisse, I.; Boué, G.; Montalto, M.; Santos, N. C.; Bonfils, X; Haghighipour, N., "SOAP-T: A tool to study the light curves and radial velocities of planets transiting rotating spotted stars", *Astronomy & Astrophysics*, Volume 549, id.A35, 8 pp, 2013.

Boué, G.; Montalto, M.; Boisse, I.; **Oshagh, M**.; Santos, N. C.; "New analytical expressions of the Rossiter-McLaughlin effect adapted to different observation techniques", *Astronomy & Astrophysics*, Volume 550, id.A53, 16 pp, 2013.

Montalto, M.; Gregorio, J.; Boué, G.; Mortier, A.; Boisse, I.; **Oshagh, M**.; Maturi, M.; Figueira, P.; Sousa, S.; Santos, N. C., "A new analysis of the WASP-3 system: no evidence for an additional companion", *Monthly Notices of the Royal Astronomical Society*, Volume 427, Issue 4, pp. 2757-2771, 2012.

Oshagh, M.; Boué, G.; Haghighipour, N.; Montalto, M.; Figueira, P.; Santos, N. C., "Transit-timing measurements with the model-independent barycenter method: application to the LHS 6343 system", *Astronomy & Astrophysics*, 540, A62, 2012.

Boué, G.; **Oshagh, M.**; Montalto, M; Santos, N. C., "Degeneracy in the characterization of non-transiting planets from transit timing variations", *Monthly Notices of the Royal Astronomical Society*, 422, L57, 2012.

Conference Proceedings

Boisse, I.; **Oshagh, M.**; Lovis, C.; Santos, N. C.; Dumusque, X.; Bonfils, X.; Montalto, M.; BouÃľ, G., " How the planetary research helps to the stellar dynamo understanding", Solar and Astrophysical Dynamos and Magnetic Activity, Proceedings of the International Astronomical Union, IAU Symposium, Volume 294, pp. 471-475, 2013.

Oshagh, M.; Grigahcéne, A.; Benomar, O.; Dupret, M.-A.; Monteiro, M. J. P. F. G.; Scuflaire, R; Santos, N. C., "Successful asteroseismology for a better characterization of the exoplanet HAT-P-7b", Stellar Pulsations, Astrophysics and Space Science Proceedings, Volume 31, Part 5, 227-230, 2013 [DOI: 10.1007/978-3-642-29630-7-42].

Oshagh, M.; Boué, G.; Haghighipour, N.; Montalto, M.; Figueira, P.; Santos, N. C., "Transit Timing Measurements Using the model-independent barycenter method: Application to LHS 6343 System", Published in Proceedings of the 2nd CoRoT symposium, 2012.

Oshagh, M.; Haghighipour, N.; Santos, N. C., "A survey of M stars in the field of view of Kepler space telescope", Published in Proceedings of the International Astronomical Union, IAU Symposium, Volume 276, p. 448-449. 2011.

Oshagh, M.; Hemmati,S.; Behrouzi,F.; Sheidaeiand,F.; Bahmanabadi,M., "Study of number of particles crossing to a scintillation detector", published in proceeding of 31st International Cosmic Ray Conference, 2009 [Arxiv: 0907.4926].